DECHIPHERING THE EVOLUTION HISTORY OF THE SAHILI AND TURGUTLU GRANITES, MENDERES MASSIF, WESTERN TURKEY USING THE ELECTRON MICROOPROBE, ION MICROPROBE AND CATHODOLUMINESCENCE

By

COURTENEY BLAIRE BAKER

Bachelor of Science in Geology

Oklahoma State University

Stillwater, OK

2006

Submitted to the Faculty of the
Graduate College of the
Oklahoma State University
in partial fulfillment of
the requirements for
the Degree of
MASTER OF SCIENCE
May, 2010

DECHIPHERING THE EVOLUTION HISTORY OF THE SAHILI AND TURGUTLU GRANITES, MENDERES MASSIF, WESTERN TURKEY USING THE ELECTRON MICROOPROBE, ION MICROPROBE AND CATHODOLUMINESCENCE

Thesis Approved:

Dr. Anna Cruse

Thesis Adviser

Dr. Estella Atekwana

Dr. Jeffrey Byrnes

Dr. A. Gordon Emslie

Dean of the Graduate College

ACKNOWLEDGMENTS

I would like to dedicate this thesis to Dr. Elizabeth Catlos, my advisor and mentor. Without her patience, support, guidance and friendship I would not have been able to make it through this exciting process. She let me into her scientific world and showed me all the wonderful things you can accomplish if you just put your mind to it. Dr. Catlos has opened many doors for me and given me more opportunities than I could ever imagine. I owe her more thanks than I can ever convey through words.

A thank you also goes to Dr. Anna Cruse who became my thesis advisor the last semester of my graduate career. She blindly accepted that task and has offered her knowledge, guidance and support as well. Thank you to Dr. Estella Atekwana for her support, useful feedback and wise counsel. I would also like to thank Dr. Çemen for his scientific guidance, encouragement and unwaivering support. Finally thank you Dr. Byrnes for joining my committee and offering your guidance and support.

I would also like to extend a special thanks to Kurtis who has supported me from the very beginning. His encouragement, love and support got me through those stressful times. Very special thanks to my parents who are always there for me. My mother Alice always has faith me and made feel like I could accomplish anything and who told me to never give up. My father Rod who always had time to listen to me when I needed to talk, to give encouragement when I was not at my best, and to make me laugh when I was feeling down. A thank you goes to Oklahoma State University Geology department for

the support and for the wonderful education I received. Thank you to the NSF grant that supported me through my graduate career, which gave me the opportunity to visit Turkey to conduct my research. One final thanks to all of the friends I have made at Oklahoms State University. Kristi thanks for always being there for me and listening to me when I was ready to give up and for helping me get through it all. Thank you everyone for all of the amazing memories.

TABLE OF CONTENTS

LIST OF TABLES

LIST OF FIGURES

Figure Page

Figure Page

Figure Page

CHAPTER I

INTRODUCTION

1.1. Introduction to the geologic and tectonic settings of the Aegean and western Turkey

At some point in the Cenozoic, the Aegean region experienced a switch from compressional to extensional tectonics (Seyitoglu et al., 1992; Jolivet et al., 1994; Hetzel et al., 1995a; Seyitoglu and Scott, 1996; Gessner et al., 2001; Lips et al., 2001). The Menderes Massif in western Turkey (Figure 1.1) is an ideal region to study this transition. The massif's complex tectonic history has been of interest to many geologists since the 1960s (Schuiling, 1962). The Menderes Massif is a large topographic feature consisting of high grade igneous and metamorphic rocks surrounded by sediments, and covers a region of 40,000km^2 (Bozkurt and Park, 1997a) and is considered a metamorphic core complex (Dewey, 1988; Gessner et al., 2001).

This study focuses on one of the main exhumation mechanisms of the Menderes Massif: the Alasehir Detachment, which bounds its northern edge. This low angle detachment extends ~180 km along strike with a northward dip of 10-20˚ and is cut by high angle, more recently active faults (Hetzel et al., 1995; Catlos and Çemen, 2005). Determining the timing of movement along the Alasehir detachment has implications for our understanding of extension in the Aegean. The ages can be used to evaluate the relationship of the Menderes Massif top other extensional domains (ie. Kazdag, Rhodope, Crete, and Cycladic Massifs) (Figure 1.1), which may have experienced a similar tectonic history. Models that have been proposed for the change from collision to extension involve the basic plate tectonic processes, including subduction, collision,

and orogenic collapse, and lateral extrusion along strike slip faults, (Figure 1.2) (Şengör and Yilmaz, 1981; Şengör et al., 1985; Çemen et al., 1999, Dewey, 1988; Le Pichon and Angelier, 1979; Meulenkamp et al., 1988; Catlos and Çemen, 2005)

To address the timing of extension, granodiorites samples (S-type, peraluminous) were collected from two outcrops along the Alasehir detachment, located near the towns Salihli and the Turgutlu. Monazite $(CeLaTh)PO_4$ in the rocks were dated in situ (in thin section) using an ion microprobe. Ages range from the Late to Early Miocene. To better understand the reason for these results x-ray element maps and cathodoluminscence (CL) images of the dated samples were obtained. The CL images provided evidence of fluid flow that indicate dissolution/reprecipitation reactions. The techniques (ion microprobe, CL) used here to acquire and interpret the ages of the granodiorites are novel. They are means to decipher the complicated history of the Menderes Massif, and can be applied elsewhere to regions that have experienced a polyphase magmatic and tectonic history.

1.2. Tectonics of the Aegean

The investigation of Turkey has proved difficult in the past because of a large number of convergent events throughout its history (Şengör and Yilmaz, 1981). The Late Mesozoic-Early Cenozoic tectonic evolution of the Aegean was controlled by the collapse and closure of two Tethyan Oceanic Basin between the converging Eurasia and Arabian plate (Şengör and Yilmaz, 1981; Robertson and Dixon, 1984; Dilek and Moores, 1990; Dilek et al., 1999; Stampfli et al., 2001; Dilek and Flower, 2003; Dilek, 2006; Dilek and Altunkaynak, 2007). During this time the region experienced complex subduction events and associated collisions, resulting in mountain building, sedimentary basin evolution, escape tectonics, orogenic collapse and lithospheric scale extension (Figure 1.2) (Dilek, 2006).

The opening of the Paleo-Tethyan Ocean occurred in the Early Devonian due to sea floor spreading between a continental sliver comprised of North and South China, Indochina and Tarim

and Gondwana (Metcalfe, 1999). The Triassic to Early Jurassic is marked by the subduction of the Paleo-Tethyan basin beneath Turkey, which constituted the northern margin of Gondwana, in response to a south dipping subduction zone (Şengör and Yilmaz, 1981; Metcalfe, 1999). The Neo-Tethyan Ocean is interpreted to have opened as the Cimmerian plate separated from Gondwana during the Triassic (Şengör and Yilmaz, 1981). The closure of the Neo-Tethyan Ocean as part of the Izmir-Ankara suture zone (Şengör and Yilmaz, 1981; Gorur et al., 1984; Çemen et al., 1999) occurred in the Mesozoic-Cenozoic due to continental collisions and subsequent post-orogenic processes (Şengör and Yilmaz, 1981; Bozkurt and Mittwede, 2001; Okay et al., 2001; Dilek and Pavlides, 2006; Robertson and Mountrakis, 2006; Taymaz et al., 2007). Thus the present tectonic setting of Turkey was created by the terminal collision of Afro-Arabia with Eurasia (Arpart and Saroglu, 1975; Aksu et al., 1987; Sengor et al., 1981). Post-collisional extension in the region caused the exhumation of the Alpine Metamorphic belts; Rhodope, Kazdag, Cycladic, Menderes, and Crete Massifs (Catlos and Çemen, 2005).

1.3. Geology of the Crete, Cyclades, Rhodope, Kazdag, and Menderes Massifs

The massifs located in the Aegean from north to south, are the Rhodope, Kazdag, Menderes, Cycladic, and Crete massifs (Fig. 1.1). Each is comprised of core and cover nappes which are considered Cenozoic (Katzir, et al., 1999; Finger, et al., 2002; Ring, et al., 1999; Katzir, et al., 2000; Bonev, 2006; Bonev and Stampfli, 2007; Liati, and Gebauer, 1999; Fassoulas, et al., 1994; Seidel, et al., 2006; Buick, 1991). All Aegean massifs share a similar lithology, being comprised of mainly high-grade metamorphic and igneous rocks (Katzir, et al., 1999; Finger, et al., 2002; Ring, et al., 1999; Katzir, et al., 2000; Bonev, 2006; Bonev, 2006; Liati, and Gebauer, 1999; Fassoulas, et al., 1994; Seidel, et al., 2006; Buick, 1991).

The Rhodope Massif is located in the northeastern part of Greece and extends into the southern part of Bulgaria (Fig. 1.1). This massif is considered to be a major tectonic zone in the Aegean and represents a part of the Alpine-Himalayan orogenic system in the eastern

Mediterranean region (e.g., Bonev and Stampfli, 2007). A strike-slip fault (the Sredna Gora Zone) separates the Rhodope in the north (Bonev and Stampfli 2007). As is documented for the other massifs, the Rhodope Massif is divided into cover and basement nappes that were assembled by southward thrusting in the hanging wall of a Late-Cretaceous-Tertiary subduction zone (Ricou et al., 1998; Bonev and Stampfli, 2007). The basement nappe of metamorphic Eocene units (e.g. Lips et al., 2000; Liati, 2005; Bonev and Stampfli, 2007) was intruded by Late Cretaceous to Early Miocene granitoids (Soldatod and Christofides, 1986; Del Moro et al., 1988; Dinter, 1998; Peytcheva et al., 1999; Bonev and Stampfli, 2007). The core nappes are metamorphosed Late Cretaceous to Miocene sediments (Boyanov and Goranov, 2001; Bonev and Stampfli, 2007) and Late Eocene-Oligocene volcanic and volcanic-sedimentary successions (Harkovska et al., 1989; Bonev and Stampfli, 2007). Crustal shortening and thickening was accompanied by syn- to post-thickening extension followed by post-orogenic Aegean back-arc extension (Burg et al., 1996; Dinter, 1998; Krohe and Mposkos, 2002; Bonev et al., 2006; Bonev, 2006 and Bonev and Stampfli, 2007).

The Kazdag Massif (Fig. 1.1) is shown to correlate with the Rhodope Massif both in terms of lithology and the metamorphic conditions experienced by its rocks (Papanikolaou and Demirtasli, 1987; Okay and Satir, 2008). Located in the northwestern part of Turkey, the Kazdag Massif is a metamorphic core complex created during the Late Oligocene (Okay and Satir 2000). Described as a topographic dome, the Kazdag is composed of high-grade metamorphic rocks, including gneiss, marble, amphibolite, and meta-ultramafic rocks (Schulling, 1959; Okay et al., 1991; Pickett and Robertson, 1996; Okay et al., 1996; Okay and Satir, 2000). The massif is overlain by a deformed Permo-Triassic basic volcanic and clastic rocks whose lower parts experienced greenschist-facies regional metamorphism. These rocks are unconformably overlain by little- deformed Jurassic –Lower Cretaceous sandstone and limestone (Bingol et al., 1975; Okay, Siyako and Burkan, 1991; Okay et al., 1996; Leven and Okay, 1996; Okay and Satir, 2000).

The Cycladic Massif lies in the Hellenic arc (Buick 1991) and records a cycle of orogenic thickening (Lister et al., 1984; Ridley, 1984; Avigad and Garfunkel, 1991; Gautier and Brun, 1994; Katzir et al., 1999) followed by an extensional collapse. Low-angle detachments push low-pressure metamorphic and unmetamorphosed rocks on top of exhumed high pressure/temperature units (Lister et al., 1984; Ridley, 1984; Avigad and Garfunkel, 1991; Gautier and Brun, 1994; Katzir et al., 1999). The Cycladic Massif consists of three nappes; an ophiolitic mélange, Permocarboniferous to Mesozoic sequence, and a Carboniferous basement (Ring et al., 1999, Gessner et al., 2001). During the middle Oligocene exhumation is believed to have occurred when normal faulting was caused by subduction rollback of the Hellenic Slab (Lister et al., 1984; Buick, 1991; Raouzaios et al., 1996; Gessner, 2001).

The Menderes Massif, located in western Turkey, has been thought to correlate to the Cycladic Massif based on lithostratigraphic comparison, but recent studies have suggested that the two massifs are in fact not related (Durr et al., 1978; Oberhansli et al., 1998; Ring et al., 1999). Although the Menderes Massif's categorization of a metamorphic core complex is accepted, the timing and the mechanism of extensional events is not understood (Bozkurt and Park 1994, 1997a, 1997b; Verge, 1995; Hetzel et al., 1995a, 1995b, 1998; Hetzel and Reischmann, 1996; Işik et. al, 2003; Catlos and Çemen, 2005). The Menderes Massif is comprised of nappes termed the Selimiye, Cine, Bozdag, and Bayindir (Ring et al., 1999; Gessner et al., 2001; Catlos and Çemen, 2005). The two lower nappes; Bayindir and Bozdag, consist of a metapelitic assemblage with amphibolite and marble lenses (Gessner et al., 2001; Ring et al., 1999; Catlos and Çemen, 2005). The Cine nappe overlies the Bayindir and Bozdag nappes and is comprised of a Proterozoic-Cambrian basement (Gessner et al., 2001; Ring et al., 1999; Catlos and Çemen, 2005). The upper Selimiye nappe consists of a metasedimentary succession of intercalated marble and calcschist (Gessner et al., 2001; Ring et al., 1999; Catlos and Çemen, 2005). The Bayindir nappe it thought to have experienced only one major Alpine

tectonometamorphic event whereas the overlying Bozdag, Cine, and Selimiye nappes record two events during the pre-Alpine and Alpine (Ring et al., 1999; Catlos and Çemen, 2005).

The Crete Massif has a horst structure in the central forarc of the Hellenic subduction zone also thought to be due to the roll back of the Hellenic (African) slab (Seidel et al., 2006). As with other massifs, the Crete Massif is divided into two nappes. The upper nappe rests unconformably on the top of the basement and consists of meta-andesite, meta-conglomerate, marble, quartzite and schist (Finger et al., 2002). The lower (or basement) consists of Pre-Alpine phyllite and quartzite, mica schist, paragneiss, amphibolite, marble and orthogneiss units overthrusting a phyllite/marble sequence (Zulauf et al., 2002; Finger et al., 2002). Theses two nappes may be separated by a low angle normal detachment fault termed the Cretan detachment (Seidel and Theye, 1993; Fassoulas et al., 1994; Jolivet et al., 1994, 1996; Kilias et al., 1994; Seidle et al., 2006). Alternatively, the Cretan detachment may be a thrust based on structural and petrological data (Campbell et al., 2003; Klein et al., 2004; Romano et al., 2004). In this scenario, Oligocene-early Miocene nappes were stacked in a southward direction during a north south compression event (Fassoulas et al., 1994) followed by mid-Miocene rapid exhumation due to displacement along a N-S low angle normal detachment fault (Seidel 2006). This exhumation caused a thinning of the nappes and uplift of the high-pressure/high-temperature metamorphic rocks (Fassoulas et al., 1994).

1.4. Models for Extension in the Aegean

The cause of the transition between compression and extension of the Aegean lithosphere is of interest as it has implications for our understanding of basic plate tectonic processes. Broad scale models have been proposed for this process operated in the Menderes Massif (Seyitoglu and Scott, 1996; Dewey, 1988; McKenzie, 1978; Le Pichon and Angelier, 1979; Royden, 1993; Dewey and Sengor, 1979; Çemen et al., 1999; Zhu et al., 2006). These models include tectonic escape, back-arc spreading along the Hellenic Arc, and orogenic collapse (Figure 1.2).

Tectonic escape and lateral extrusion (Figure 1.2) in the Aegean scenario is driven due to the terminal collision of the Arabian and Eurasia (Şengör and Yilmaz, 1981; Şengör et al., 1985; Çemen et al., 1999, Catlos and Çemen, 2005). In response to this collision the Anatolian block moved eastward along the North and East Anatolia transform faults (Şengör and Yilmaz, 1981; Şengör et al., 1985; Çemen et al., 1999, Catlos and Çemen, 2005). Shortening is believed to have generated a compressional regime with N-trending Tibet-type grabens in which Early Miocene sediments accumulated (Şengör et al., 1985; Şengör, 1987; Seyitoglu and Scott, 1996).

The second proposed model is back-arc spreading along the Hellenic Arc (Figure1.2) (LePichon and Angelier, 1979, 1981; Meulenkamp et al., 1988; Catlos and Çemen, 2005). The Hellenic arc is a curved belt to the north of the present day active trench system, which marks the site of the northeastward direction subduction of the African plate beneath the Eurasian plate (Buick 1991). The Hellenic Arc is a key element for the back arc spreading model, which suggests that the migration of the trench system to the south and southwest gave rise to an extensional regime in the back-arc, Aegean region (Seyitoglu and Scott, 1996). Subduction may have occurred around 26 Ma but the roll-back process probably did not commence immediately because the descending slab had insufficient length and density to overcome resistive forces acting upon it (Seyitoglu and Scott, 1996; Le Pichon and Angelier, 1979; Le Pichom and Angelier, 1981; McKenzie, 1978; Jackson and McKenzie, 1988; Meulenkamp et al., 1988; Spakman et al., 1988). Back-arc spreading has been proposed to have initiated extension in the Aegean region during the Late Miocene (Le Pichon and Angelier, 1979; Le Pichom and Angelier, 1981; Meulenkamp et al., 1988; Seyitoglu and Scott, 1996).

The third model proposed is orogenic collapse (Figure 1.2) when thermally weakened crust lithosphere that experienced Paleogene contraction extends (Dewey 1988; Seyitoglu and Scott, 1996; Catlos and Çemen, 2005). In this scenario subsequent to collision along the Izmir Ankara Shear Zone, the crust collapses and extends (Dewey 1988; Seyitoglu and Scott, 1996; Catlos and Çemen, 2005). Lithospheric extension is located along orogenic belts because thicker continental

crust can contain structural inhomogeneities, and suffer extensional collapse due to body forces resulting form isotactically compensated elevation and sharp elevation gradients (Dewey, 1988). This mechanism would occur when rapid thinning of the shortened thermal boundary conduction layer occurs beneath an orogen and causes rapid uplift, and may be enhanced by subduction rollback into small remnant oceans (Dewey 1988).

Each model proposed; tectonic escape, orogenic collapse, and subduction roll-back (Figure 1.2) possibly contributed to the extensional tectonics individually or as a whole. The timing of initiation of N-S extensional tectonics is the key element for the evaluation of these models (Işik et al., 2003). Latest Oligocene Early Miocene initiation of the N-S extensional tectonics perhaps contradicts the tectonic escape model since their triggering events are younger than this time of initiation (Seyitoglu and Scott, 1996; Işik et al., 2003). Conversely, Oligocene age for the initiation of roll-back process indicates that back arc spreading and orogenic collapse are equally important (Thomson et al., 1998; Okay and Sati, 2000; Işik et al., 2003).

Çemen et al., (2006) proposes a three-stage continuous extension model for the structural development of the terrane. Where the first stage, extension, initiated in the late Oligocene along an extensional simple shear zone (Çemen et al., 2006). It has been suggested that this late Oligocene may have been initiated by an orogenic collapse of thermally weakened crust of the Izmir-Ankara suture zone (Seyitoğlu and Scott, 1996; Çemen et al., 2006). However, extension probably started due to a simple shear-rolling hinge model (Wernicke, 1985; Wernicke et al., 1988; Axen and Bartley, 1997; Çemen et al., 2006). The second stage probably triggered by the subduction roll-back, which started in the early Miocene is the continued extension that produced the Alasehir and Büyük Menderes detachment surfaces (Çemen et al., 2006). The Alaşehir detachment surface dip angle has been controversial, but it is thought that the surface may have formed with a steep dip in the early Miocene and then rotated to its present low angle as the extension continued (Seyitoğlu et al., 2000, 2002; Çemen et al., 2006). The third and final stage proposed in the extension model started in the late Miocene (Catlos and Çemen, 2005; Çemen et

al., 2006). This coincides with the formation of the North Anatolian strike-slip fault zone, produced continuous extension along the Simaz, Alasehir, and Buyuk Menderes detachments, and oblique slip movement along the Southwest Anatolian shear zone (Barka, 1997; Çemen et al., 2006). The structural development of Western Anatolian within the last 5 m.y. was influenced by the North Anatolian Fault zone (Şengör, 1979; Şengör and Yilmaz, 1981; Çemen et al., 2006). This fault zone also accommodated the tectonic escape or lateral extrusion of the Turkey plate westward and together with subduction rollback of the Aegean subduction zone, these mechanisms may have been responsible for the third and final stage of the proposed model (Şengör, 1979; Şengör and Yilmaz, 1981; Çemen et al., 1993, 1999, 2006)

1.5. Outline of the thesis

This thesis is organized into seven chapters. The work present here is part of collaborative efforts, included in two American Geophysical Union conference abstracts and one Microscopy Society of America conference abstract. Chapter 1 is divided into four sections; an introduction into the geologic and tectonic setting of the Aegean and western Turkey, models for extension in the Aegean. Chapter 2 describes the geologic background, lithologies, and ages of the Menderes Massif, and describes the sample collection process and the mineral assemblages of the Salihli and Turgutlu granites. Chapter 3 describes the electron microprobe, ion microprobe, cathodoluminescence, whole rock and chemical analysis methodology used in this thesis. The results from the electron microprobe, ion microprobe, geochemical and cathodoluminescence techniques are presented in Chapters 4, 5, and 6. Geochemical results are described in Chapter 4, which contains major and trace element data. Ages from previous studies and this study of the Salihli and Turgutlu monazites are presented in Chapter 5. Chapter 5 also contains backscattered and secondary electron images of the dated monazites. Chapter 6 contains the cathodoluminescence images of the Salihli and Turgutlu granites. Chapters 7 and 8 wil summarizes the results.

Figure 1.1. Generalized map of the metamorphic belts; Rhodope, Kazdag, Menderes, Cycladic, Crete Massifs and structural elements (Catlos and Çemen, 2002).

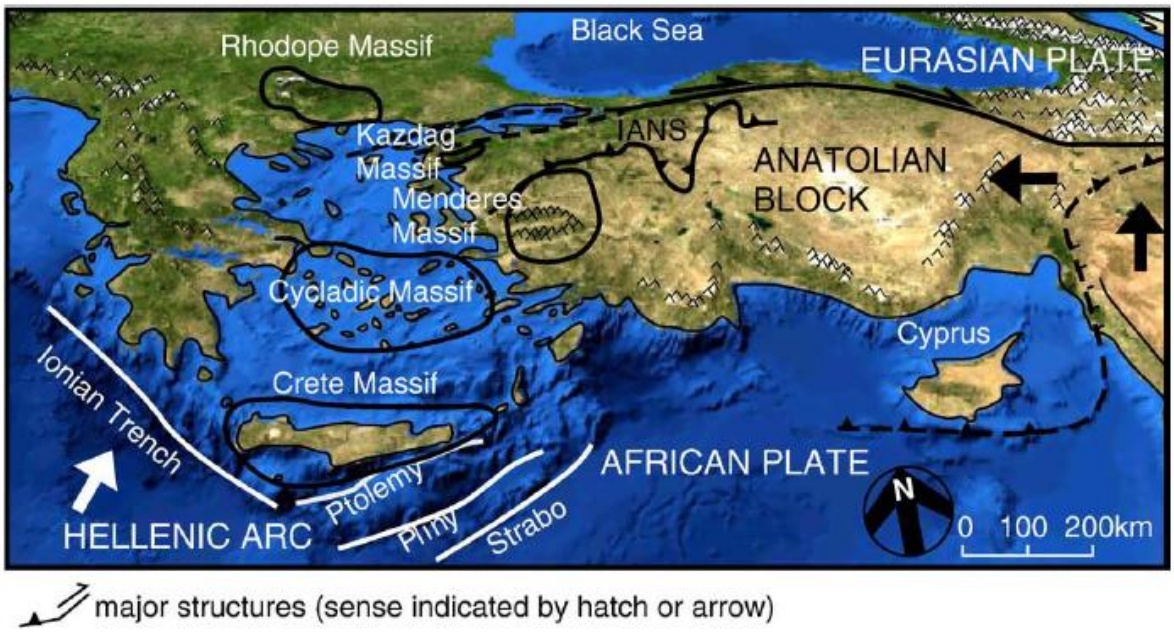

Figure 1.2. NASA World Wind image (10 vertical ezaggeration) of the Aegean region and Turkey showing the location of major structures and massifs (After Catlos et al., 2009). Abbreviations: IANS=Izmir-Ankara Neotethyan Suture.

CHAPTER II

REVIEW OF LITERATURE

2.1. Geologic background of the Menderes Massif

The Menderes Massif consists of metamorphic rocks that are Precambrian to Paleocene in age and is one of the most complex and studied regions in western Turkey (e.g., Schulling, 1962; Akkok, 1981; Satir and Friedrischen, 1986; Sengor et al., 1984; Seyitoglu and Scott, 1991; Hetztel et al., 1995a, 1995b; Oberhansli et al., 1997; Hetzel et al., 1998; Gokten et al., 2001). Recent extension within the Menderes Massif is concentrated along four E-W trending grabens (Glodny and Hetzel, 2007). The two largest of these grabens, the Alasehir graben in the north and the Buyuk Menderes graben (Guney Detachment) in the south (Fig. 2.1), separate the central Menderes Massif from the northern and southern submassifs (Glodny and Hetzel, 2007). The Alasehir detachment accommodates this extension and contains two granitic intrusions the; Turgutlu and Salihli granites (Glodny and Hetzel, 2007). This thesis focuses on these two granites that outcrop along the central Menderes Massif's north-dipping Alasehir detachment.

2.2. Menderes Massif lithologies and ages

In the past the Menders Massif has been described as a core-cover sequence. The cover unit consists of Paleozoic schist and Mesozoic-Cenozoic marble (Sengor and Yilmaz, 1981; Sengor et al., 1984; Satir and Friedrichsen, 1986; Loos and Reischmann, 1999) and the core unit comprised of Cambro-Ordovician augen gneiss (Sengor and Yilmaz, 1981). However this traditional core-cover interpretation has been further interpreted, and the Menderes Massif has

been divided into a series of nappes (Fig. 2.1). From the base to the top, these nappes are termed the: Bayindir, Bozdag, Cine, and Selimiye nappes (Fig. 2.1) (see Ring et al., 1999; Gessner et al., 2001; Isik and Tekeli, 2001; Catlos and Çemen, 2005).

The lower Bayindir nappe contains phyllite, quartzite, marble, and greenschist of inferred Permo-Carboniferous and Mesozoic age (Candan, 1999; Okay, 2000; Ring et al., 2001). The depositional age of the nappe is likely Early Tertiary (Ring et al., 2001). A single Alpine greenschist metamorphism affected the rocks 37 Ma (Ring et al., 2001). The Bozdag nappe consists of amphibolite, eclogite and marble lenses (Ring et al., 2001). The age of the protolith is unknown, but is thought to be Precambrian (Gessner et al., 2000; Ring et al., 2001). A granitoid intruded this nappe 230-240 Ma (Koralay et al., 2000; Ring et al., 2001). The Cine nappe is comprised of deformed orthogneiss and undeformed metagranite (Ring et al., 2001). The Cine nappe was intruded by orthogenesis 540-560 Ma (Hetzel and Reischmann, 1996; Dannat, 1997; Loos and Reischmann, 1999; Ring et al., 2001). The uppermost Selimiye nappe contains metapelite, metabasite, and marble (Ring et al., 2001; Catlos and Çemen, 2005). A metagranite intrudes the lowest part of this nappe that yields a zircon age of 549 Ma (Reischmann, 1999; Ring et al., 2001). The age of the metagranite indicates a Precambrian age for the surrounding metapelite (Ring et al., 2001) and Devonian and Carboniferous ages to the metasediments (Schuiling, 1962; Caglayan et al., 1980; Ring et al., 2001). The Alasehir detachment located along the northern margin of the Menderes Massif (Fig. 2.1) exposes garnet-bearing schists and gneisses of the Bayinidir and Bozdag nappes which are intruded by the Salihli and Turgutlu granites. These two granites are S-type peraluminous (e.g., Isik et al., 2003; see Chp 4).

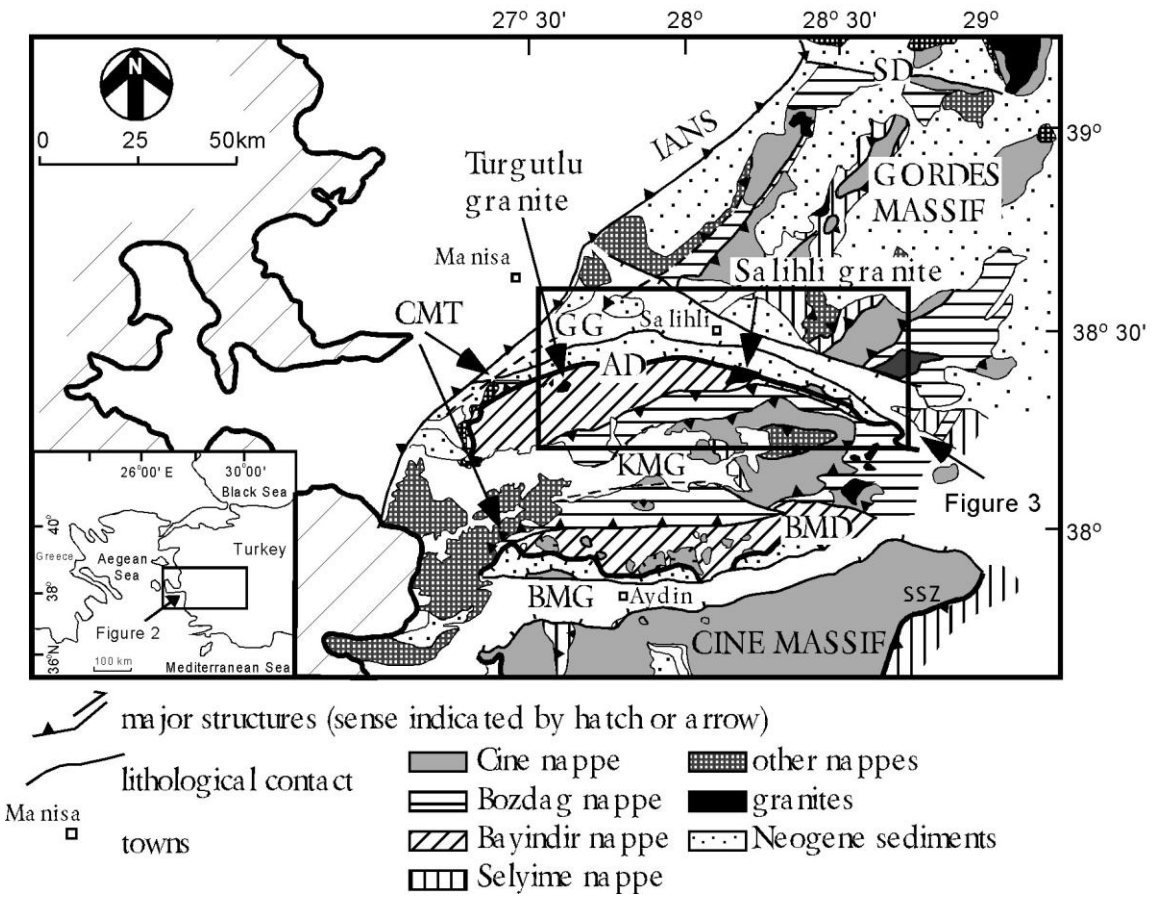

Figure 2.1. Map of the Menderes Massif after Sozbilir (2001) and Gessner et al., (2001). Inset shows the location of the massif in relation to western Turkey. See Figure 4 for Sample locations. Abbreviations: GG=Gediz Graben; AD=Alasehir detachment; KMG=Kuyuk Menderes Graben; BMG=Buyuk Menderes Graben; CMT=Cyclades Menderes Thrust.

Numerous attempts have been made to obtain the metamorphic history of the region (Table 2.1-2.3) (Satir and Freidrichsen, 1986; Reishcmann et al., 1991; Seyitoglu et al., 1992; Seyitoglu and Scott, 1996; Hetzel and Reischmann, 1996; Hetzel et al., 1998; Koralay et al., 1998; Loos and Reischmann, 1999; Lips et al., 2001; Catlos et al., 2002; Isik et al., 2004; Glodny and Hetzel, 2007). The approaches include U-Pb zircon, $^{207}Pb/^{206}Pb$ single zircon isotope, Th-Pb monazite, K-Ar and $^{40}Ar/^{39}Ar$ biotite, muscovite, and amphibole, Rb-Sr whole rock, and mica, apatite and zircon fission track geochronology that are used to determine ages (Table 2.2-2.3) (Satir and Freidrichsen, 1986; Reishcmann et al., 1991; Seyitoglu et al., 1992; Seyitoglu and Scott, 1996; Hetzel and Reischmann, 1996; Hetzel et al., 1998; Koralay et al., 1998; Loos and Reischmann, 1999; Lips et al., 2001; Isik et al., 2004; Catlos and Çemen, 2005; Glodny and Hetzel, 2007). Although the number and timing of different episodes are still being debated, it is now commonly agreed that the Menderes Massif has a complex, polyphase metamorphic history (Bozkurt and Oberhaensli, 2001; Catlos and Çemen, 2005; Çemen, 2006).

Rock of the Cine Massif (Fig 2.1) have been interpreted as Cambro-Ordovician or older based on $^{207}Pb/^{206}Pb$ single zircon and Rb-Sr whole rock (Satir and Friedrichsen, 1986; Hetzel and Reischmann, 1996; Loos and Reishmann, 1999; Catlos and Çemen, 2005). Recently monazite dating within garnets and within the surrounding matrix reveals a two stage metamorphic history of the Cine metamorphic assemblages (Catlos and Çemen, 2005). Monazite ages within the garnets yield ages of 501±18 Ma and the matrix grains have an average age of 42±5 Ma (Catlos and Çemen, 2005).

In the central Menderes Massif extension along the northern Alasehir detachment is thought to have occurred in early to late Miocene time which has been interpreted from $^{40}Ar/^{39}Ar$ amphibole that yielded an age of 19.5±1.4 to 7±1 Ma (Hetzel et al., 1995a, b; Lips et al., 2001). The early Miocene age has recently been discounted as it was affected by excess argon (Catlos and Çemen, 2005; Glodny and Hetzel, 2007). The Salihli and Turgutlu granites were dated using U-Pb monazite

Granites that intrude the Alasehir detachment are separated by an E-W distance of ~ 50 km (Fig. 3), and their petrology and structural setting suggest syntectonic emplacement during extension and low- to mid-greenschist facies conditions during ductile deformation (Hetzel et al., 1995a,b; Isik et al., 2003; Glodny and Hetzel, 2007). $^{40}Ar/^{39}Ar$ ages of 13.1±0.2 Ma from Turgutlu and 12.2±0.4 Ma from Salihli biotite grains indicate extension was already active by the Late Miocene (Hetzel et al., 1995a,b). A reported 19.5±1.4 Ma $^{40}Ar/^{39}Ar$ amphibole age was thought to constrain intrusion of the Salihli granite (Hetzel et al., 1995a), but has been discounted due to the presence of excess argon (Catlos and Çemen, 2005; Glodny and Hetzel, 2007). Recently, 16.1±0.2 Ma and 15.0±0.3 Ma U-Pb ages were reported from aliquots of monazite and allanite grains separated from the granites (Glodny and Hetzel, 2007). Turgutlu allanite grains (Fig. 2.2) in the samples we collected are typically anhedral with diffuse boundaries, filling cracks or crystal faces within other minerals, typically feldspar (see Catlos et al., 2008). In contrast, Salihli allanite grains (Fig. 2.2) are large (mm-sized), appear zoned, can significantly affected by radiation damage (Catlos et al., 2008). These grains often contain inclusions of other minerals, including zircon, apatite, and quartz. The radiation-damage induced cracks in the Salihli allanite are often filled by re-crystallized material, suggesting the presence of a fluid phase. BSE images reported in Catlos et al., (2008) suggest that the precise ages reported for allanite from the Salihli samples should be interpreted with caution. Biotite Ar ages from an unspecified granite located on the Alasehir detachment range from 36.4±2.2 Ma to 16.6±0.3 Ma (Dlaloye and Bingol, 2000), the ~20 m.y. difference likely due to the presence of excess argon. The northern Gordes Massif (2.1) yielded ages from spores and pollen of 20-14 Ma and K-Ar biotite ages from igneous rocks of 16.9±0.5 to 18.4±0.8 Ma (Seyitoglu et al., 1994; Seyitoglu and Scott, 1996). Recently zircons from the Bozdag and Cine nappes were dated using the ion microprobe and yielded ages of 508±92 Ma ($^{207}Pb/^{206}Pb$) (Catlos and Çemen, 2005).

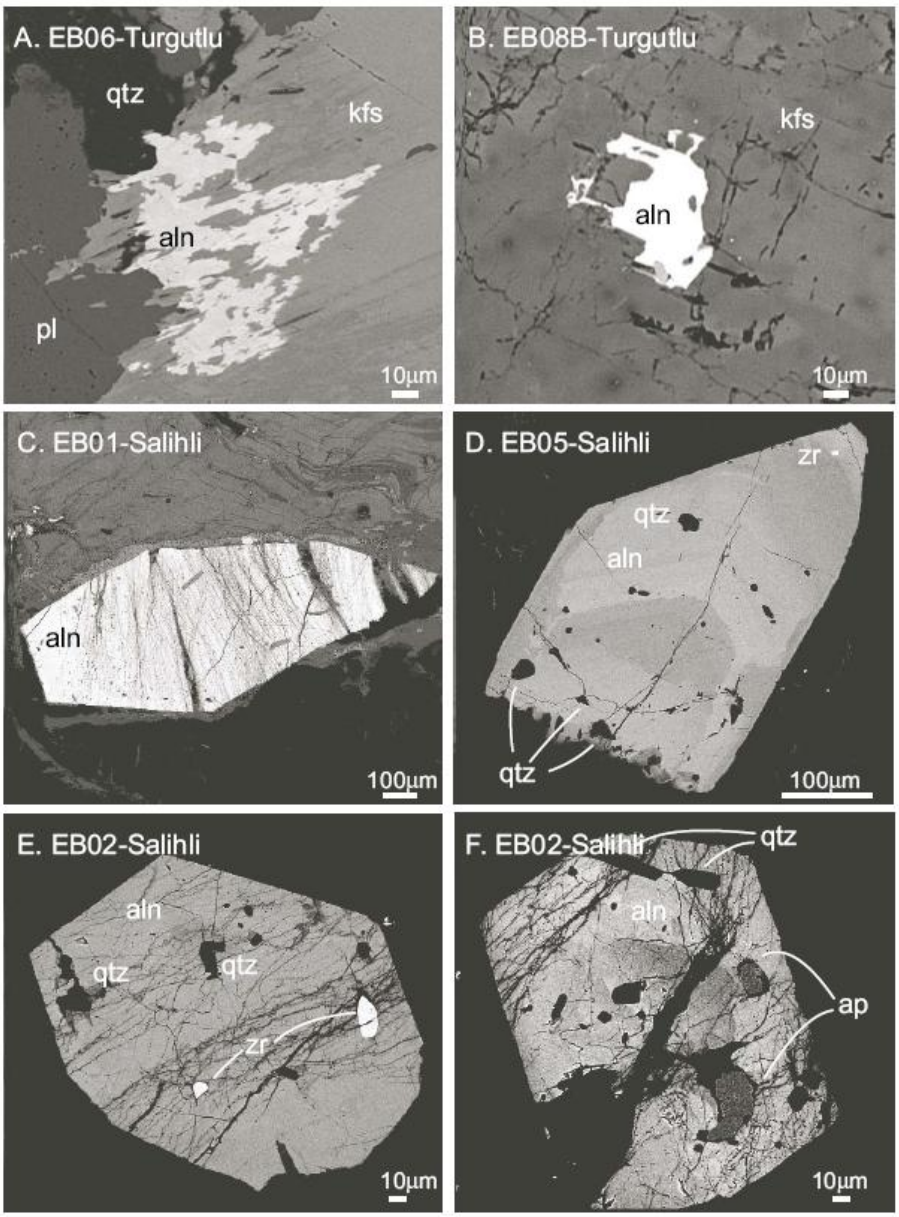

Figure 2.2. Backscattered electron images (BSE) of allanite grains in Turgutlu (A-B) and Salihli samples (C-F). Sample numbers are indicated. Abbreviations after Kretz.

Table 2.1. Ages from the Northern Menderes Massif

Lithology/Locality	Age Ma	Method	Authors
Metagranites and orthogneisses; entire Anatolide belt	2555-1740	207Pb/206Pb Single Zircon evaporation	Reischmann et al., 1991
Granodiorite whole rock	471±9	Rb/Sr	Satir and Freidrichsen, 1986
Granite gneiss	288±5, 229±5	Rb/Sr	Satir and Freidrichsen, 1986
Egrigoz granitoid, Northern Menderes Massif	23-20	40Ar/39Ar biotite isochron age	Reishcmann et al., 1991; Isik et al., 2004
Acid Vocanic domes	18.4±0.8 to 16.3±0.5	K-Ar biotite isochron age	Seyitoglu et al., 1992
Tourmaline Leucogranite dykes	24.2±0.8 to 21.1±1.1	K-Ar muscovite isochron age	Seyitoglu et al., 1992

Table 2.2. Ages from the Central Menderes Massif

Lithology/Locality	Age Ma	Method	Authors
Birgi metagranite	551±1.4	U-Pb zircon dating	Hetzel et al., 1998
Granites; Bozdag nappe	~240-250	207Pb/206Pb Single zircon evaporation	Koralay et al., 1998
Salihli granodiorite	19.5±1.4	40Ar/39Ar Amphibole isochron age	Hetzel et al., 1995
Alasehir graben	19-20 to 14-15	Sporomorph	Seyitoglu and Scott, 1996
Turgutlu and Salihli granodiorites	13.1±0.2 to 12.2±0.4	40Ar/39Ar Biotite isochron age	Hetzel et al., 1995
Kuzey detachment	7±1	40Ar/39Ar Muscovite isochron age	Lips et al., 2001
Kuzey detachment	4.5±1.0	Th-Pb monazite	Catlos and Çemen, 2005
Turgutlu and Salihli granodiorites	16.1±0.2, 15.0±0.3	U-Pb monazite dating, U-Pb allanite dating	Glodny and Hetzel, 2007

Table 2.3. Ages from the Southern Menderes Massif

Lithology/Locality	Age	Method	Reference
Metaranites and orthogneisses	659±7; 563±3-512±8	207/PB/206Pb Single zircon evaporation, U-Pb dating	Loos and Reischmann, 1999
Metagranite in Kayabuku shear zone	546.2±1.2	207Pb/206Pb Single Zircon evaporation	Hetzel and Reischmann, 1996
Granite gneiss	502 ±10	Rb/Sr	Satir and Freidrichsen, 1986
Granite gneiss	61±1	Rb/Sr	Satir and Freidrichsen, 1986
Granite gneiss	48±1	Rb/Sr	Satir and Freidrichsen, 1986
Augen gneiss, schist	43-37	40Ar/39Ar Muscovite isochron age	Hetzel and Reischmann, 1996
Orthogneiss, Guney detachment	36±2	40Ar/39Ar Muscovite isochron age	Lips et al., 2001
Cine nappe	501±Ma; 42±5 Ma	Th-Pb monazite	Catlos and Çemen, 2005

2.3. Sample collection and mineral assemblages

Samples EB01, EB02, EB03, EB05 and CC20 were collected from the Salihli granite and samples EB06, EB08A, EB08B, EB09A, EB09B were collected from the Turgutlu granite (Fig 2.3). Overall the Salihli samples we analyzed contain Qtz + Pl + Kfs + Bt + Ap + Zrn ± Ilm ± Chl ± Ms ± Px ± Aln ± Ep ± Xtm ± Mnz ± Th ± Ttn ± Rt ± Hem ± Cld (Table 2.4). Only Salihli sample CC20 contains monazite. Chloritoid was found in Salihli samples CC20 and EB05. Turgutlu samples in general have a similar mineral assemblage of Qtz + Pl + Kfs + Bt + Ms + Ap + Mnz + Zrn ± Chl + Ilm + Xtm ± Aln ± Rt ± Ttn ± ± Sil ± Hem. However, the Turgutlu samples do not contain pyroxene, epidote, thorite or chloritoid and fibrous sillimanite was found in Turgutlu sample EB09B. All granites analyzed are S-type, subalkalic, and permaluminous.

The next chapter describes the dating technique we applied to date monazite in these rocks, the imaging used to facilitate the interpretation of the results, including the conditions and instrumentation that were used to obtain the CL, BSE, and secondary electron (SE) images are also described. Whole rock fusion ICP and trace element ICP/MS analyses were obtained from granites in this study from Activation Laboratories; compositions are also reported.

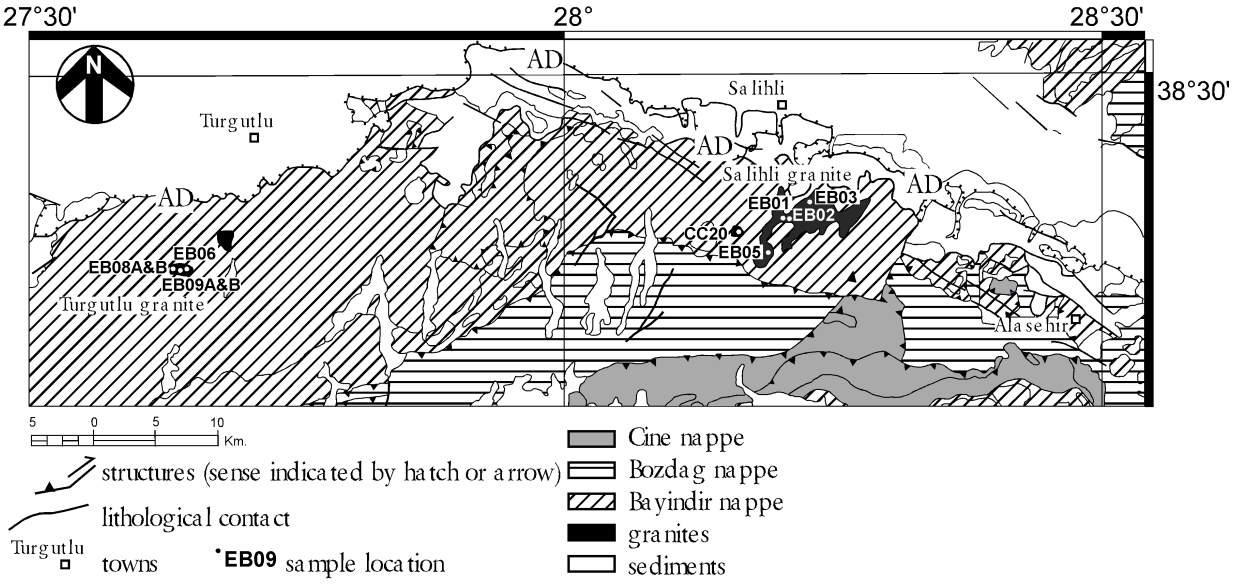

Figure 2.3. Geologic and sample location map modified after Konak (2002), Seyitoglu et al., (2002), Isik et al., (2003), and our observations. Abbreviations: AD=Alasehir detachment, EB and CC samples were collected from the granites.

Table 2.4. Mineral assemblages of the Salihli and Turgutlu granitic samples

Sample	Mineral Assemblage
	Salihli granitic samples
EB01	Ilm + Chl + Ms + Px + Aln + Ep + Ttn + Hem
EB02	Ilm + Chl + Ms + Px + Aln + Ep + Ttn
EB03	Ilm + Chl + Ms + Px + Aln + Ep + Ttn
EB05	Chl + Aln + Ep + Ttn + Cld
CC20	Ilm + Ms + Cld + Xtm + Mnz + Rt + Th
	Turgutlu granitic samples
EB06	Ilm + Ms + Aln + Xtm + Mnz + Rt + Htn
EB08A	Ilm + Chl + Ms + Xtm + Mnz + Rt
EB08B	Ilm + Chl + Ms + Aln + Mnz + Rt
EB09A	Ilm + Chl + Ms + Xtm + Mnz + Ttn + Hem
EB09B	Ilm + Ms + Sil + Xtm + Mnz + Hem

(a) (mineral abbreviations after Kretz, 1983).

CHAPTER III

METHODOLOGY

3.1. Introduction

This thesis reports Th-Pb ion microprobe monazite $(CeLaTh)PO_4$ ages, bulk rock geochemical data and cathodoluminescence (CL) images from the Salihli and Turgutlu granites. To better understand the chronology of extension monazite ages from granites exposed along detachment faults are frequently used (Murphy and Harrison, 1999; Catlos et al., 2004; Gilotti and McClelland, 2005; Catlos et al., 2008). CL has been used to document mineral zoning, deformation and fluid alteration in a variety of lithologies (Marshall, 1988; Ramseyer et al., 1992; Sorensen et al., 2006; Pidgeon et al., 2007; Catlos et al., 2008) and as a precursor to understand compositional zoning in zircon and as a guide for the dating of specific zones within minerals (Aleinikoff et al., 2002; Liati et al., 2002; Hoskin, 2005; Catlos et al., 2008) CL investigations have been stated to be necessary in order to obtain valid information about the origin of granites (Ramseyer et al., 1992).

3.2. Monazite paragenesis

Monazite is frequently used to date igneous and metamorphic rocks (Catlos et al., 2002). The mineral preferentially incorporates ThO_2 (e.g., Overstreet, 1967), sustains little radiation damage (e.g., Meldrum et al., 1998), and remains relatively impervious to Pb loss at high crustal temperatures (e.g., Smith and Giletti, 1997). Monazite appears in pelites near the garnet isograd (e.g., Smith and Garreiro, 1990; Harrison et al., 1997) and inclusions in garnet are armored

against daughter product loss (e.g., Montel et al., 2000). Monazite ages can be affected by fluid-mediated dissolution-reprecipitation reactions that occur along a retrograde path (Seydoux-Guillaume et al., 2002; Catlos et al., 2008). In granites, monazite has been reported to form at low Ca activity, whereas allanites, a radiogenic rare-earth epidote-group mineral, precipitates at higher Ca levels (Lee and Dodge, 1964; Cuney and Friedrich, 1987; Broska and Siman, 1998; Broska et al., 2000).

Monazite contains <1 to 30 wt% of ThO_2 (Overstreet, 1967), although 4-12 wt% is a more common range (Deer et al., 1992; Stern and Sanborn, 1998) and preferentially incorporates light rare earth elements (REE) over heavy REE (Overstreet, 1967; Rappa and Watson, 1986; Montel, 1993; Pan, 1997; Finger et al., 1998; Zhu and O'Nions, 1999a,b; Boska et al., 2000; Catlos et al., 2002). Th enters the monazite structure through coupled substitutions $Th^{4+} + Si^{4+} \rightarrow REE^{3+} + P^{5+}$, $Th^{4+} + Ca^{2+} \rightarrow 2REE^{3+}$ and $Th^{4+} + 2Si^{4+} \rightarrow Ca^{2+} + 2P^{5+}$ (e.g., Burt, 1989). Monazite grains are typically zoned, and their compositions are used to explain changing environmental conditions during mineral growth (see Zhu and O'Nions, 1999b).

Bulk rock composition and pressure-temperature (P-T) conditions vary the formation of monazite (Wing et al., 1999; Catlos et al., 2002). Allanite, apatite, REE and Th oxides are precursor minerals in prograde metamorphic rocks (e.g., Smith and Barreiro, 1990; Kingsbury et al., 1993; Catlos et al., 2002). Along the retrograde path, monazite has been identified as a replacement after allanite (Pan, 1997; Finger et al., 1998) and after preexisting monazite (e.g., Ayers et al., 1999; Townsend et al., 2000). Petrographic and thermobarometric studies suggest that monazite appears in metapelites during prograde metamorphism at ~500-600 ºC via allanite breakdown reactions (e.g., Smith and Barreiro, 1990; Ayers et al., 1999; Rubatto et al., 2001; Catlos et al., 2002).

3.3. Electron Microprobe Analysis

Thin sections were first examined using an optical microscope to determine the rock's mineral assemblages. However, monazites are detected using backscattered electrons (BSE) using an electron microprobe. Monazites chosen for geochronology were identified using qualitative Energy Dispersive Spectrometer (EDS) measurements and imaged in detail using (BSE) (see also Scherrer et al., 2000; Catlos et al., 2002). Monazites appear bright which is due to their chemical composition, which includes radiogenic and rare earth elements (REE) (Catlos et al., 2002). Standard operating conditions for the electron microprobe are: accelerating potential of 15 kV and a probe current of ~30 nA (Catlos et al., 2002). The grains were X-ray element mapped in Y, Th, Ca, Si, and U using Wavelength Dispersive Spectrometers (WDS). For this application, the probe current was increased 10 fold for best results.

3.4. Ion Microprobe Analysis

The high-sensitivity/high-resolution ion microprobe has been used successfully for over ten years to date zircon by the U-Pb method (Compston et al., 1984; Harrison et al., 2005). A similar methodology permits precise (±2%) Th-Pb dating of monazites using an ion microprobe (Harrison et al., 2005). An in situ ion microprobe method for dating monazite is clearly warranted for rocks that experienced a complicated metamorphic history, as the monazite grain itself and its textural context is preserved (Catlos et al., 2002; Catlos and Çemen 2005).

3.4.1. Sample preparation

Ion microprobe samples were prepared in the lab after electron microprobe analyses were performed. The conductive carbon coat was removed from each thin section by abrasion. The portions containing monazite used for geochronology were cut out using a high-precision diamond saw. The fragments were cleaned and mounted with a prepolished block of age standards (monazite 544, Force, 1997) on dual-sided tape. A 1-inch metallic ring was coated

with release agent and placed around the thin section chips and age standards. Epoxy was then poured into a ring with a depth of ~10 mm. After the epoxy has hardened, the rings are broken away from the tape and the epoxy plugs are removed. The back of the plug is then cut to a desired thickness of ~5 mm. A reflected light image mosaic of the mount is then acquired using an optical microscope with a digital camera to facilitate location of monazite grains during ion microprobe analysis. The finished mount is then cleaned and coated with gold.

3.4.2. Th-Pb dating method

During ion microprobe analyses, an oxygen (O^-) primary beam with a 30-μm-diameter (2 to 13 nA) sputters positive ions (Th+, Pb+) from the surface of the monazite (e.g., Catlos et al., 2002; Harrison et al., 2005). A mass resolving power of ~5000 is sufficient to separate molecular interferences and distinguish between Pb isotopes in the 204-208 mass range (Harrison et al., 1999). Typically, a 50 eV energy window with a 10-15 eV offset for $^{232}Th^+$ is used (Catlos et al., 2002). The magnet is stepped through six different mass species: $^{204}Pb^+$, $^{207}Pb^+$, $^{208}Pb^+$, $^{232}Th^+$, ThO_2^+, U^+ (Catlos et al., 2002). This cycle was repeated 15 times to correct for variations in beam stability, and average values were used to calculate ages (Catlos et al., 2002).

Details of the Th-Pb method is outlined by Harrison et al., (1995) and Catlos et al., (2002). Briefly summarized: determination of the Pb/Th sensitivity factor is accomplished by dividing the measured $^{208}Pb^+/^{232}Th^+$ of a standard monazite at a reference ThO_2^+/Th^+ value by the standard's known daughter to parent ratio. The age of an unknown, measured under identical operating conditions, is determined by applying this sensitivity factor to the measured $^{208}Pb^+/^{232}Th^+$ vs. $^{208}Pb^+/Th^+$ measured from a monazite standard. Limiting factors on the precision of ion microprobe age determinations include: the reproducibility of the calibration line, high amounts of common Pb, and if values of the unknown monazite not lie within range defined by the standard. All analyses in this study utilize monazite standard 554 a peraluminous granodiorite

from the Santa Catalina Mountains in Arizona (Force, 1997). In our study, Th-Pb isotope dilution analysis of monazite-554 has produced radiogenic ^{208}Pb yields >98% and an average age of 45.3±1.4 Ma (±1σ) (Catlos et al., 2002). This age is consistent with the 45±1 Ma Th-Pb age determined by ion microprobe analysis (Harrison et al., 1999; Catlos et al., 2002). Because we were limited by the size and irregular shape of the grain (typically <60-μm diameter) and diameter of the primary beam (typically ~20-30 μm) many monazites grains reported in this thesis were typically analyzed with one spot (Catlos et al., 2002).

3.5. Cathodoluminescence Imaging

To better understand the ion microprobe ages that were obtained the rocks were imaged using the CL technique with a Premier American Technologies luminoscope model ELM-3R located in the Smithsonian Institution's Department of Mineral Sciences at the National Museum of Natural History (Sorensen et al., 2006). The electron beam was run with a < 100 torr between 20 kV and 0.5 mA vacuum. A microscope is attached to the luminoscope and an Olympus Opelco MagnaFire Model S9986 camera. Three digital grayscale images with a 1300x 1030 pixel monochrome CCD is captured through a rotating Red-Blue-Green (R-B-G) color filter wheel. A final image is produced using complementing MagnaFire software by combining the three R-B-G images. Exposure times varied depending on sample and ranges from >1-5 minutes.

3.6. Whole rock and chemical analysis

Whole rock fusion Inductively Coupled Plasma (ICP) and Inductively Coupled Plasma Mass Spectrometry (ICP/MS) analysis were obtained from granites from Activation Laboratories. ICP is a technique capable of measuring 40 to 70+ elements in a variety of materials and ICP/MS provides multi-element and isotopic data. Geochemical data from the Salihli and Turgutlu granites have been analyzed both in this study and by others (Delaloye and Bingol, 2000; Glodny and Hetzel, 2007; Catlos et al., 2008).

CHAPTER IV

GEOCHEMICAL RESULTS

4.1. Introduction

Geochemical data from the Salihli and Turgutlu granites collected from the Alasehir detachment are reported in Tables 4.1-4.4. See Figure 2.3 for sample locations and Table 2.4 for specific mineral assemblages. The data was plotted on a series of diagrams in order to discriminate between magma sources and gain insight into their tectonic evolution and relationship to each other (Figures 4.1-4.2). The same granites were also geochemically analyzed by Delaloye and Bingöl (2000) and Glodny and Hetzel (2007). We include their data with our analyses to make interpretations about the possible tectonic history and source of these rocks.

4.2. Major elements

All granites analyzed in the study are S-type, peraluminous, and subalkalic (Figure 4.1.A and B and Figure 4.2). S-type granites form from a sedimentary source and contain higher amounts of SiO_2 (Chappell and White, 1983; Frost et al., 2001). In a total alkalis ($Na_2O + K_2O$) vs silica (SiO_2) diagram (de LaRoche, 1980), the majority of Salihli samples are granodiorites (Figure 4.1), with the exception of CC20 which we consider a leucogranite. Geochemically, Turgutlu rocks can be considered granite, granodiorite, monzogranite, or seyenogranite (Figure 4.1). For simplification in this thesis, all samples are referred to as granites. The majority of the Turgutlu granites are ferroan with the exception of one which plots in the magnesia field (Frost et al., 2001). All Salihli granites are magnesium rich (Figure 4.2). The Turgutlu granites are alkali-

calcic or calc-alkalic, whereas all Salihli granites are dominantly calcic (Figure 4.2) (Frost et al., 2001). The Salihli and Turgutlu samples are peraluminous, which indicates that the portion of Al_2O_3 exceeds that of $Na_2O + K_2O$.

The geochemical data of the Alasehir detachment granites show that these samples range in SiO_2 from 60.12 wt% (Delaloye and Bingöl, 2000) to 77.16 wt% (Tables 4.1-4.4; Figure 4.2). Most Turgutlu samples that were analyzed have higher SiO_2 contents than Salihli rocks (69.0±3.3 wt% vs 72.0±3.3 wt%). While the granites' SiO_2 content increases the CaO, MgO, Fe_2O_3(total), MnO, Al_2O_3, TiO_2 and P_2O_5 wt% decrease, and their Na_2O and K_2O wt% are scattered, but generally increase **(**Figure 4.2). These trends are consistent fractional crystallization, with some alkali fluid mobility.

Linear regression techniques were applied to the major element compositional data from both granites to differentiate if the Turgutlu and Salihli granites outline a single liquid line of descent within $\pm 1\sigma$ in SiO_2 verses the other major elements. Table 4.5 reports the results of these linear regressions. In general, the granites show statistically different slopes and intercepts in SiO_2 versus Na_2O, Fe_2O_3, MnO, and P_2O_5.

4.3. Trace Elements

To better understand the evolution of granites in western Turkey discriminations diagrams are often used (e.g. Erdogan and Gungor, 2004; Ibbeyli et al., 2004; Altunkaynak, 2007; Yilmaz et al., 2007). These diagrams rely on the assumption that the trace element geochemistry of the rocks have not been significantly affected by alteration (e.g. Pearce et al., 1984; Twist and Harmer, 1987). The whole rock geochemical composition of these rocks are influenced by many factors, including source rock characteristics (composition, mineralogy), tectonic setting, depth of emplacement, and degree of alteration. Interpretations of tectonic setting from geochemical data from granites can be open to dispute (Twist and Harmer, 1987; Arculus, 1987; Forster et al., 1997).

Most Salihli and Turgutlu granites are characteristics of a volcanic arc setting (Figure 4.3.A and B) (also Delaloye and Bingöl, 2000) as seen with a discrimination diagram of Rb versus Yb+Nb (Pearce et al., 1984; Forster et al., 1997). However, two of the analyses from the Turgutlu granites plot closer to the syn-collisional field (see Figure 4.3.A). Volcanic arc rocks may plot in this region if politic source rocks were melted (see Forster et al., 1997). In an Rb versus Yb+Ta diagram, the Turgutlu granites plot within the syn-collisional field (Figure 4.3.B). Any ambiguities in identifying a source using discrimination diagrams with this data may be the results of the Menderes Massif's complex, polyphase tectonic history, and may be common in orogenic system that are followed by extension (e.g., Forster et al., 1997).

Menderes Massif granites are similar in their degree of enrichment of geochemically important high field strength (HFSE) and rare earth elements (REE) (Figure 4.4). A flatter REE profile is seen in the Turgutlu samples EB09A and EB09B ($(La/Lu)_{Nn}$ is 2±1 vs 15±4) and average 10 times less ∑REE total (28±6 ppm REE vs 298±60 ppm) (Figure 4.4). This may be the results of higher degrees of metamorphism (e.g. Bea and Montero, 1999). The majority of the granites have negative Eu anomalies, whereas EB09 samples have positive Eu anomalies. Eu anomalies are controlled by feldspars, particularly in a felsic melt (Rollinson, 1993). A negative anomaly is caused by removal of feldspar from a melt by crystal fractionation, whereas the presence of hornblende, sphene, clinopyroxene, orthopyroxene and garnet can contribute to a positive Eu anomaly (Rollinson, 1993). Sample CC20 also differs from the general HFSE and REE patterns than the other granites. Samples EB09 and CC20 contain higher amounts of SiO_2 (by 5-9 wt%) and less Fe_2O_3 (by 2-3%), MnO (0.4-0.7 wt%) and MgO (by 0.5-1.5 wt%) (Figures 4.5-4.8). Samples from the EB09 locality differ in that it has been metamorphosed, where as CC20 is a leucogranite.

Linear regression techniques were applied to the trace elements versus the major element compositional to decipher if the granites followed a single line of descent (Figures 4.5-4.8 and Table 4.5). In general these granites show a decrease in Zr and Ce with increasing SiO_2 content

(Figure 4.6 and 4.8), consistent with fractional crystallization of minerals that contain these elements. Turgutlu granites show a decrease in Y with increasing SiO_2 (Figure 4.8), and Salihli samples contain relatively constant amounts of Y (18±3 ppm). Turgutlu granites generally show a decrease in the heavier REE with an increase in SiO_2 whereas Salihli granites contain 67±3 ppm. These granites decrease in V, Sm, Sr, Nd, Sc, La, Eu, Pr, Co, Ti, Gd, and Th with increasing SiO_2. Tugutlu granites show a decrease in Rb, Er, Dy, Ba, and Ho with an increase in SiO_2 while Salihli granites show relatively constant amounts of Rb, Er, Dy, Ba, and Ho. Salihli granites show a decrease in Hf, Ga, and Nb with an increase in SiO_2 while the Turgutlu granites show relatively constant amounts of Hf, Ga, and Nb. Tugutlu granites increase in Cs, Ta, and Be with increasing SiO_2 and Salihli granites contain relatively constant amounts of Cs, Ta, and Be.

Turgutlu and Salihli granites increase in La, Th, Ce, Sc, Sm, Ti, Eu, Er, Nd, V, Sr, Gd, Pr, Co, Zr, and Hf with increasing Fe_2O_3. Both granites contain a relatively constant amount of Rb and both granites show a decrease in Pb with an increase in Fe_2O_3. The Salihli granites have relatively constant amounts of Ba Ta, Y, Dy, Be, Sn, and Cs, while Turgutlu granites show relatively constant amounts of U, and Nb. Salihli granites have an increase in Nb, and Ga with increasing Fe_2O_3 while the Turgutlu granites show an increase in Yb, Lu, Y, Ba, Tm, Dy, and Ho. Turgutlu granites display a decrease in Ta, Be, Ga, Sn, and Cs and Salihli granites show a decrease in Yb, Tm, Er, Lu, U, and Ho with increasing Fe_2O_3.

4.4. Conclusions

Geochemical data has been used to study and interpret the Salihli and Turgutlu granites. Both granites are peraluminous- S-type rocks. The majority of the Salihli samples are granodiorites whereas the majority of Turgutlu samples are granites. The Salihli granodiorites are magnesian whereare the Turgutlu granites plot in the ferroan field with the exception of one (CC20) which is magnesian. Turgutlu granites are alkali-calcic and calcic-alkalic, whereas the Salihli samples are clacic. All samples can be considered volcanic-arc granites.

Based on the geochemistry, questions whether Salihli and Turgutlu granites were generated from the same source and experienced the same tectonic history arise. Both granites are classified as volcanic arc granites, and are enriched in Rb, Th, U, Ta, Nb, Hf, and Y and depleted in Ba, Sr, P, Zr, and Ti (Figure 4.5) (Brown et al., 1984).

The Salihli granodiorites are magnesian and calcic which indicates that these granites are enriched in MgO and that their weight percent of SiO_2 is greater than 61 percent (Frost et al., 2001). Turgutlu granites are ferroan, alkali-calcic and calcic-alkalic. Ferroan granites are enriched in iron, calc-alkalic rocks have weight percents of silica between 56-61 percent, and alkali-calcic granites have silica weight percents between 51-55 percent (Frost et al., 2001). The whole-rock geochemical data suggests that the Salihli and Turgutlu granites may have been generated under a compressional régime due to north dipping subduction of the Eastern Mediterranean floor along the Hellenic trench. The major and trace element geochemistry show differences between the two granites; which could indicate that the Salihli and Turgultu granites do in fact have different sources.

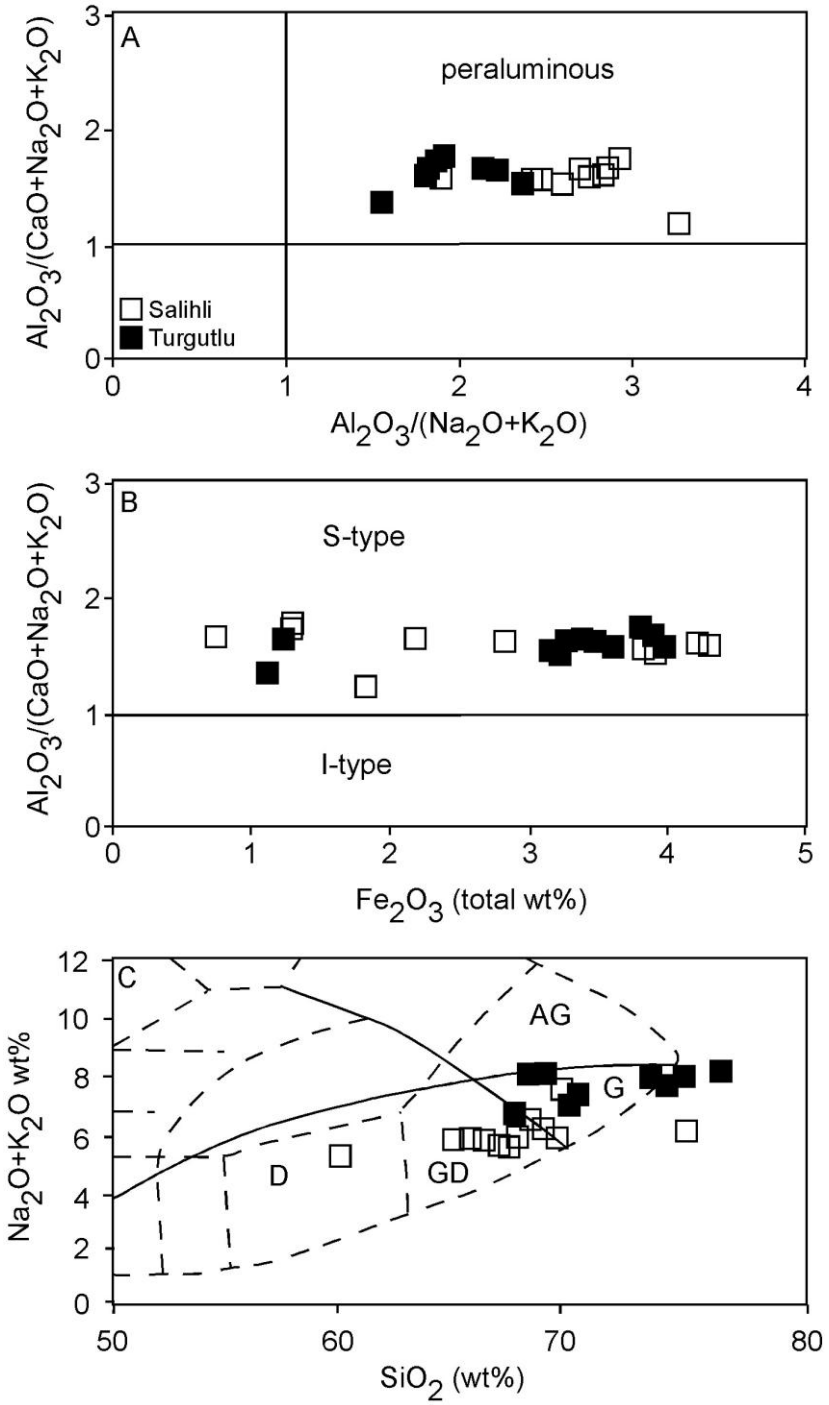

Figure 4.1. (A) Shand's index for granitic protolith (Maniar and Piccoli, 1989). The data plotted are from the Turgutlu and Salihli samples (our data, Glodny and Hetzel, 2007 Salihli and Turgutlu samples) and from an unspecified Alasehir detachment sample (Delaloye and Bingöl, 2000 unspecified Alasehir samples). (B) $Al_2O_3/(CaO+Na_2O+K_2O)$ vs. Fe_2O_3 total after Marc (1992). (C) The chemical classification and nomenclature of plutonic rocks using the total alkalis versus silica (TAS) diagram of Cox et al. (1989) and Wilson (1989). The solid line divides the alkali from subalkalic rocks. Abbreviations: AG=Alkali granite, G=Granite, GD=Granodiorite, D=Diorite.

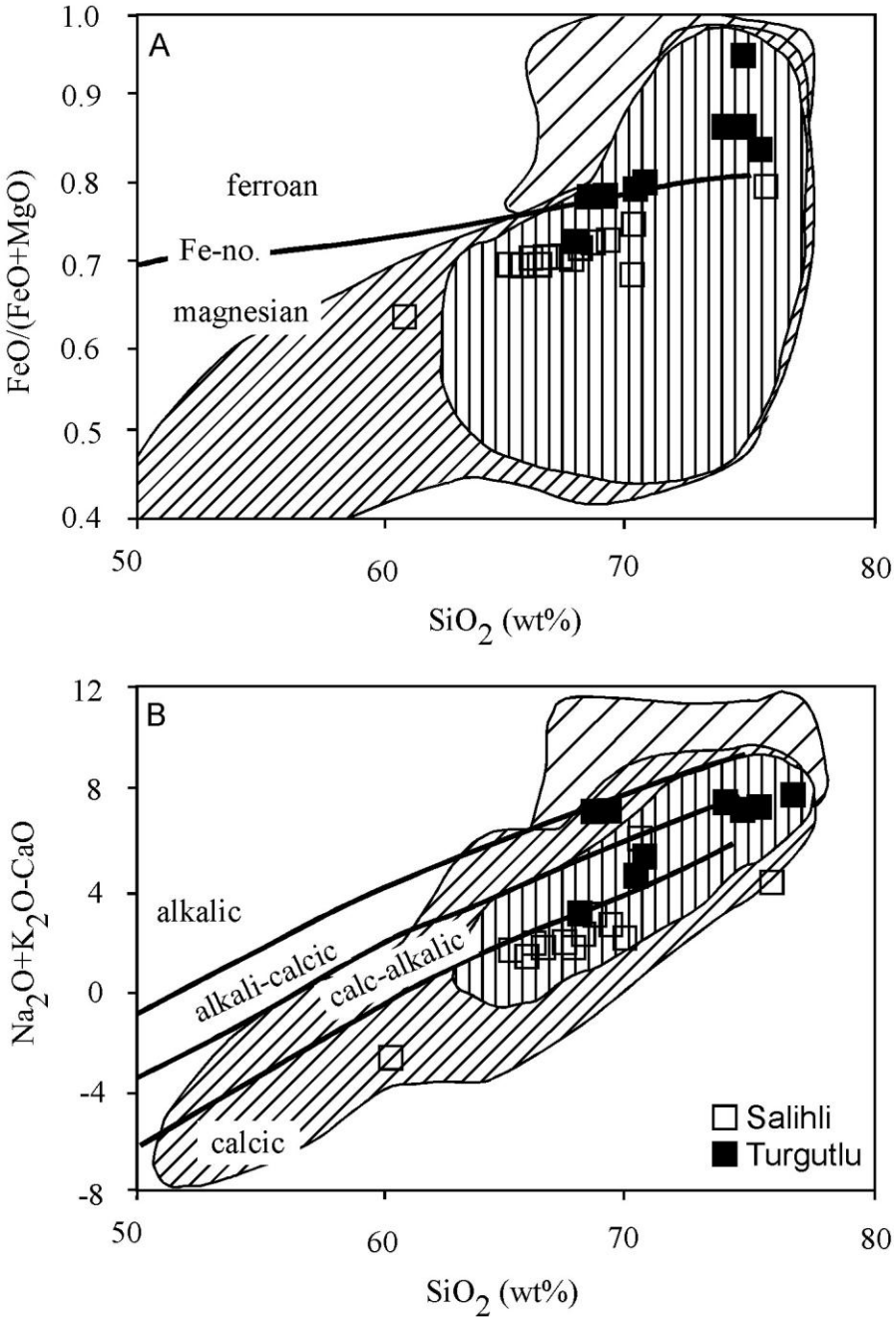

Figure 4.2. (A) FeO/(FeO+MgO) vs. SiO_2 (wt%) (Frost et al., 2001) shows the composition range for rocks from the Salihli and Turgutlu granites (our data, Glodny and Hetzel, 2007) and from an unspecified Alasehir detachment sample (Delaloye and Bingöl, 2000). (B) Na_2O+K_2O-CaO vs. SiO_2 (wt%).

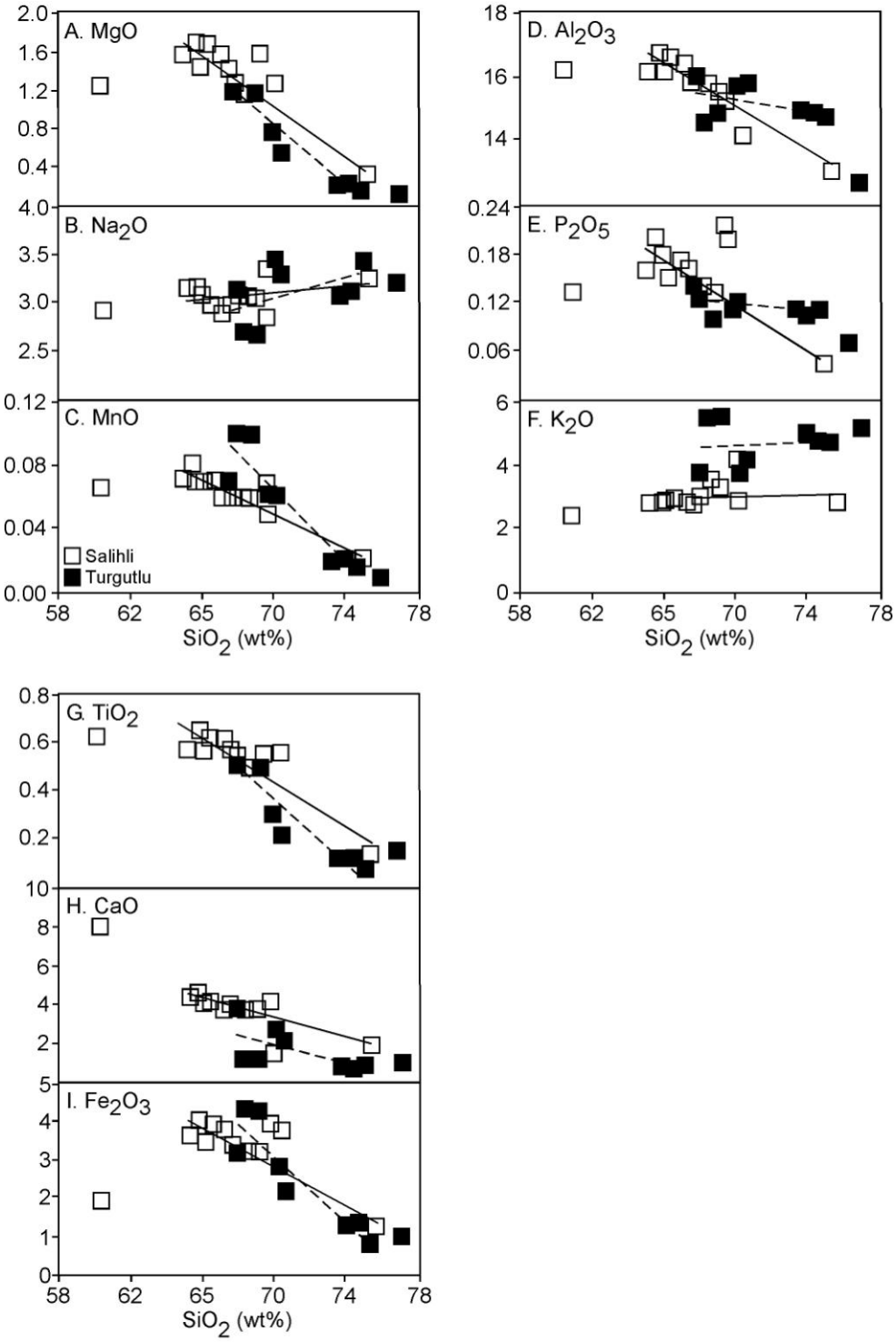

Figure 4.3. Major-element (wt%) versus SiO_2 (wt%) variation diagrams for Salihli and Turgutlu granites. Best-fit linear regressions are indicated. Table 4.5 contains the slope and intercept data. Delaloye and Bingöl, 2000, analyses are from two unspecified granites from the Alasehir Detachment are plotted. Glodny and Hetzel, 2007, analyses are from the Salihli and Turgutlu granite outcrops.

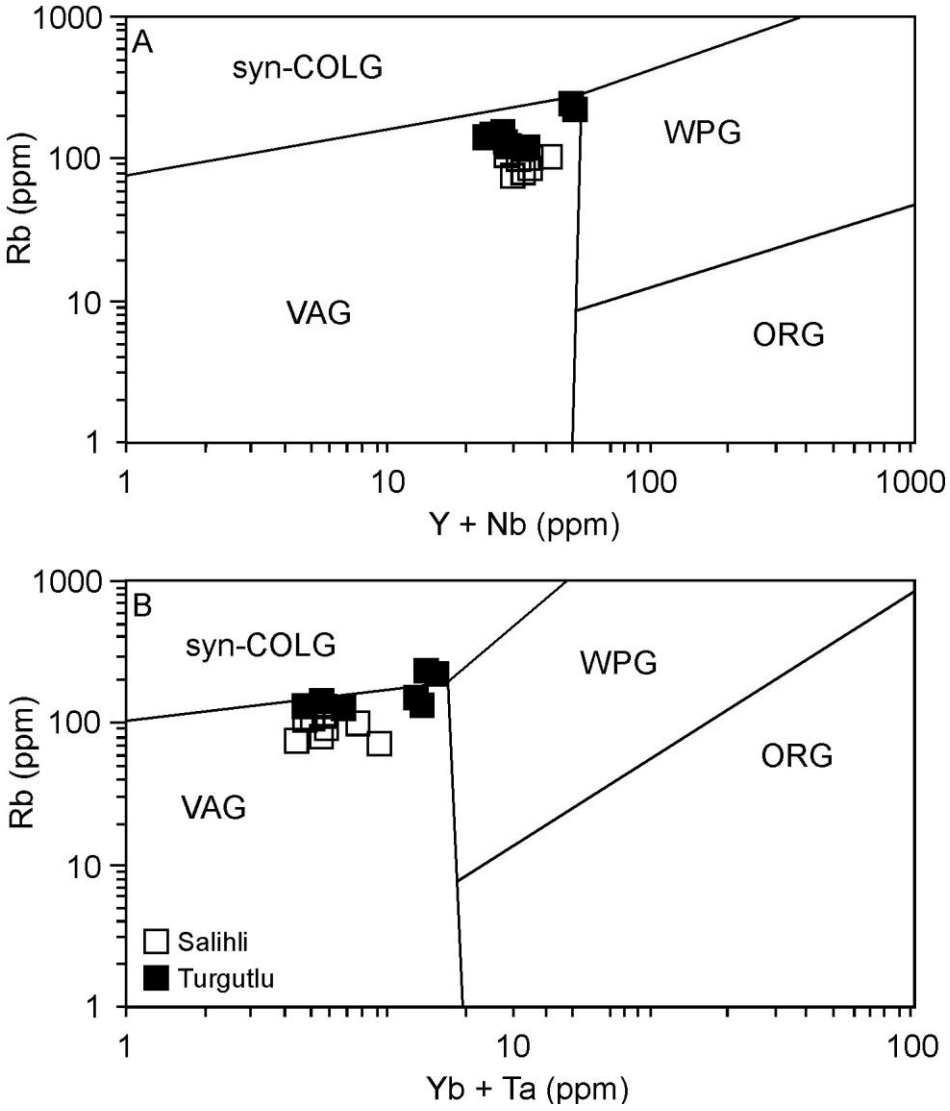

Figure 4.4. (A) Y-Nb (ppm) vs. Rb (ppm) discrimination diagram for granites (after Pearce et al., 1984) showing the fields of syn-collisional granites (syn-COLG), with-in plate granites (WPG), volcanic-arc granites (VAG), and oceanic ridge granites (ORG). (B) Yb-Ta (ppm) vs. Rb (ppm) discrimination diagram for granites (after Pearce et al., 1984). Fields are the same as in (A).

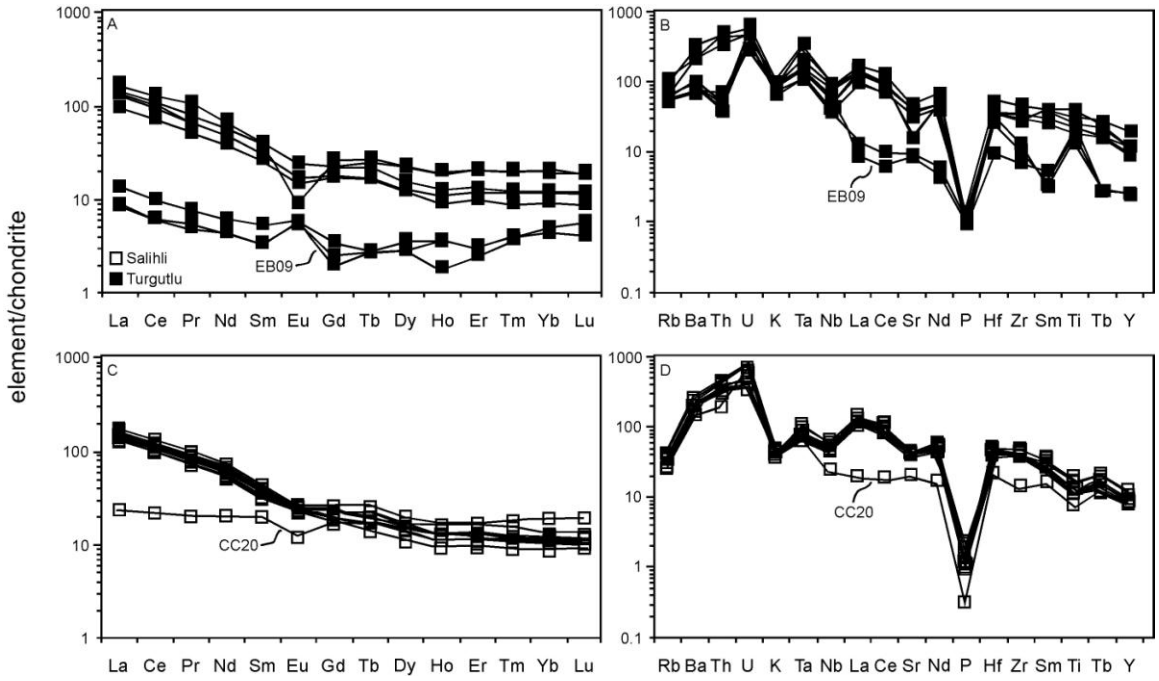

Figure 4.5. (A and C) REE Chondrite-normalized graphs (McDonough and Sun, 1995) and (B and D) High field strength element (HFSE) patterns for the Salihli and Tugutlu granites.

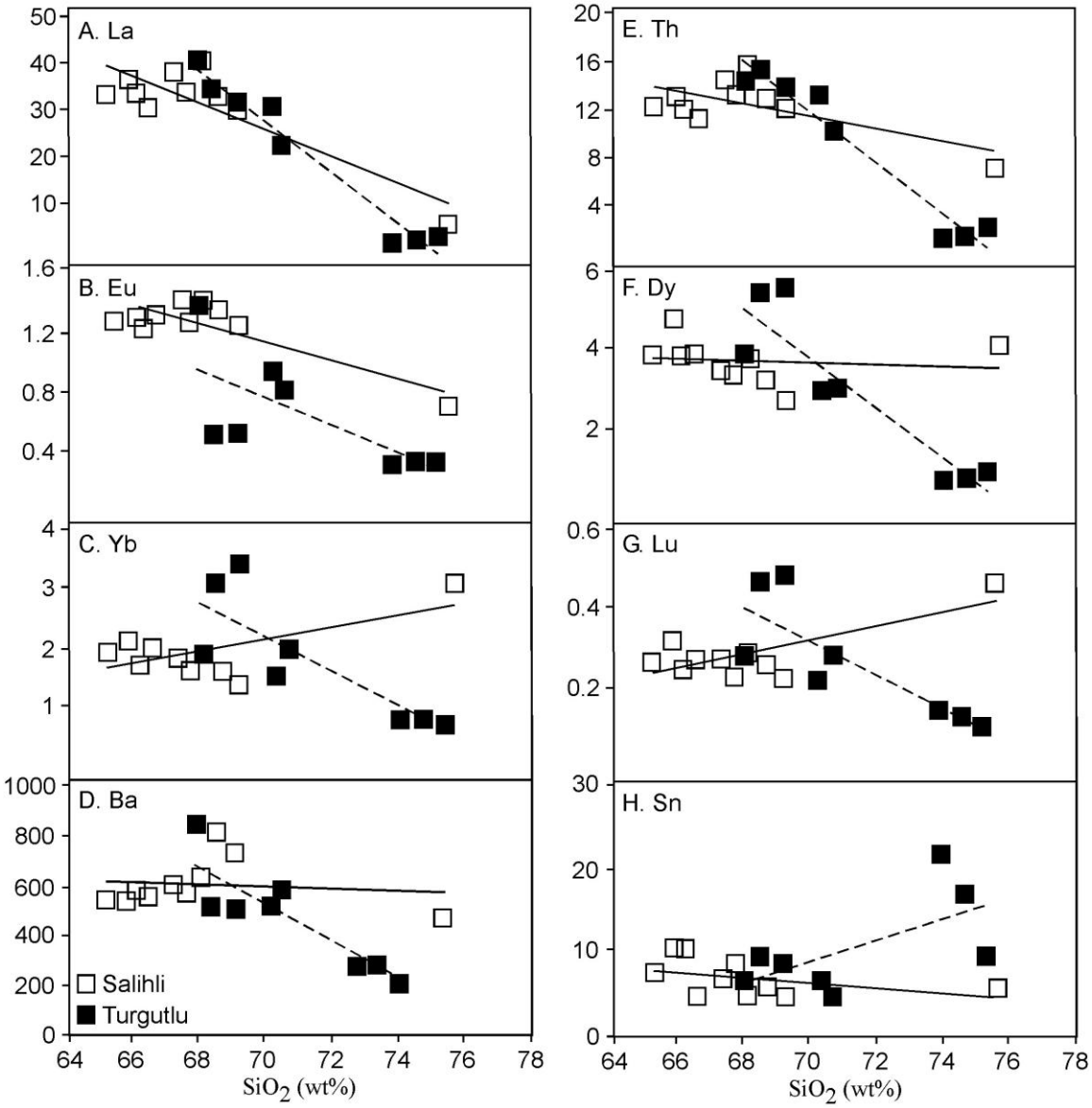

Figure 4.6. Trace element (ppm) versus SiO_2 (wt%) diagrams for the Salihli and Turgutlu granites. Table 4.5 contains slope and intercept information.

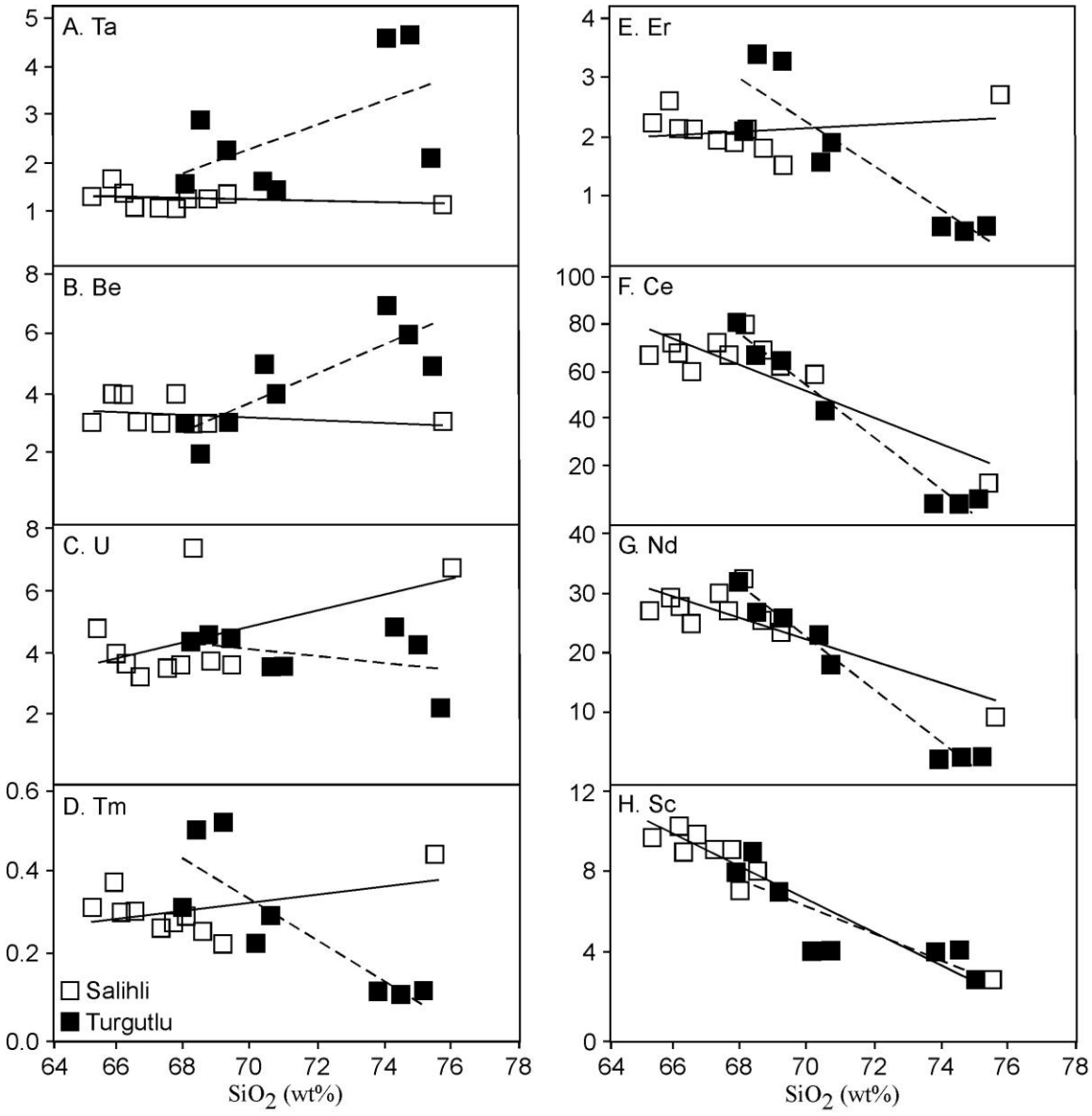

Figure 4.7. Trace element (ppm) versus SiO_2 (wt%) diagrams for the Salihli and Turgutlu granites. Table 4.5 contains slope and intercept information.

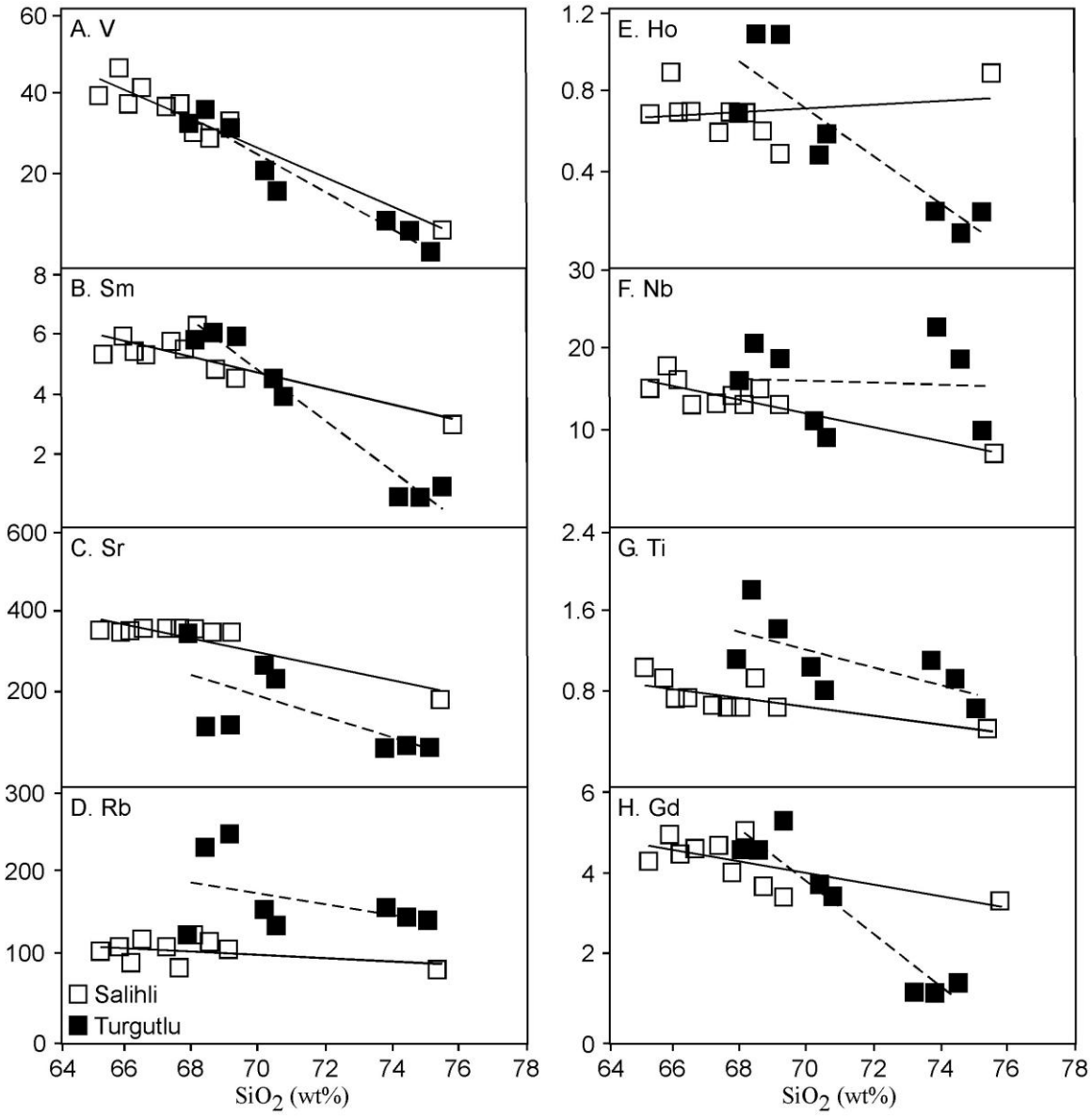

Figure 4.8 Trace element (ppm) versus SiO_2 (wt%) diagrams for the Salihli and Turgutlu granites. Table 4.5 contains slope and intercept information.

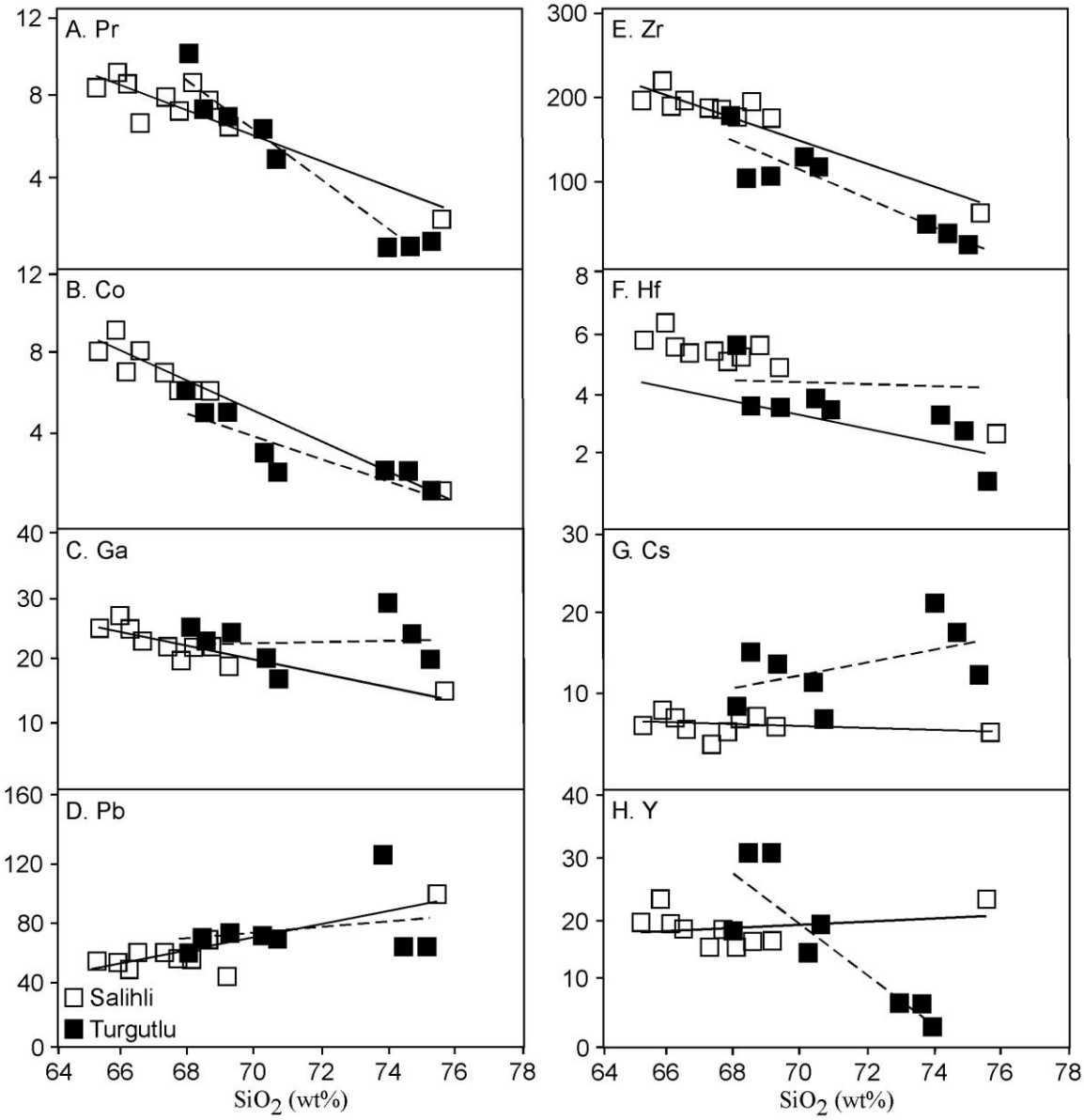

Figure 4.9. Trace element (ppm) versus SiO_2 (wt%) diagrams for the Salihli and Turgutlu granites. Table 4.5 contains slope and intercept information.

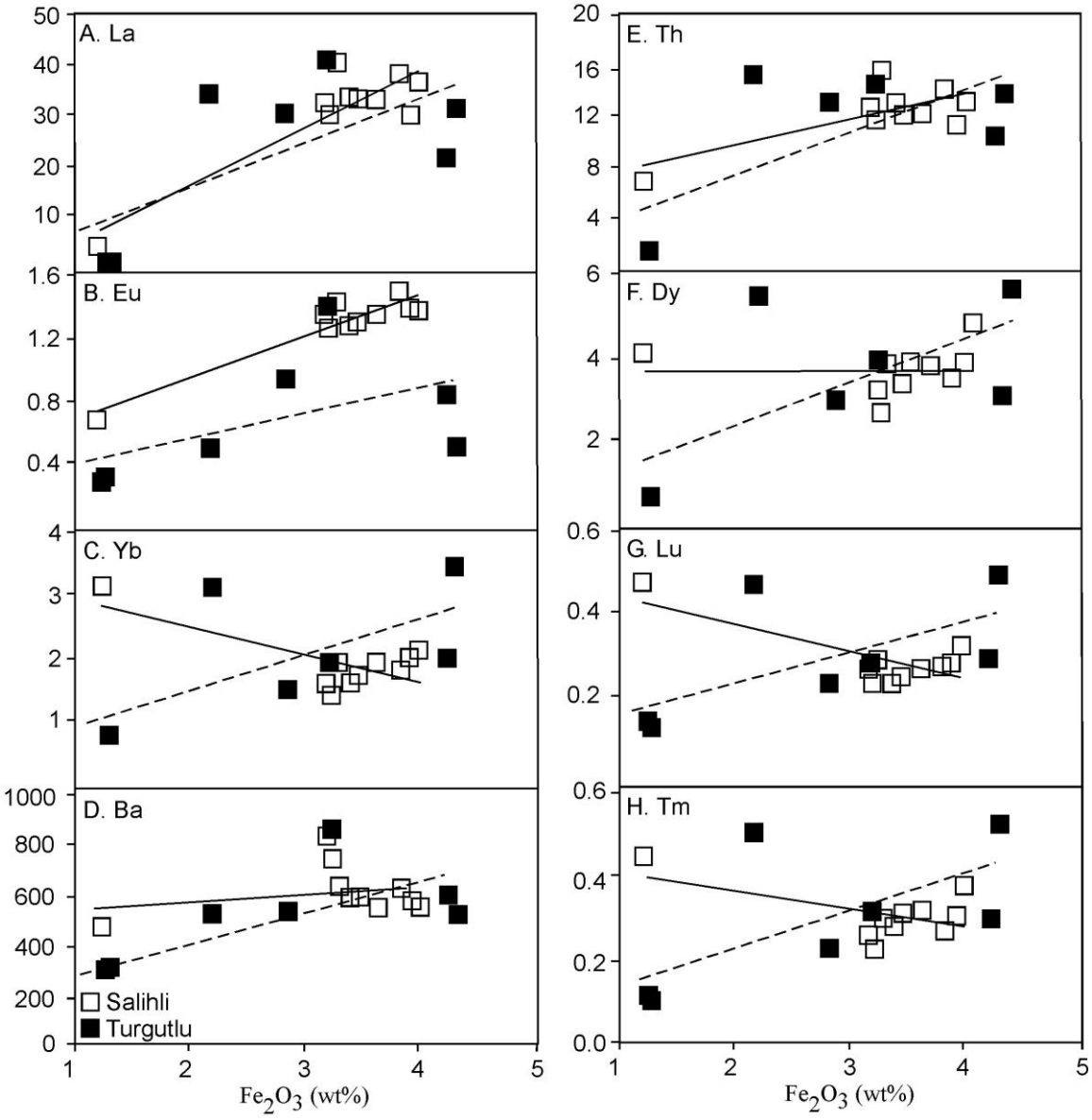

Figure 4.10. Trace element (ppm) versus Fe_2O_3 (wt%) diagrams for the Salihli and Turgutlu granites. Table 4.5 contains slope and intercept information.

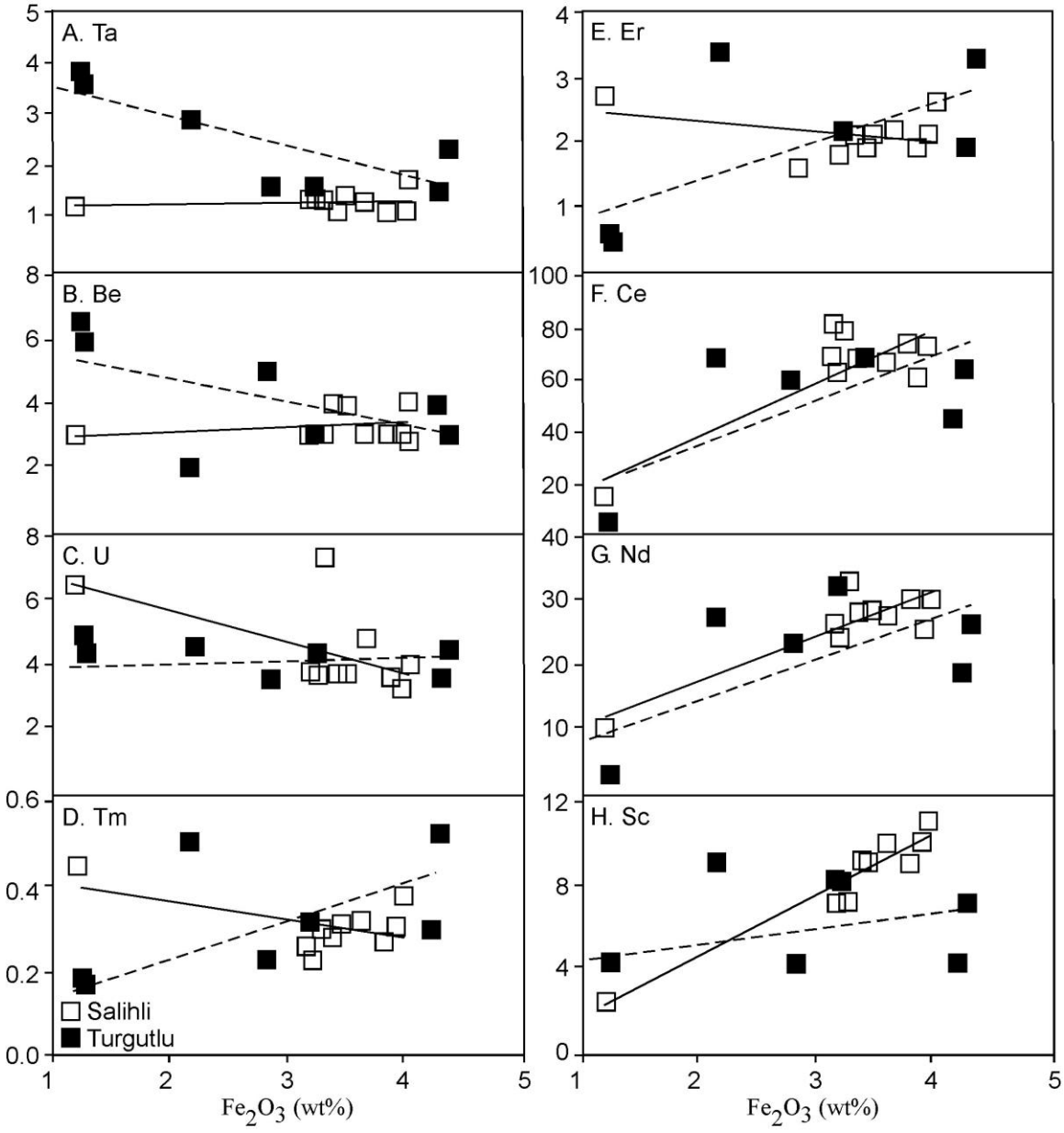

Figure 4.11. Trace element (ppm) versus Fe_2O_3 (wt%) diagrams for the Salihli and Turgutlu granites. Table 4.5 contains slope and intercept information.

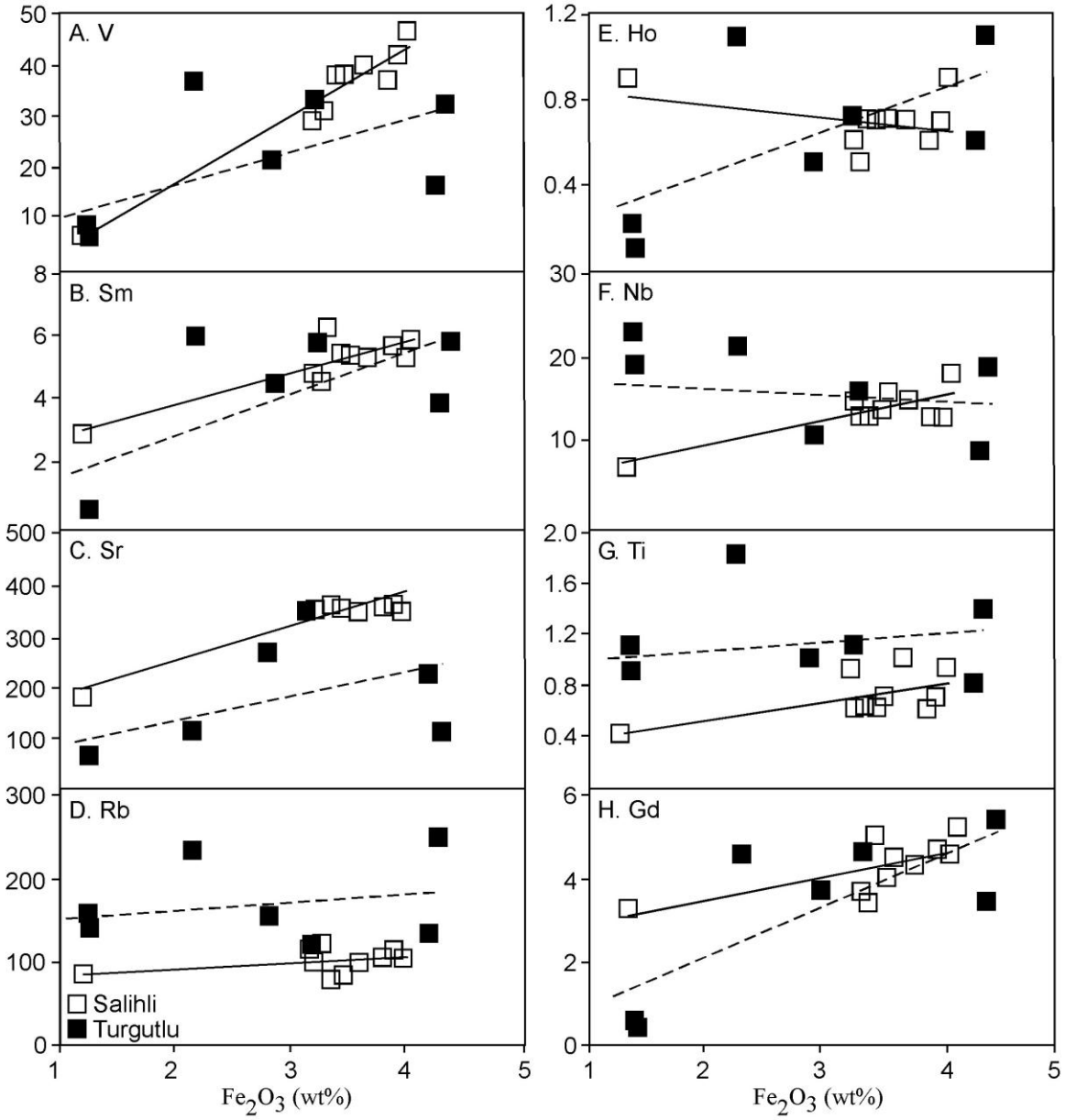

Figure 4.12. Trace element (ppm) versus Fe_2O_3 (wt%) diagrams for the Salihli and Turgutlu granites. Table 4.5 contains slope and intercept information.

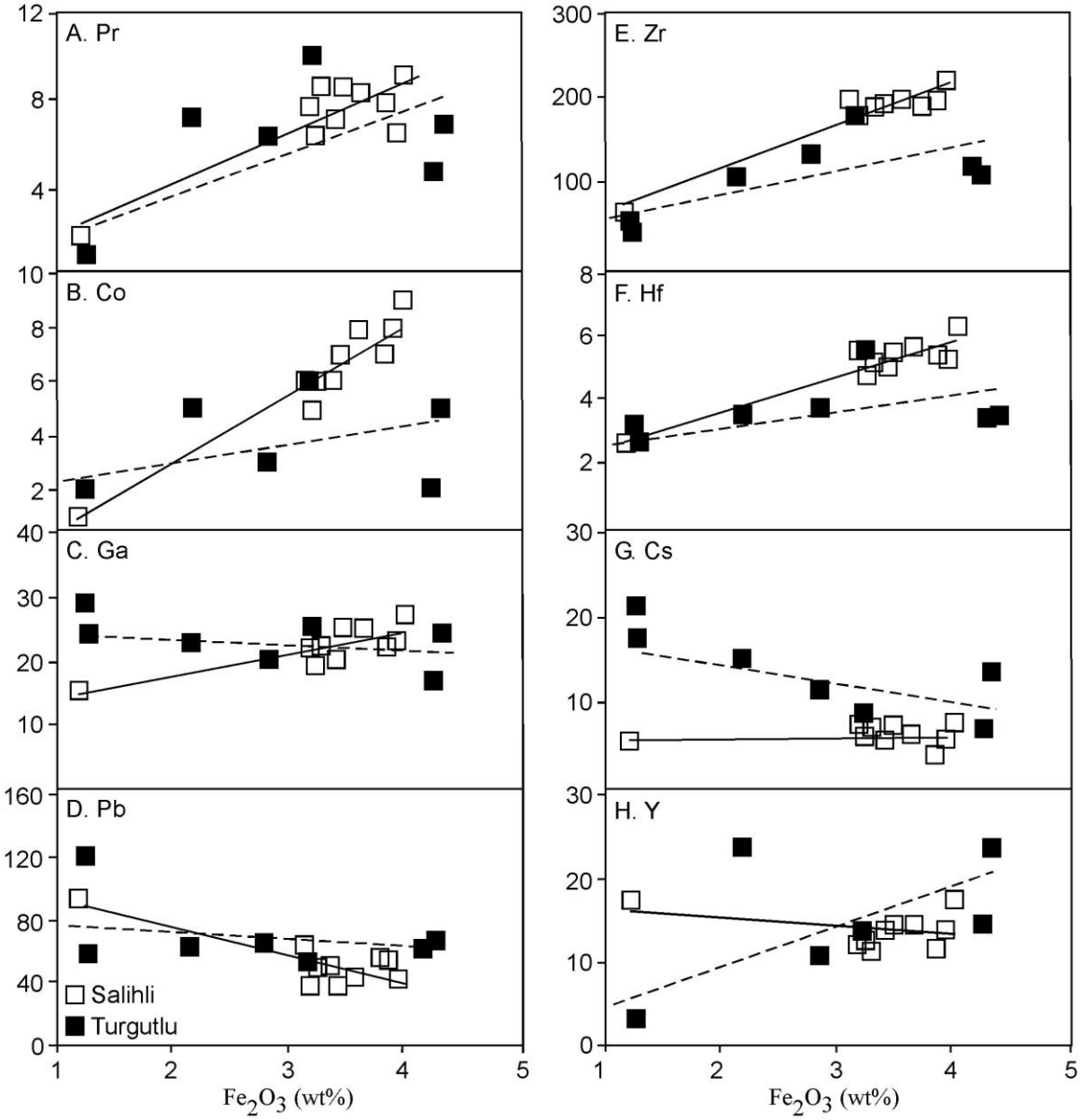

Figure 4.13. Trace element (ppm) versus Fe_2O_3 (wt%) diagrams for the Salihli and Turgutlu granites. Table 4.5 contains slope and intercept information.

Table 4.1. Major element compositional data from the Salihli granites (western, Turkey).

Element	EB01	EB01	EB01	EB02	EB02	EB03	EB05	EB05	EB05	CC20
SiO2	67.72	66.16	67.32	65.86	66.54	65.25	69.24	68.64	68.12	75.69
Al2O3	15.79	16.11	16.38	16.69	16.59	16.08	15.52	15.77	16.09	12.95
Fe2O3	3.38	3.45	3.81	3.97	3.90	3.61	3.21	3.16	3.27	1.22
MnO	0.06	0.07	0.07	0.08	0.07	0.07	0.06	0.06	0.06	0.02
MgO	1.39	1.42	1.56	1.69	1.66	1.54	1.18	1.18	1.26	0.32
CaO	3.94	4.07	3.77	4.60	4.13	4.31	3.72	3.59	3.80	1.80
Na2O	2.95	3.06	2.87	3.13	2.96	3.13	3.03	3.04	3.02	3.24
K2O	2.62	2.81	2.73	2.75	2.83	2.71	3.24	3.46	2.95	2.80
TiO2	0.56	0.56	0.61	0.64	0.61	0.57	0.49	0.49	0.54	0.13
P2O5	0.16	0.18	0.17	0.20	0.15	0.16	0.13	0.14	0.14	0.04
LOI	1.11	1.04	1.25	0.77	0.90	1.56	0.76	0.63	0.90	1.41
Total	99.68	98.93	100.50	100.40	100.30	98.98	100.60	100.20	100.20	99.62

(a) Compositional data is in wt% oxide, all granites contain monazite with the exception of CC20 which contains allanite. See Table 2.4. for mineral assemblages.

Table 4.2. Major element compositional data from the Turgutlu granites (western, Turkey).

Element	EB06	EB06	EB08B	EB08A	EB08A	EB09A	EB09A	EB09B
SiO2	68.01	70.33	70.68	68.48	69.23	74.69	75.35	74.02
Al2O3	15.96	15.67	15.71	14.51	14.76	14.83	14.66	14.90
Fe2O3	3.19	2.82	2.17	4.29	4.21	1.29	0.74	1.27
MnO	0.07	0.06	0.06	0.10	0.10	0.02	0.01	0.02
MgO	1.19	0.75	0.54	1.18	1.18	0.20	0.14	0.20
CaO	3.75	2.55	2.11	1.01	1.01	0.60	0.73	0.61
Na2O	3.07	3.43	3.26	2.67	2.64	3.11	3.41	3.06
K2O	3.67	3.62	4.10	5.40	5.48	4.67	4.64	4.94
TiO2	0.50	0.31	0.22	0.50	0.49	0.11	0.08	0.11
P2O5	0.14	0.11	0.12	0.12	0.10	0.10	0.11	0.11
LOI	0.58	0.54	0.86	0.69	0.92	1.04	0.64	1.67
Total	100.10	100.20	99.84	98.95	100.10	100.70	100.50	100.90

(a) Compositional data is in wt% oxide, granites contain both monazite only and/or allanite. See table 2.4. for mineral assemblages.
(b) In some cases more than one analyses of a granite sample were made.

Table 4.3. Trace element compositional data from the Salihli granites (western, Turkey).

Element	EB01A	EB01B	EB01	EB02	EB02	EB03	EB05A	EB05B	EB05	CC20A
Sc	9	9	9	11	10	10	7	8	7	2
Be	4	4	3	4	3	3	3	3	3	3
V	38	38	37	47	42	40	33	29	31	6
Ba	573	575	607	539	562	538	734	816	623	467
Sr	361	353	361	351	363	353	355	351	358	180
Y	18	19	15	23	18	19	16	16	15	23
Zr	186	189	189	219	195	196	177	196	178	64
Co	6	7	7	9	8	8	5	6	6	1
Ga	20	25	22	27	23	25	19	22	22	15
Ge	2	2	1	2	1	2	1	2	1	2
Rb	80	85	105	104	117	100	102	114	121	77
Nb	14	16	13	18	13	15	13	15	13	7
Sn	8	10	6	10	4	7	4	5	4	5
Cs	5.2	7	3.7	7.7	5.4	6	5.9	7.1	6.9	5.2
La	33.9	33.5	38.1	36.5	30.4	33.4	30.4	33	40.3	5.6
Ce	67.4	68.2	73.3	73.5	60.2	67.6	61.7	68.8	80.1	13.3
Pr	7.26	8.66	7.91	9.17	6.6	8.45	6.5	7.88	8.69	1.87
Nd	27.5	27.8	29.8	29.5	24.9	27	23.6	25.9	32.4	9.2
Sm	5.5	5.4	5.7	5.9	5.3	5.3	4.5	4.8	6.3	2.9
Eu	1.27	1.29	1.49	1.37	1.38	1.34	1.26	1.35	1.42	0.69
Gd	4	4.5	4.7	5.2	4.6	4.3	3.4	3.7	5	3.3
Tb	0.6	0.8	0.7	0.9	0.7	0.7	0.5	0.6	0.7	0.6
Dy	3.4	3.9	3.5	4.8	3.9	3.9	2.7	3.2	3.8	4.1
Ho	0.7	0.7	0.6	0.9	0.7	0.7	0.5	0.6	0.7	0.9
Er	1.9	2.1	1.9	2.6	2.1	2.2	1.5	1.8	2.1	2.7
Tm	0.27	0.3	0.26	0.37	0.3	0.31	0.22	0.25	0.29	0.44
Yb	1.6	1.7	1.8	2.1	2	1.9	1.4	1.6	1.9	3.1
Lu	0.23	0.25	0.27	0.32	0.28	0.27	0.23	0.26	0.29	0.47
Hf	5	5.5	5.4	6.3	5.3	5.7	4.8	5.5	5.2	2.6
Ta	1.1	1.4	1.1	1.7	1.1	1.3	1.4	1.3	1.3	1.2
Ti	0.6	0.7	0.6	0.9	0.7	1	0.6	0.9	0.6	0.4
Pb	50	37	54	43	53	42	38	63	49	93
Th	13.2	12.1	14.3	13.1	11.3	12.1	12	12.9	15.7	7
U	3.6	3.6	3.5	3.9	3.2	4.7	3.6	3.7	7.3	6.7

(a) Compositional data is in ppm, all granites contain monazite with the exception of CC20 which contains allanite. See Table 2.4. for mineral assemblages. Cr, Ni, Cu, Zn, As, Mo, Ag, In, Sb, and W elements analyzed, but were deleted because they are below the detection limits <20 ppm.

(b) Dection limit in ppm (< #) indicated for elements that were not detected.

Table 4.4. Trace element compositional data from the Turgutlu granites (western, Turkey).

Element	EB06	EB06	EB08B	EB08A	EB08A	EB09A	EB09A	EB09B
Sc	8	4	4	9	7	4	2	4
Be	3	5	4	2	3	6	5	7
V	33	21	16	37	32	6	< 5	8
Ba	839	522	580	511	510	243	171	242
Sr	349	269	231	113	114	64	66	63
Y	18	14	19	31	31	4	< 2	4
Zr	180	131	116	106	108	38	27	51
Co	6	3	2	5	5	2	1	2
Ga	25	20	17	23	24	24	20	29
Ge	2	1	1	2	2	3	2	3
Rb	123	153	133	232	251	143	138	156
Nb	16	11	9	21	19	19	10	23
Sn	6	6	4	9	8	17	9	22
Cs	8.5	11.3	6.9	15.2	13.9	17.7	12.2	21.4
La	40.8	30.6	22.5	34.3	31.6	2.1	3.2	2
Ce	81.4	59.4	44.2	67.8	63.7	3.8	6.2	3.8
Pr	10.1	6.36	4.8	7.29	6.99	0.46	0.72	0.51
Nd	31.9	22.9	17.9	26.9	26	2	2.8	2
Sm	5.8	4.5	3.9	6	5.9	0.5	0.8	0.5
Eu	1.39	0.95	0.84	0.52	0.52	0.33	0.33	0.31
Gd	4.6	3.7	3.4	4.6	5.3	0.4	0.7	0.5
Tb	0.8	0.6	0.6	0.9	1	< 0.1	0.1	0.1
Dy	3.9	3	3.1	5.5	5.6	0.7	0.9	0.7
Ho	0.7	0.5	0.6	1.1	1.1	0.1	0.2	0.2
Er	2.1	1.6	1.9	3.4	3.3	0.4	0.5	0.5
Tm	0.31	0.22	0.29	0.5	0.52	0.09	0.1	0.1
Yb	1.9	1.5	2	3.1	3.4	0.8	0.7	0.8
Lu	0.28	0.22	0.29	0.47	0.49	0.13	0.1	0.14
Hf	5.6	3.8	3.4	3.5	3.5	2.7	1	3.2
Ta	1.6	1.6	1.5	2.9	2.3	4.7	2.1	4.6
Ti	1.1	1	0.8	1.8	1.4	0.9	0.6	1.1
Pb	53	65	62	62	67	58	57	120
Th	14.5	13.2	10.4	15.3	13.8	1.4	2.1	1.1
U	4.3	3.5	3.5	4.5	4.4	4.2	2.2	4.8

(a) Compositional data is in ppm, all granites contain both monazite only and/or allanite. See Table 2.4. for mineral assemblages. Cr, Ni, Cu, Zn, As, Mo, Ag, In, Sb, and W elements analyzed, but were deleted because they are below the detection limits <20ppm.

(b) Detection limit in ppm (< #) indicated for elements that were not detected.

Table 4.5. Linear regression data for the Salihli and Turgutlu granites.

Element	Salihli Granites			Turgutlu Granites		
vs. SiO_2	Slope (±1σ)	Intercept (±1σ)	R^2	Slope (±1σ)	Intercept (±1σ)	R^2
Al_2O_3	-0.341	39.00	0.902	-0.077	20.67	0.164
Fe_2O_3	-0.252	20.47	0.91	-0.428	33.03	0.848
CaO	-0.248	20.69	0.952	-0.251	19.49	0.410
MgO	-0.128	10.09	0.930	-0.154	11.7	0.927
TiO_2	-0.047	3.721	0.919	-0.060	4.623	0.907
P_2O_5	-0.013	1.076	0.890	-0.002	0.290	0.308
MnO	-0.005	0.421	0.937	-0.011	0.841	0.857
Na_2O	0.016	1.925	0.213	0.050	-0.544	0.245
K_2O	0.016	1.750	0.035	0.026	2.674	0.011
Sr	-16.88	1488.0	0.804	-25.36	1968.0	0.454
Zr	-13.35	1088.0	0.888	-16.32	1259.0	0.833
Ce	-5.388	430.0	0.745	-10.78	811.0	0.965
Ba	-3.937	871.3	0.013	-69.13	5385	0.827
V	-3.616	280.2	0.918	-4.606	347.7	0.935
La	-2.796	221.8	0.742	-5.407	406.7	0.963
Rb	-2.103	243.6	0.165	-6.807	651.8	0.171
Nd	-1.845	151.3	0.744	-4.204	316.5	0.970
Ga	-1.046	93.18	0.818	0.094	16.00	0.005
Sc	-0.823	64.21	0.932	-0.704	55.54	0.714
Co	-0.721	55.41	0.936	-0.558	43.11	0.792
Pr	-0.646	51.30	0.830	-1.229	92.37	0.947
Th	-0.521	47.84	0.462	-2.110	159.5	0.948
Gd	-0.515	14.58	0.473	-0.676	51.16	0.932
Nb	-0.484	71.42	0.769	-1.104	23.42	0.003
Sn	-0.347	29.92	0.190	1.340	-85.53	0.401
Hf	-0.312	26.39	0.899	-0.347	28.12	0.638
Sm	-0.269	23.50	0.717	-0.839	63.35	0.960
Cs	-0.104	13.12	0.067	0.797	43.48	0.239
Eu	-0.065	5.720	0.767	-0.092	7.241	0.495
Be	-0.055	7.096	0.117	0.484	-30.15	0.703
Ti	-0.043	3.680	0.506	-0.084	7.079	0.434
Dy	-0.023	5.288	0.014	-0.636	48.35	0.840
Ta	-0.015	2.316	0.058	0.255	-15.54	0.323
Ho	0.010	-0.043	0.067	-0.118	9.012	0.775
Tm	0.010	-0.387	0.224	-0.050	3.879	0.728
Lu	0.017	-0.916	0.565	-0.042	3.291	0.685
Er	0.031	-0.082	0.070	-0.368	28.00	0.792
Yb	0.105	-5.264	0.447	-0.296	22.93	0.691
U	0.263	-13.57	0.295	-0.114	12.10	0.160
Y	0.264	0.195	0.071	-3.647	275.3	0.79
Pb	4.751	-271.1	0.738	2.312	-96.98	0.098
vs. Fe_2O_3	Slope (±1σ)	Intercept (±1σ)	R^2	Slope (±1σ)	Intercept (±1σ)	R^2
Pb	-17.19	108.8	0.677	-4.179	78.43	0.069
Y	-1.363	22.69	0.132	6.609	-1.381	0.560
U	-1.136	8.128	0.383	0.130	3.598	0.045

Yb	-0.418	3.288	0.492	0.552	0.394	0.518
Er	-0.162	2.627	0.128	0.624	0.152	0.491
Lu	-0.068	0.511	0.587	0.076	0.074	0.477
Ho	-0.054	0.878	0.116	0.199	0.065	0.474
Tm	-0.045	0.449	0.310	0.088	0.044	0.483
Dy	0.026	3.631	0.001	1.080	0.226	0.523
Ta	0.043	1.145	0.034	-0.593	4.144	0.377
Ti	0.139	0.238	0.361	0.068	0.916	0.062
Be	0.163	2.761	0.070	-0.726	6.189	0.342
Cs	0.213	5.306	0.019	-2.156	18.77	0.379
Eu	0.263	0.417	0.877	0.163	0.239	0.336
Gd	0.579	2.358	0.485	1.231	-0.174	0.667
Sn	0.904	3.318	0.090	-3.026	17.68	0.442
Sm	1.034	1.749	0.739	1.406	-0.026	0.583
Hf	1.168	1.276	0.880	0.551	1.960	0.347
Th	2.127	5.355	0.538	3.499	0.236	0.562
Pr	2.332	-0.394	0.756	1.936	-0.182	0.507
Co	2.700	-2.606	0.917	0.717	1.458	0.282
Nb	3.012	3.766	0.679	-0.894	18.23	0.051
Sc	3.095	-2.007	0.922	0.777	3.307	0.187
Ga	3.604	10.11	0.680	-0.881	24.95	0.104
Nd	7.082	2.402	0.767	6.837	-0.526	0.554
Rb	10.21	66.82	0.272	10.04	141.0	0.080
La	10.92	-4.527	0.793	8.646	-0.706	0.532
V	13.86	-11.963	0.945	6.609	2.616	0.416
Ce	20.78	-5.143	0.776	17.30	-1.928	0.536
Ba	26.76	515.1	0.042	124	142.5	0.575
Zr	51.51	9.001	0.925	28.58	23.23	0.552
Sr	66.47	119.3	0.872	48.15	38.35	0.354

(a) See Figure 4.3 and Figures 4.6-4.9 for accompanying graphs.
(b) Linear regression data is assuming the equation of a straight line.

CHAPTER V

GEOCHRONOLOGY OF THE SALIHLI AND TURGUTLU GRANITES

5.1. Introduction

Monazite ($CeThPO_4$) ages from granites exposed along detachment faults are widely used in studying the chronologies of extension (e.g., Murphy and Harrison, 1999; Catlos et al., 2004; Gilotti and McClelland, 2005). The mineral remains impervious to diffusive Pb loss at conditions >900°C (Cherniak et al., 2004) and appears resilient to radiation damage (Meldrum et al., 1998). Ages can be affected by fluids as dissolution-reprecipitation reactions occur along a retrograde path (e.g., Seydoux-Guillaume et al., 2002). However, the mineral's ability to recrystallize during multiple geologic events provides a record of information about complexly metamorphosed regions (e.g., Catlos et al., 2002; Catlos and Çemen, 2005) and can be used as a complement to zircon or $^{40}Ar/^{39}Ar$ ages.

In this study, we used an in situ (in thin section) approach to dating the mineral. Preservation of the grain and rock fabric is obtained by using the ion microprobe method. Multiple monazite ages from the Salihli and Turgutlu granites were collected using the ion microprobe. The combination of the ion microprobe, whole rock and geochemical information from the grain itself can allow for a clear interpretation of the age. The work has implications for Aegean tectonics, the transition from compression to extension in orogens overall, and for development of monazite as a geochemical and chronologic monitor of extension.

5.2. Age of Salihli granites

5.2.1. Previous work

^{40}Ar-^{39}Ar dating of biotite in the Salihli granodiorites yielded ages of 12.2±0.4 Ma (Hetzel et al., 1995; Glodny and Hetzel, 2007). The biotite ages were originally interpreted to reflect cooling through approximately 300-350°C, because the samples lacked foliation (Hetzel et al., 1995). Further cooling of the Salihli granites is constrained by two zircon apatite fission track ages of 5.2±0.3 Ma and 1.9±0.4 Ma (Gessner et al., 2001). Matrix monazite grains from metamorphic rocks within the eastern part of the Alasehir detachment, analyzed by ion microprobe, gave ages of 17±5 and 4.5±1.0 Ma, interpreted to record extension (Catlos and Çemen, 2005).

5.2.2. This study

Six monazites were dated from the CC20 Salihli leucogranites (Figure 5.1); those ages ranges from 21±74.5 to 9.6±1.6 Ma (Table 5.1) (See Figure 2.3 for sample locations). CC20 monazite 2 (Figure 5.1) adjacent to potassium feldspar and plagioclase and has an ion microprobe age of 13.0±1.1 Ma. Monazite 5 from CC20 yielded an age of 18.6±4.5 Ma and is located within plagioclase. The largest monazite found in CC20 (monazite 6) has three ion microprobe ages that range from 11.9±2.5 to 21.7±4.5 Ma. This monazite is located within a biotite grain. The youngest monazite from CC20 (monazite 1) is located within plagioclase and has an age of 9.6±1.6 Ma.

5.3. Ages of the Turgutlu granites

5.3.1. Previous Works

Turgutlu granites were also dated using the ^{40}Ar/^{39}Ar method (Hetzel et al., 1995; Glodny and Hetzel, 2007). Magmatic biotite from the Turgutlu graniodiorite yeilds an 13.2±0.2 Ma ^{40}Ar-

^{39}Ar plateau age (Hetzel et al., 1995; Glodny and Hetzel, 2007). Turgutlu granite monazites dated using the U-Pb methods yield ages of 16.1±0.2 Ma (Glodny and Hetzel, 2007).

5.3.2. This study

Turgutlu samples with multiple monazites were analyzed using the ^{232}Th-^{208}Pb ion microprobe technique (see methods section for details). Ages from four different samples ranged from 19.2±.1 to 11.5±1.0 Ma (Figures 5.2-5.4 and Table 5.1). Turgutlu sample EB08 contains multiple monazites that have a wide range of ages. EB08 monazite 3A (12.2±1.4 Ma) is found within a plagioclase adjacent to biotite. Monazite 2A is located next to a large biotite grain and has an age of 14.0±0.8 Ma. A second monazite 2B is large enough for two ion microprobe spots and is 15.4±1.0 and 15.8±1.3. This found next to biotite and quartz. Monazite 3B is located within plagioclase next to a large biotite grain and has an age of 14.3±0.7 Ma. EB08 monazite 1 is found at the tip of a biotite grain next to a quartz crystal is 15.3±1.3 Ma. A large monazite 4 has two ion microprobe ages of 11.5±0.8 and 14.3±0.8 Ma and is found next to a potassium feldspar crystal.

Sample EB09 monazite 1 has an age of 16.8±1.1 Ma and is found next to an L-shaped biotite grain and a quartz crystal. Monazite 4 is also located within a plagioclase grain with an age of 14.9±1.2 Ma. Sample EB09 monazite 3A appears to be between two biotite grains within a plagioclase and has an age of 15.0±0.8 Ma; monazite 2A is also located between two grains of biotite within a plagioclase, however its age is younger (13.2±0.8 Ma). A second monazite 3B is large enough for two ion microprobe spots; those ages are 13.8±0.9 and 19.2±5.1 Ma. This monazite is located within a plagioclase crystal next to a biotite grain. Another monazite 2B has an age of 16.1±1.4 Ma and is found next to a biotite grain, a plagioclase and quartz crystal. EB06 contains monazite grains which are 15.4±1.3 and 15.5±1.2 Ma. Monazite 4, which has an age of 15.1±1.0 Ma, is located between a biotite grain and a potassium feldspar crystal.

5.4. Conclusions

The range of monazite ages may suggest that the Menderes Massif has undergone multiple stages of crystallization. The most uncertain ages are the oldest (21.7±4.5 Ma; 18.3±1.8 Ma sample CC20). The level of uncertainty reported for these Menderes Massif monazite grains is higher than is typically reported, and is attributed to lower than average radiogenic ^{208}Pb* contents and the unknown analyses not lying in the region defined by the calibration. The average ^{208}Pb* for the dated grains is 71±4%, whereas our measured standard (monazite 554; Force, 1997) ^{208}Pb* contents is 98±1%.

The abundant ~15 Ma ages recorded by these granites (Table 5.1; see also Glodny and Hetzel, 2007) likely time the crystallization of the monazite grain in this rock, but the younger ages, however, may be affected by dissolution-reprecipitation reactions. The youngest monazite ages, which, in the Turgutlu granite, is located in the rim of a feldspar grain (11.5±0.8 Ma), and in the Salihli granite, is located along the edge of a plagioclase grain (9.6±1.6 Ma). The average of all the monazites date is 15.0±2.8 Ma (MSWD=3.8).

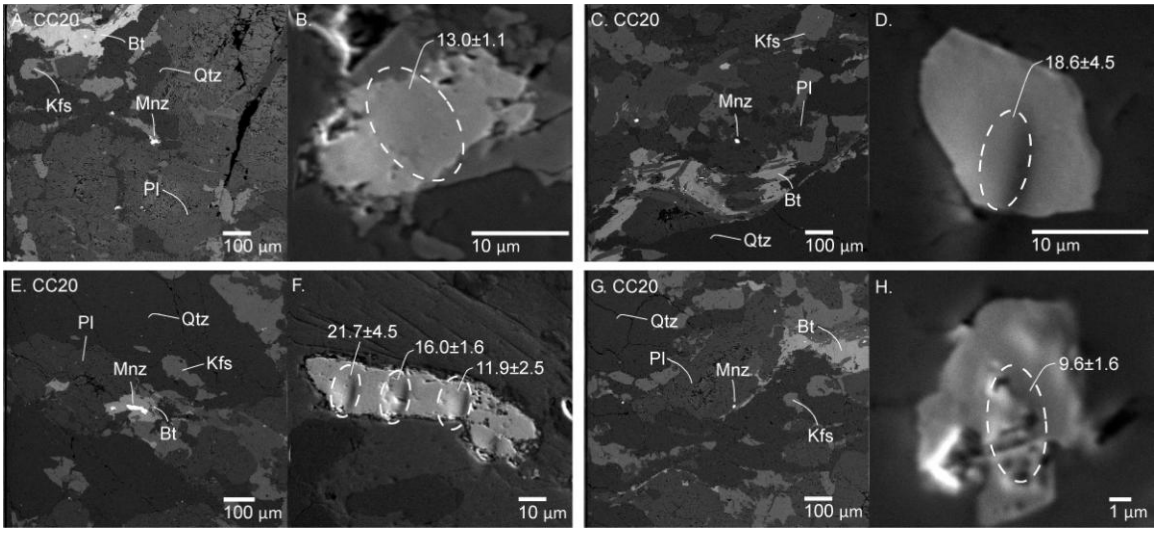

Figure 5.1. Images of Salihli monazites with ion microprobe ages (Ma). Abbreviations after Kretz (1983). Bt=biotite, Kfs=potassium feldspar, Mnz=monazite, Pl=plagioclase, Qtz=quartz. Ion microprobe spots are outlined with dashed black circle.

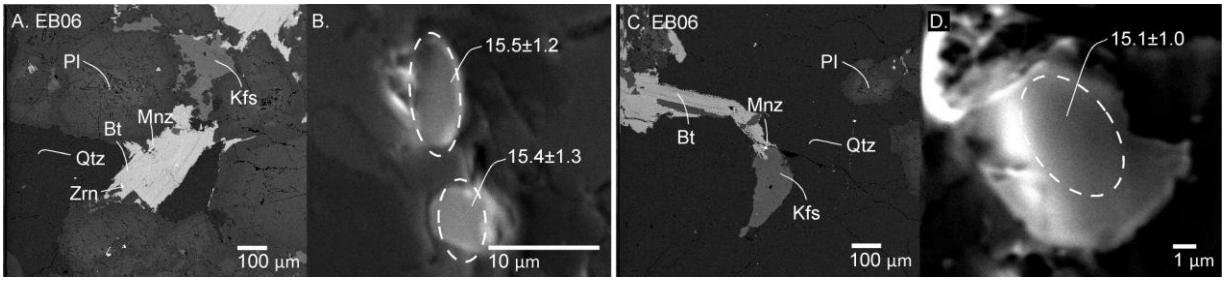

Figure 5.2. Images of Turgutlu monazites with ion microprobe ages (Ma). Abbreviations after Kretz (1983). Abbreviations are the same as in Figure 5.1 with the addition of Zrn=zircon. Ion microprobe spots are outlined with dashed black circle.

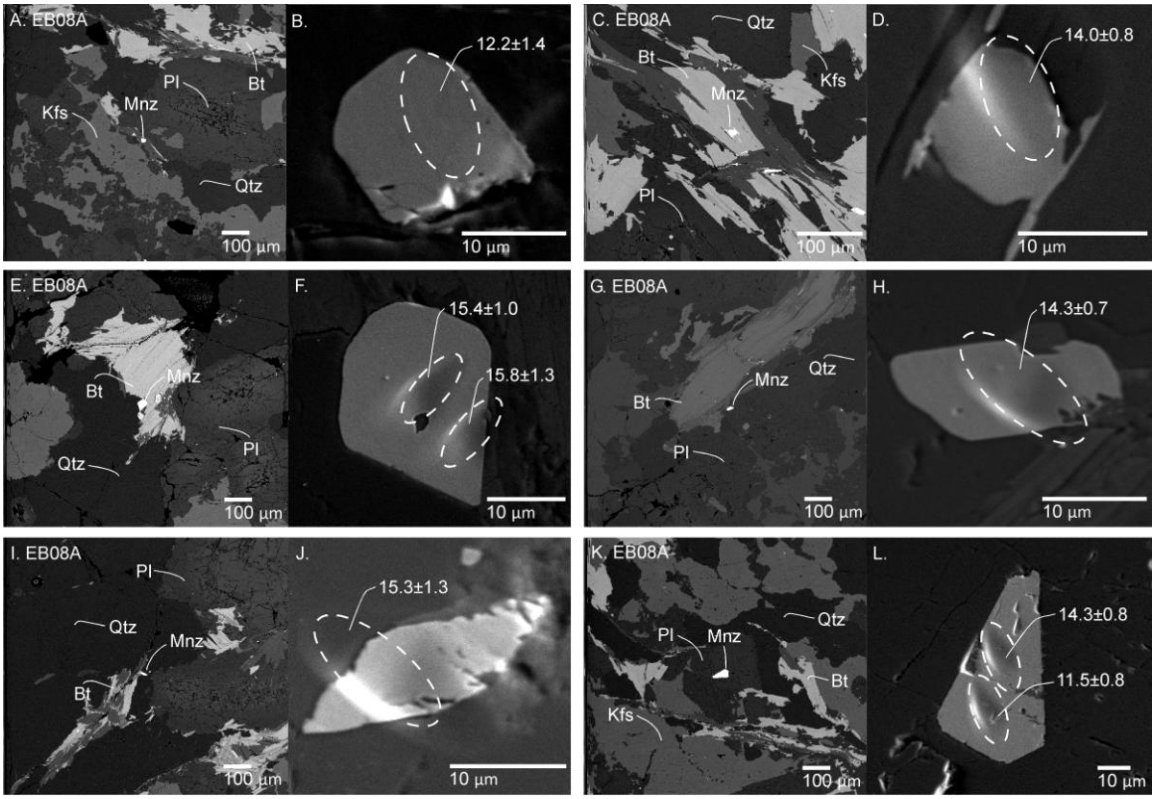

Figure 5.3. Images of Turgutlu monazites with ion microprobe ages (Ma). Abbreviations after Kretz (1983). Abbreviations are the same as in Figure 5.1. Ion microprobe spots are outlined with dashed black circle.

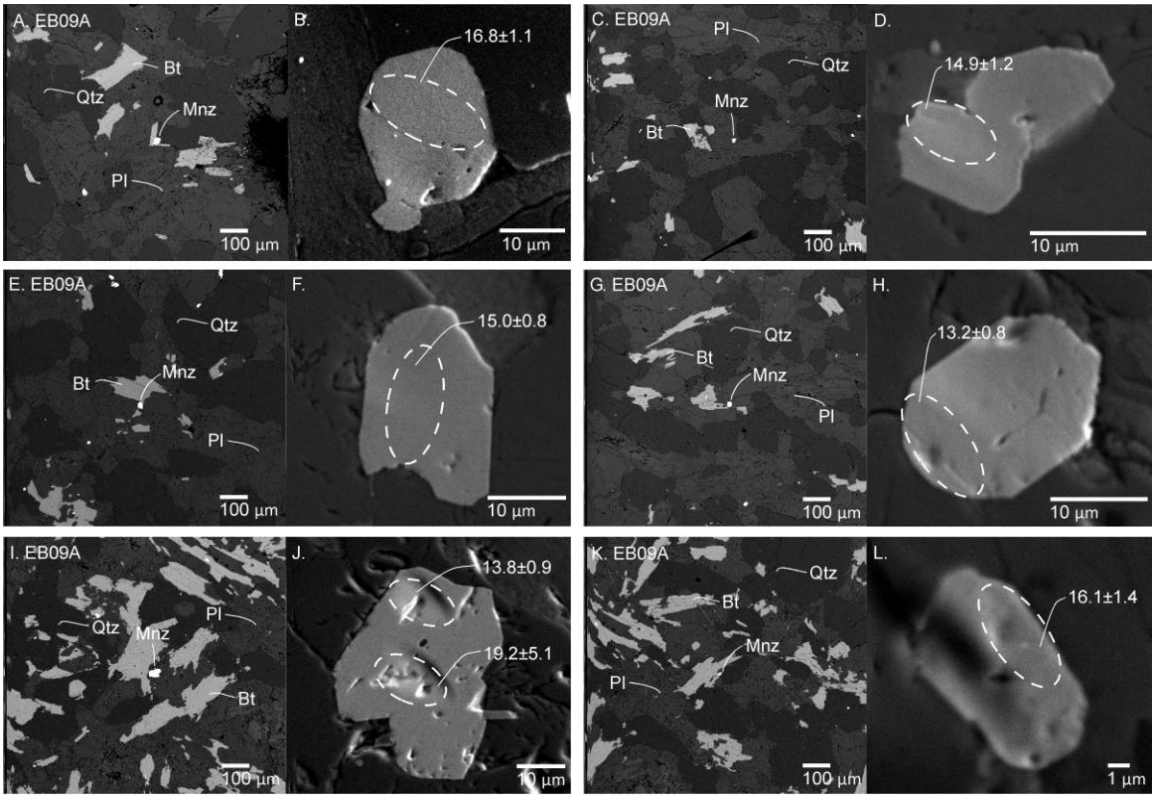

Figure 5.4. Images of Turgutlu monazites with ion microprobe ages (Ma). Abbreviations after Kretz (1983). Abbreviations are the same as in Figure 5.1. Ion microprobe spots are outlined with dashed black circle.

Table 5.1. Th-Pb ion microprobe monazite ages from the Salihli and Turgutlu granites.

Sample[a]	Age (Ma) (±1σ)	ThO_2^+/Th^+(±1σ)[b]	^{208}Th*/Th(±1σ)[c]	%^{208}Pb*(±1σ)[d]
Salihli leucogranite; average 15.0±2.8 Ma				
CC20 (N 38°24'24.0" E2 8°11'43.0")[e]				
m6_3	21.7±4.5	1.543±0.016	1.076E-03±2.250E-04	59.7±2.5
m5_1	18.6±4.5	2.209±0.014	9.205E-04±2.232E-04	43.9±6.3
m2_1	18.3±1.8	2.209±0.015	9.046E-04±8.872E-05	65.1±1.2
m6_1	16.0±1.6	2.125±0.016	7.923E-04±8.060E-05	80.4±0.9
m2_1	13.0±1.1	2.479±0.023	6.449E-04±5.559E-05	57.7±1.6
m6_4	11.9±2.5	1.661±0.017	5.911E-04±1.222E-04	18.0±2.1
m3_1	11.0±2.6	1.574±0.016	5.440E-04±1.266E-04	13.2±1.7
m1_1	9.6±1.6	2.285±0.017	4.761E-04±8.106E-05	19.0±2.7
Turgutlu granodiorite; average 15.0±1.7 Ma				
EB06 (N 38°22'58.5" E 27°40'32.2")[e]				
m2_1	15.5±1.2	3.182±0.048	7.651E-04±5.950E-05	71.4±3.0
m2_2	15.4±1.3	3.098±0.038	7.611E-04±6.304E-05	66.2±3.6
m4_1	15.1±1.0	2.837±0.014	7.483E-04±4.962E-05	82.2±1.4
EB08A (N 38°22'55.8" E 27°39'40.7")[e]				
m2_2	15.8±1.3	2.436±0.011	7.799E-04±6.205E-05	96.6±0.5
m2_1	15.4±1.0	2.866±0.011	7.643E-04±4.747E-05	96.3±0.5
m1_1	15.3±1.3	2.418±0.006	7.552E-04±6.355E-05	58.2±1.4
m1_1	15.0±1.4	2.617±0.022	7.397E-04±6.744E-05	56.9±3.0
m4_1	14.3±0.8	3.065±0.017	7.056E-04±4.016E-05	93.4±0.8
m3_1	14.3±0.7	3.561±0.028	7.072E-04±3.449E-05	92.5±1.2
m2_1	14.0±0.8	3.058±0.027	6.915E-04±4.109E-05	85.1±1.2
m1_1	13.9±1.0	2.840±0.027	6.885E-04±4.746E-05	84.5±1.7
m3_1	12.2±1.4	2.594±0.027	6.032E-04±6.880E-05	40.4±3.5
m4_2	11.5±0.8	2.699±0.018	5.694E-04±3.966E-05	93.0±1.3
EB09A (N 38°22'55.1" E 27°39'41.5")[e]				
m3_2	19.2±5.1	3.267±0.033	9.508E-04±2.500E-04	61.3±7.9
m1_1	16.8±1.1	2.906±0.037	8.303E-04±5.405E-05	87.7±1.3
m4_1	16.7±1.6	2.937±0.026	8.274E-04±7.737E-05	80.9±3.7
m2_1	16.1±1.4	3.254±0.025	7.986E-04±6.852E-05	68.3±4.2
m3_1	15.0±0.8	3.608±0.016	7.405E-04±3.948E-05	87.8±1.9
m4_1	14.9±1.2	3.075±0.029	7.364E-04±5.872E-05	54.8±2.6
m3_1	13.8±0.9	3.238±0.025	6.843E-04±4.382E-05	72.0±2.4
m2_1	13.2±0.8	3.121±0.035	6.511E-04±4.106E-05	85.3±1.8
EB09B (N 38°22'55.1" E 27°39'41.5")[e]				
m2_4	16.3±1.3	2.646±0.027	8.055E-04±6.549E-05	81.9±3.1
m2_1	15.7±1.3	2.660±0.021	7.774E-04±6.592E-05	83.5±2.9
m2_2	14.9±1.2	2.922±0.024	7.391E-04±6.026E-05	76.8±3.8
m2_3	14.6±4.2	2.342±0.020	7.247E-04±2.072E-04	42.9±11.3
m1_1	14.1±1.0	3.028±0.021	6.985E-04±4.750E-05	84.2±2.8

(a) The nomenclature in the grain #_ion microprobe spot #.
(b) Measured in the sample. Ideally, the unknown ThO_2^+/Th^+ ratio lies within the range defined by the standard (from 2.837±0.031 to 3.960±0.021)
(c) The reported Pb*/Th (±1σ) ratio includes the radiogenically derived $^{208}Pb/^{204}Pb$ of 39.5±0.1 (Stacey and Kramers, 1975).

(d) Percent radiogenically derived ^{208}Pb.
(e) Sample number and GPS location. See Figure 2.3 for sample locations.

CHAPTER VI

CATHODOLUMINESCENCE OF THE SALIHLI AND TURGLUT GRANTIES

6.1. Introduction and background

Cathodoluminescence (CL) is visible light emitted from a specimen when it is bombarded with electrons (Smith and Stenstrom, 1965; Marshall, 1977; Kopp, 1981; Finch and Klein, 1999; Sorensen, 2006). CL has been used to provide information about many kinds of geologic materials (Long and agrell, 1965; Sippel and Glover, 1965; Smith and Stenstrom, 1965; Kopp, 1981). With the use of CL, minerals (quartz, feldspar, and plagioclase) can be rapidly identified and structural and composition variations with potential genetic implications can be revealed (Smith and Stenstromm, 1965). In addition, textural information from a variety of rocks can be obtained with the use of the CL (Smith and Strenstrom, 1965; Marshall, 1977; Kopp, 1981; Ramseyer et al., 1992; Finch and Klein, 1999; Leichmann et al., 2003; Slaby and Götze, 2004; Sorensen, 2006; Weibe et al., 2007). Variations in mineral compositions (mainly quartz and feldspars) and textures (growth zonations or hydrothermal alterations) are visible (AlDahan et al., 1988; Hopson and Ramseyer, 1990; Ramseyer et al., 1992).

Not all geologic materials luminescence. However the CL colors and intensities produced by those that do result from several factors including (1) the nature of the host lattice, (2) the kinds and amounts of "activators" and "quenchers" (Kopp, 1981).

Activators can include impurities, abnormally ionized atoms (for example, Al, and Ti), and quenchers reduce intensity (for example, iron) (Kopp, 1981). As a result it is possible that two different specimens of the same mineral species will behave differently or may have the same appearance when viewed with CL (Smith and Stenstrom, 1965; Greer and Weber, 1968; Marshall, 1977; Kopp, 1981; Finch and Klein, 1999; Sorensen, 2006). The definition of luminescence color, based on naked eye observations is subjective (Greer and Weber, 1968; Marshall, 1977).

CL has been used to obtain different types of information about rocks and minerals (Smith and Stenstromm, 1965; Greer and Weber, 1968; Marshall, 1977; Kopp, 1981; AlDahan et al., 1988; Hopson and Ramseyer, 1990; Ramseyer et al., 1992; Cox et al., 1996; Finch and Klein, 1999; Stirling et al., 1999; Goetze et al., 2000; Janousek et al., 2001; Leichmann et al., 2003; Slaby and Götze, 2004; Sorensen, 2006; Weibe et al., 2007). For example the CL technique has been used to study quartz, plagioclase and k-feldspar from granitic rocks in the Siljan impact area, central Sweden (Ramseyer et al., 1992). Feldspar alteration was investigated by Leichmann et al., (2003) with the use of this technique. Feldspar minerals are commonly targeted by CL, as they can record magmatic and subsoildus evolution of the rock (Cox et al., 1996; Stirling et al., 1999; Goetze et al., 2000; Janousek et al., 2001; Leichmann et al., 2003). CL has been used to characterize the mutual relationship between plagioclase and k-feldspar and their alteration in a sedimentary environment (Walker, 1984; Fedo et al., 1997) and in magmatic systems (Mora and Ramseyer, 1992; Garcia et al., 1996; Leichmann et al., 2003). The process of K-metasomatism in ash-flow tuffs was studied with the use of CL, which quickly yields information about the mineralogical changes and reaction

mechanism that take place during alteration for large samples suites and links these properties to geochemical changes (Rougvie and Sorensen, 2002; Leichmann et al., 2003). Sorensen et al., (2006) used the CL to show that the petrogenesis of jadeitite is relevant to the study of fluid-rock interactions in subduction zones.

Mineral zoning, deformation, and fluid alteration in a variety of lithologies have been documented with the use of CL (Marshall, 1988; Ramseyer et al., 1992; Pidgeon et al., 2001; Sorensen et al., 2006). However, the application of the CL technique for the petrological evaluation of igneous rocks is uncommon (Kopp, 1981; Ramseyer et al., 1992; Leichmann et al., 2003). For the purpose of this study the CL was used to show evidence for fluid interaction, including tracks of pathways and infilled cracks. Inconsistent monazite ages can often be explained by dissolution-reprecipitation reactions. X-ray element maps or backscattered electron (BSE) imaging may not always reveal the presence of the fluids that trigger these reactions, which is why the application of the CL was considered. Although the activities for the colors were not quantitatively determined, the images document a complicated growth and retrogression history of the Salihli and Turgutlu granites.

6.2. Sample CC20 (N 38°24’24.0” E 28°11’43.0”)

Each mineral has a distinct characteristic CL color. In the Salihli granites the k-feldspar has a blue CL color. The blue CL can be broken down into five different shades; dark blue, light blue, medium blue, bright blue, and brownish-blue. Red and blue CL from alkali feldspar, with the majority giving blue was noted visually by Smith and Stenstrom (1965) (Finch and Klein, 1999). The feldspars blue CL color has been

attributed to Eu^{2+}, Ti^{4+}, and Ga^{3+} activation (Geake et al., 1973; Mariano and Ring, 1975; Mariano, 1988; De St Jorre and Smith, 1990; Finch and Klein, 1999). Plagioclase grains in the Salihli samples have a green CL color which has also been observed in lunar samples (Götze et al., 1999). Greake et al., (1972) attribute the green color to Mn^{2+} and Ca^{2+}. The green CL color can be broken down into six different shades; dark green, medium green, light green, bright green, bright yellow green, and brownish-green.

A brown CL color is seen in the Salihli granites quartz grains. This brown CL color can only be broken down into three shades; light brown, reddish-brown, and light reddish-brown. The brown luminescent color has been linked to many different quartz crystallization processes; (1) during small-scale deformation of the rock, (2) plastic deformation, (3) rapid formation of the quartz, (4) high density of lattice defects, and (5) damage to the lattice induced by particle bombardment (Kullis, 1982; Matter and Ramseyer, 1985; Ramseyer et al., 1988).

Grain boundary migration and recrystallization can be seen along the CC20 k-feldspar and plagioclase grains. This shows that these grains are texturally resorbed as the brownish-green plagioclase grains intrude the k-feldspar grains. A reddish blue CL color can be identified along some of the k-feldspar and plagioclase grain boundaries (Figures 6.1-6.4). Finch and Klein (1999) have linked this change in color from blue to red to fluid interaction. Fluids may have infiltrated cracks between the k-feldspar grains and altered them to reddish-blue. Bright blue domains are usually seen as specs throughout the k-feldspar grains or in some instances along fractures (Figures 6.1-6.4). Grains that avoided significant fluid interaction and alteration are represented by this bright blue color.

Myrmekite is replacing many of the k-feldspar grains. Multiple generations of microcracks can also be seen in many of the grains.

The CC20 plagioclase grains have rims that vary in size, texture, and color. These rims can be patchy or are replaced by myrmekite. A few grains contain bright "flame-type" structures. These bright regions may represent compositional differences. Larger plagioclase grains have dark green outer rims, medium to light green inner rims with bright yellow green cores (Figures 6.1-6.4). The cores of the majority of the plagioclase grains are often highly corroded and fractured (Figures 6.1-6.4). Within a few of the highly corroded plagioclase grains a white CL color can be observed (Figures 6.1 and 6.3) although most of the grains cores are bright yellow-green. A similar texture has been reported which suggests that the cores are "shattered" (Janoušek et al., 2004) and are thought to be relics of crystals from a previous magma (Leichmann et al., 2003; Janoušek et al., 2004). A non-corroded plagioclase grain can be identified in Figure 6.3. With the use of the CL multiple generations of microcracks and microfaults are easily identified within the plagioclase grains. The brownish-green CL can be seen along the rims of the plagioclase where myrmekites have formed (Figures 6.1-6.4). Myrmekite often comprises the outermost rims of plagioclase grains in Salihli samples.

Quartz grains have a brown to reddish-brown CL color (Figures 6.1-6.4). Fractures of different sizes can be seen throughout the quartz grains. A majority of the fractures within the grains have a brighter red CL color (Figures 6.1 and 6.3). Some of the fractures appear to be cross-cutting each other (Figure 6.3). Figure 6.1 has quartz grains that have a brighter reddish-brown CL color which are filled with microfractures. Some of the quartz grains appear to have a brighter red rim (Figure 6.3). Deformation

lamellae are visible in certain regions of the quartz grains; these have a light red almost pink CL color (Figure 6.3).

6.3. Sample EB06 (N 38°22’58.5” E 27°40’32.2”)

The Turgutlu granites quartz, k-feldspar and plagioclase grains all have the same characteristic CL colors as the Salihli samples. K-feldspar grains show the blue CL colors which range from dark, medium, bright and brownish blue. The Turgutlu plagioclase grains have the characteristic yellow-green, light, medium, dark, and brownish-green color. Quartz grains are the typical brown, light, dark brown, and reddish-brown with lighter CL color fractures. Grain boundary migration and recrystallization can also be seen along the EB06, EB08A and EB09A k-feldspar and plagioclase grains, which are also seen throughout the CC20 Salihli granites. This shows that the Turgutlu grains are texturally resorbed as the brownish-green plagioclase intrudes the k-feldspar grains.

K-feldspars in the EB06 Turgutlu granites are dark and medium blue with light blue spots (Figures 6.5-6.6). A magnified image (10x) shows a k-feldspar with a dark blue CL color with bright blue spots (Figure 6.6). The bright blue domains are not localized to the core of the grain as seen in the plagioclase grains, but can be observed near the rims or fractures of the crystals (Figures 6.5 and 6.6). The factures seen throughout the k-feldspar grains have a brownish-blue CL color.

The plagioclase grains have dark green outer rims with medium to light green inner rims and bright yellow green cores. Like the Salihli plagioclase grains the rims vary in size, texture and color and can be patchy or are replaced by myrmekite. Within some

of the grain cores the white CL color is observed. The cores are highly corroded or "shattered", which indicates that these grains are possibly relics of crystals from a previous magma (Figures 6.5-6.6) (Leichmann et al., 2003; Janoušek et al., 2004). Zoning can be seen clearly here in the plagioclase grains. The quartz grains are a dark, light and reddish brown CL color with microfractures. A magnified image (10x) of the quartz shows that the grains have a brownish-red CL color with a brighter red fractures (Figure 6.6).

6.4. Sample EB08A (N 38°22'55.8" E 27°39'40.7")

The typical corroded core seen in the plagioclase grains is uncommon in EB08A Turgutlu samples, but is still seen in a few of the minerals (Figure 6.7). The grains with the non-corroded cores are still highly fractured (Figures 6.7-6.12). The fractures have a brownish-green CL color and the cores that are corroded are yellow-green. Most of these fractures are crosscutting and a few appear to run parallel to each other. Zoning is seen in some of the larger plagioclase grains, which are outlined by dashed lines. The k-feldspar grains in the EB08A samples are dark blue (Figure 6.7). These k-feldspar grains have fractures that are brownish-green or black CL color. A few of the grains have dark blue rims with a lighter blue core (Figure 6.12). The reddish blue CL color can be identified along some of the Turgutlu EB08A k-feldspar and plagioclase grain boundaries, which indicate that fluids may have infiltrated the cracks along these grain boundaries (Figures 6.7-6.12) (Finch and Klein, 1999). Myrmekite is replacing many of the k-feldspar grains. Quartz grains are dark, light and reddish-brown and contain fractures with a brighter

reddish brown CL color (Figure 6.7). A few of these fractures are cross cutting (Figure 6.7).

6.5. Sample EB09A (N 38°22’55.1” E 27°39’41.5”)

Within the Turgutlu samples k-feldspar is not observed, which is typically seen in the Salihli and EB06 and EB08A Turgutlu granites. Non-corroded cores are seen in the Turgutlu plagioclase grains (Figures 6.13-6.17). The few grains that are corroded are yellow-green in color. The non-corroded cores of the plagioclase grains have a medium green CL color with brownish-green to dark green rims. Plagioclase rims within the granites are thin and highly fractured. Most of the plagioclase grains are highly fractured which have a brownish-green CL color and appear to run parallel to each other. Myrmekites are also not present in these granties (Figures 6.13-6.17). The quartz grains in the EB09A Turgutlu samples are brown and light brown, which could indicate two generations of quartz. Some of the smaller quartz grains are light brown with brighter red rims. These quartz grains are fractured and these fractures have a lighter brown CL color.

6.6. Conclusions

With the use of cathodoluminescence it has been revealed that the Salihli and Turgutlu granites have experience a multistage tectonic history with episodes of mineral growth and brittle deformation. Fluid interaction is apparent through the dull color at grain boundaries, the change from blue to a reddish CL color in the k-feldspar, anastomosing pathways and myrmekite. Recrystallization and grain boundary migration is seen in the Salihli and Turgutlu samples as the plagioclase intrudes the k-feldspar.

Plagioclase is replacing feldspar, which is seen by the presence of myrmekites and left-over grains. CC20 quartz grains show evidence of deformation lamellae, and shattered cores of plagioclase grains. Overgrowths are seen in the EB09A Turgutlu samples. Throughout most of the samples the plagioclase rims are revealed to have been affected by reaction textures. These rims vary in texture, size, and color. The CL documents multiple stages of brittle deformation, both at depth and at lower temperatures near the surface as the occurred along the detachment in pulses.

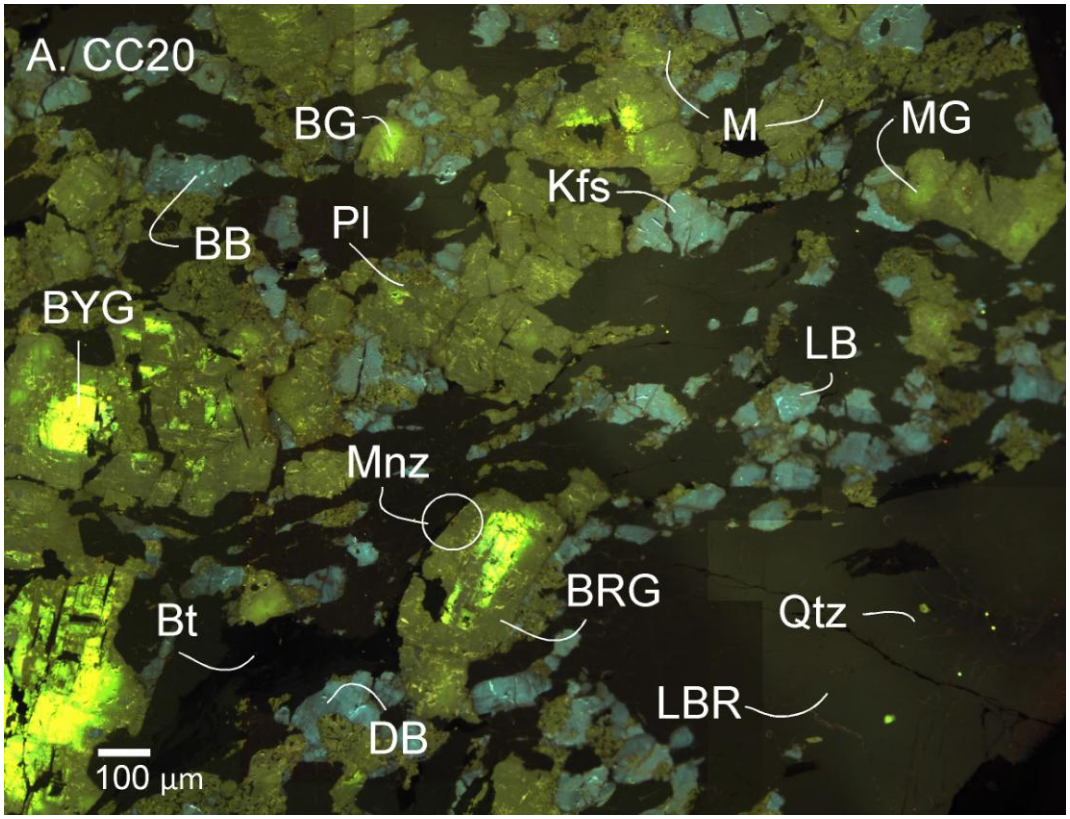

Figure 6.1. (A) CL image of the Salihli granite. Abbreviations of minerals after Kretz (1983); Qtz= quartz, Pl= plagioclase, Bt= biotite, Kfs= k-feldspar, and Mnz= monazite. Other abbreviations; BG= bright green, MG= medium green, DG= dark green, LB= light blue, DB= dark blue and M= myrmekite.

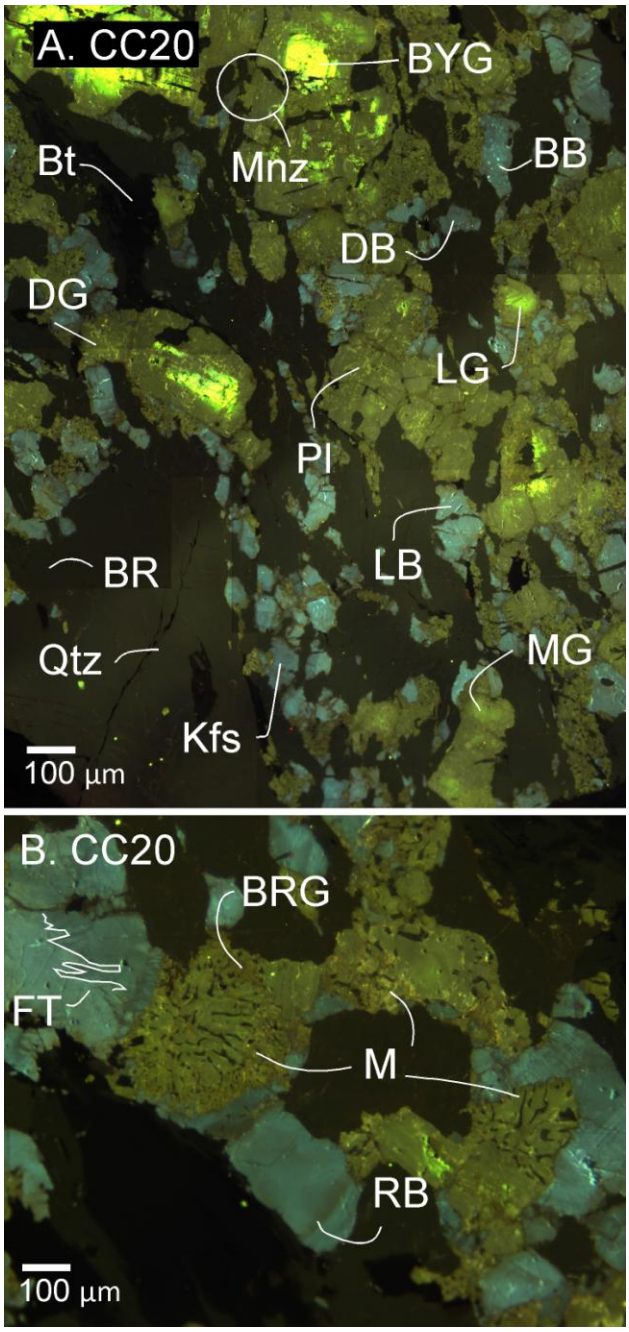

Figure 6.2. CL image of the Salihli granite. Abbreviations are the same as Figure 6.1. (A) Image shows the plagioclase with bright green cores. (B) CL image of the Salihli granite at 10x. Magnified image show myrmekites, plagioclase and k-feldspar.

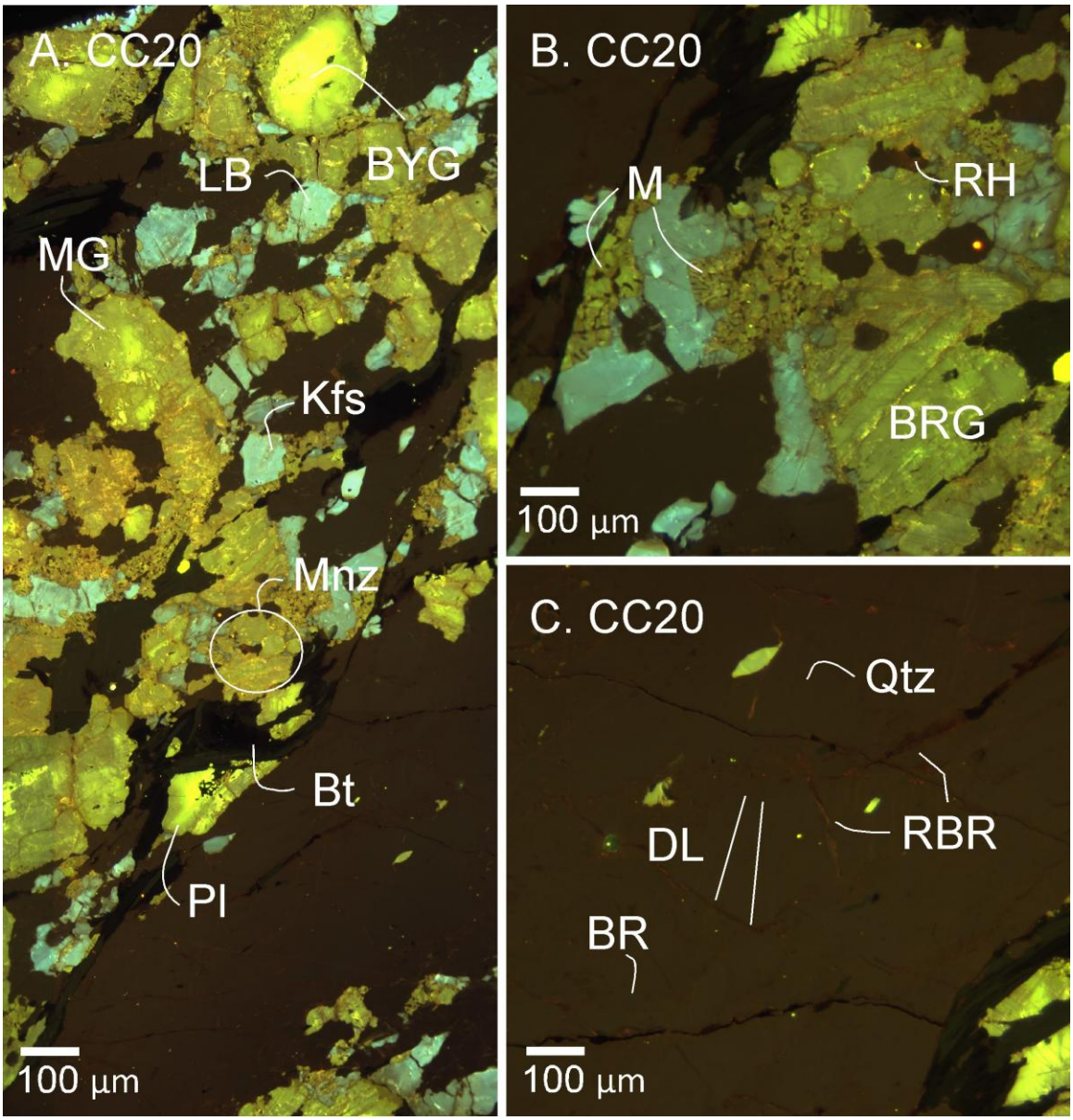

Figure 6.3. CL image of the Salihli granite. (A) Abbreviations are the same as Figure 6.1, with the exception of MB= medium blue. (B) CL image of Salihli granite at 10x. Magnified image shows myrmekites, k-feldspar and RH= radiation halo. (C) CL image of Salihli granite at 10x. Magnified image shows deformation lamellae and fractures.

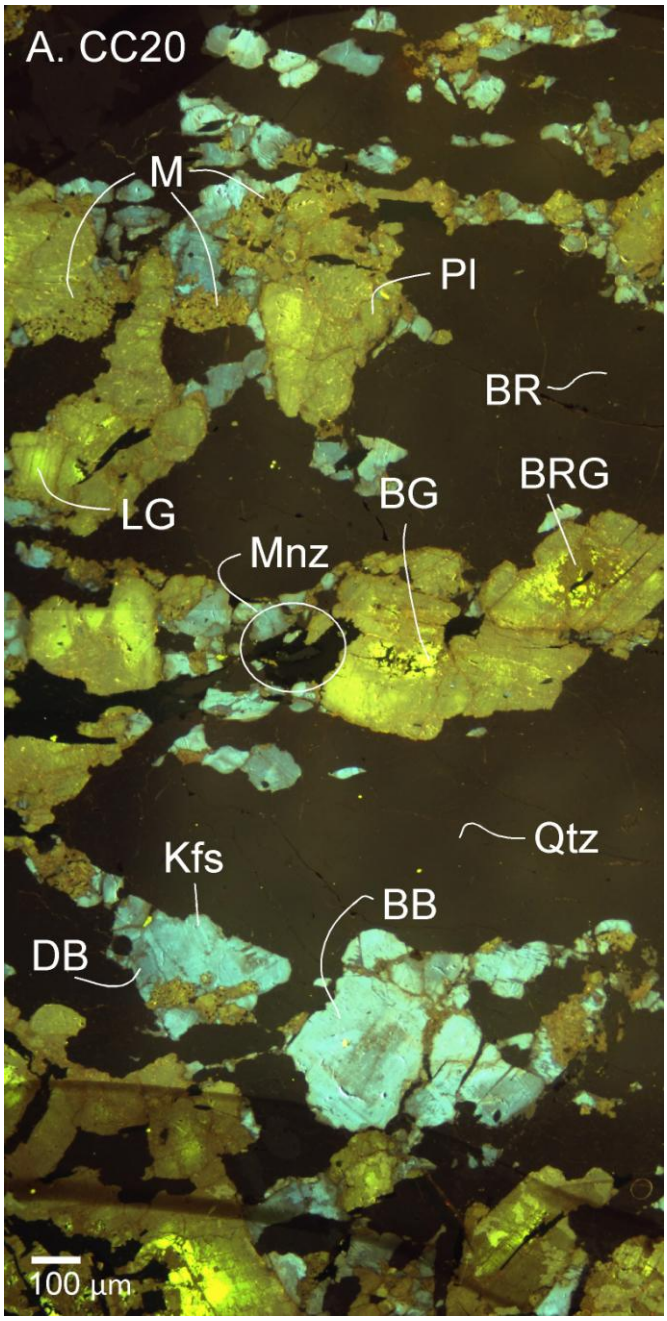

Figure 6.4. CL image of the Salihli granite. Abbreviations are the same as Figure 6.1, with the exception of BB= bright blue. Image shows plagioclase with corroded cores and the replacement of k-feldspar with plagioclase.

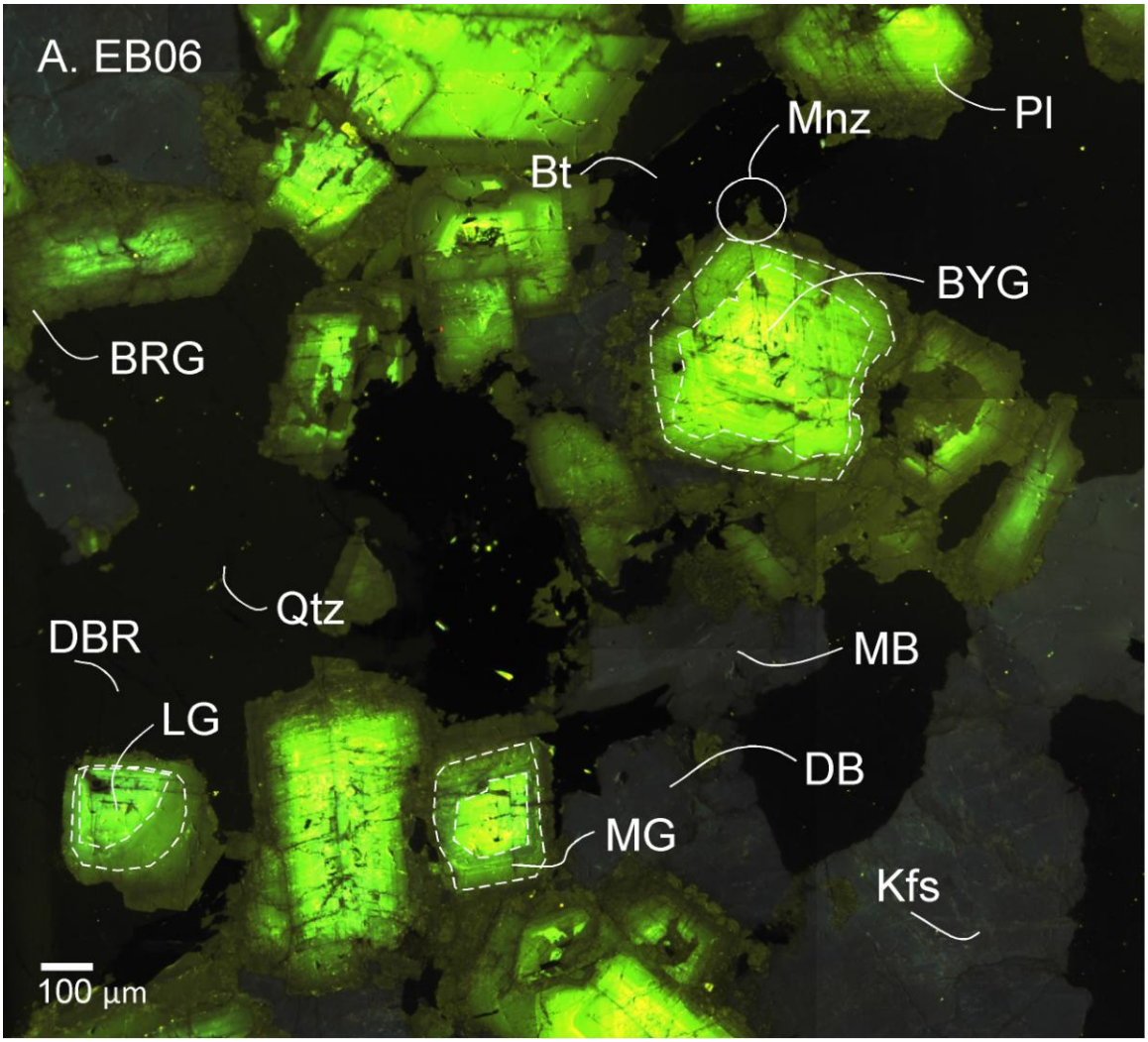

Figure 6.5. CL image of the Turgutlu granite. Abbreviations are the same as Figure 6.1, with the exception of MG= medium green. Imaging shows zonation in the plagioclase.

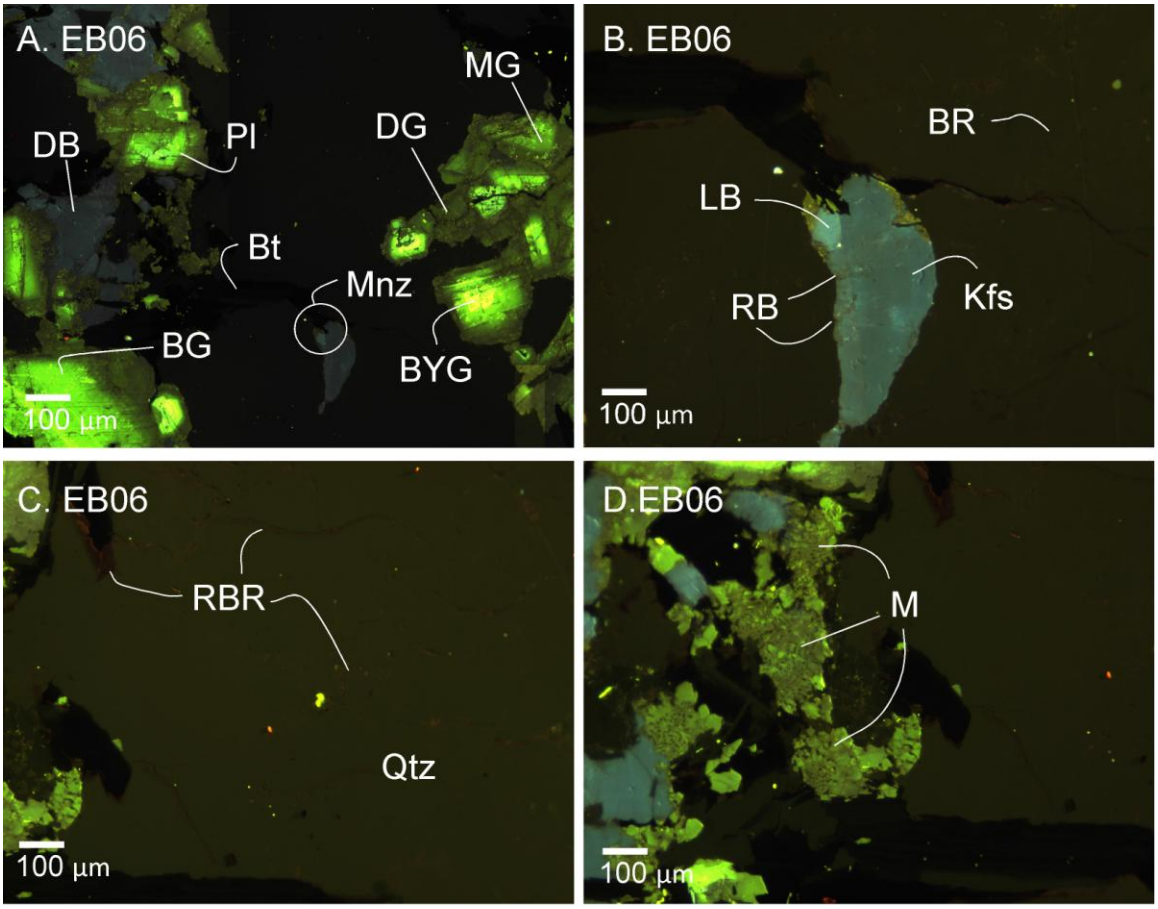

Figure 6.6. CL image of the Turgutlu granite. Abbreviations are the same as Figure 6.1. (A) CL image of granite shows plagioclase with zonation and non-corroded cores. (B) CL image of Turgutlu granite at 10x. Image shows k-feldspar, plagioclase, quartz and biotite. (C) CL image of Turgutlu granite at 10x. Image shows quartz, and fractures within the quartz. (D) CL image of Turgutlu granite at 10x. Image shows myrmekite.

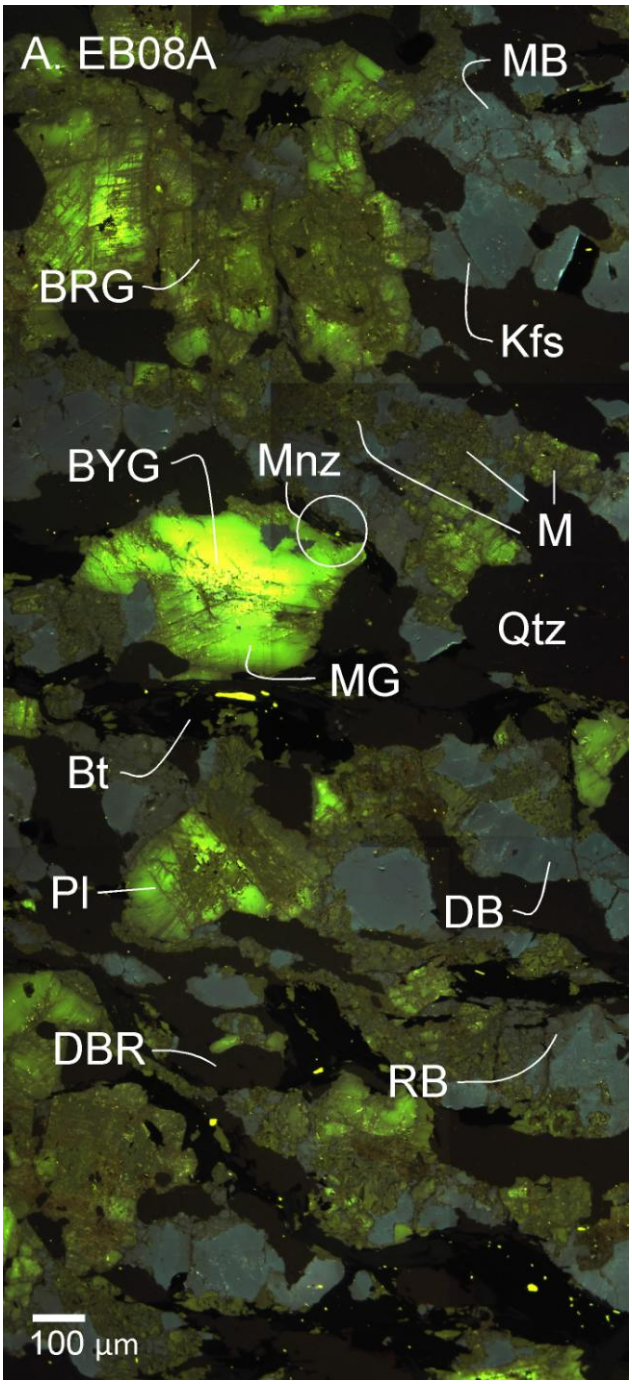

Figure 6.7. CL image of the Turgutlu granite. Abbreviations are the same as Figure 6.1.

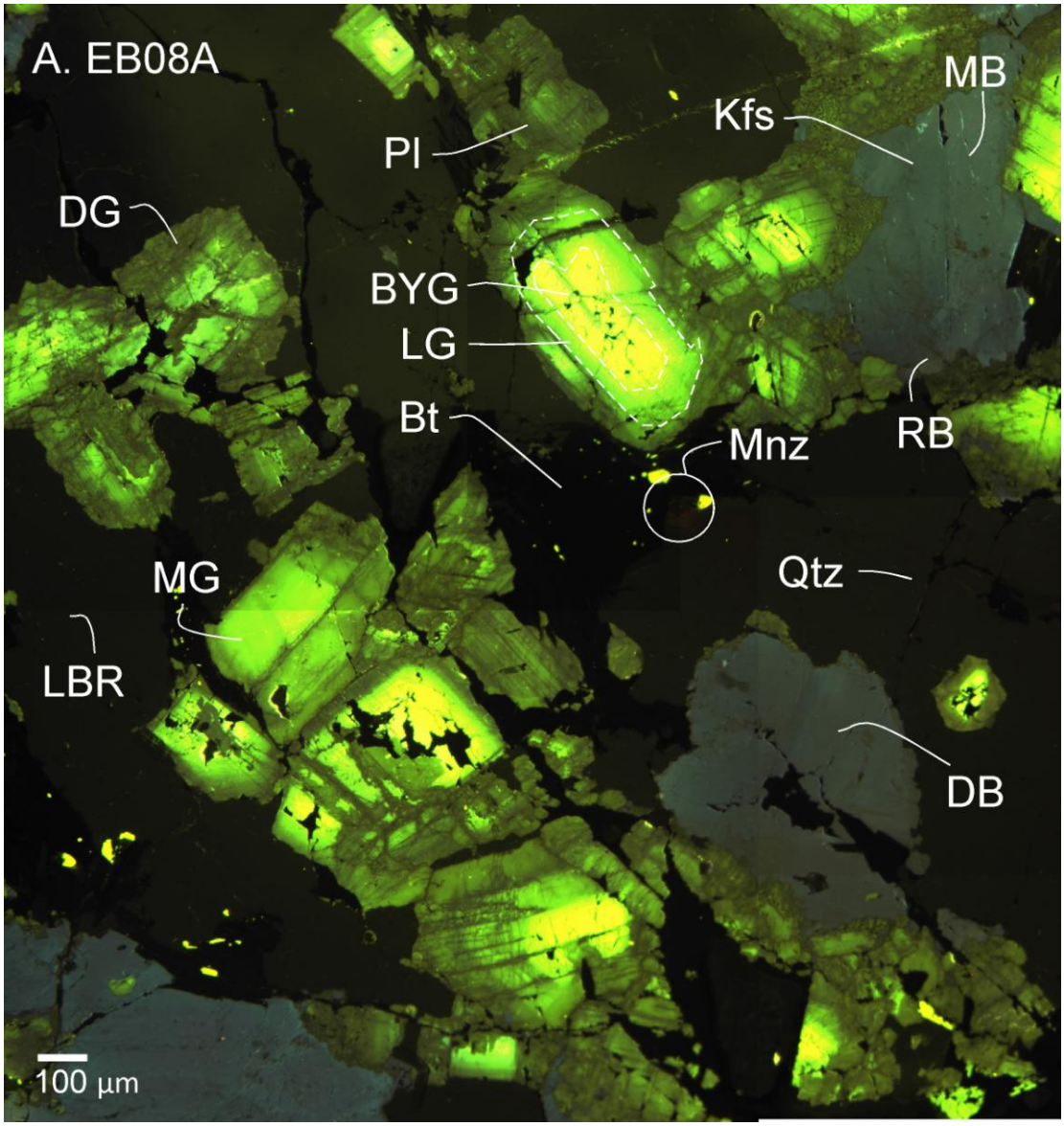

Figure 6.8. CL image of the Turgutlu granite. Abbreviations are the same as Figure 6.1.

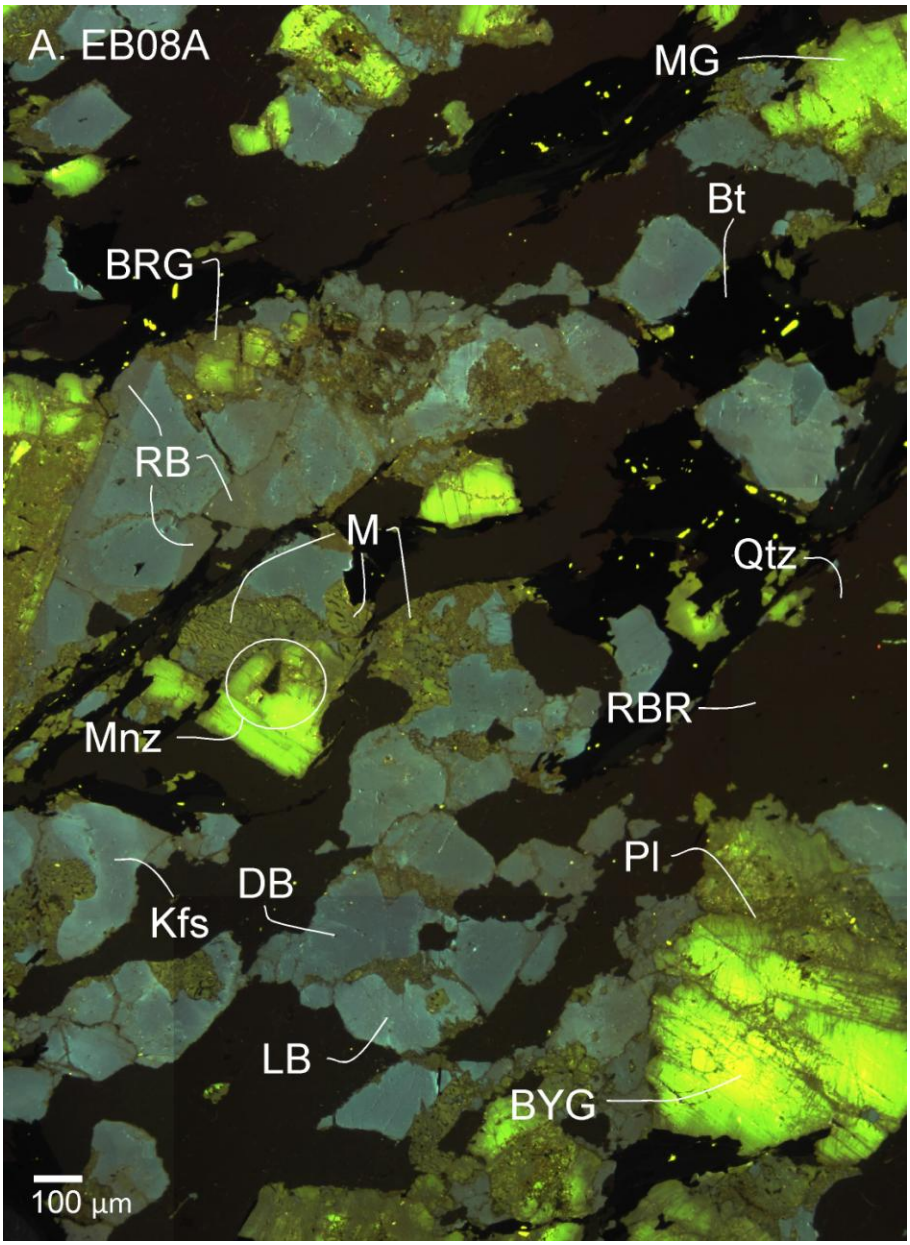

Figure 6.9. CL image of the Turgutlu granite. Abbreviations are the same as Figure 6.1.

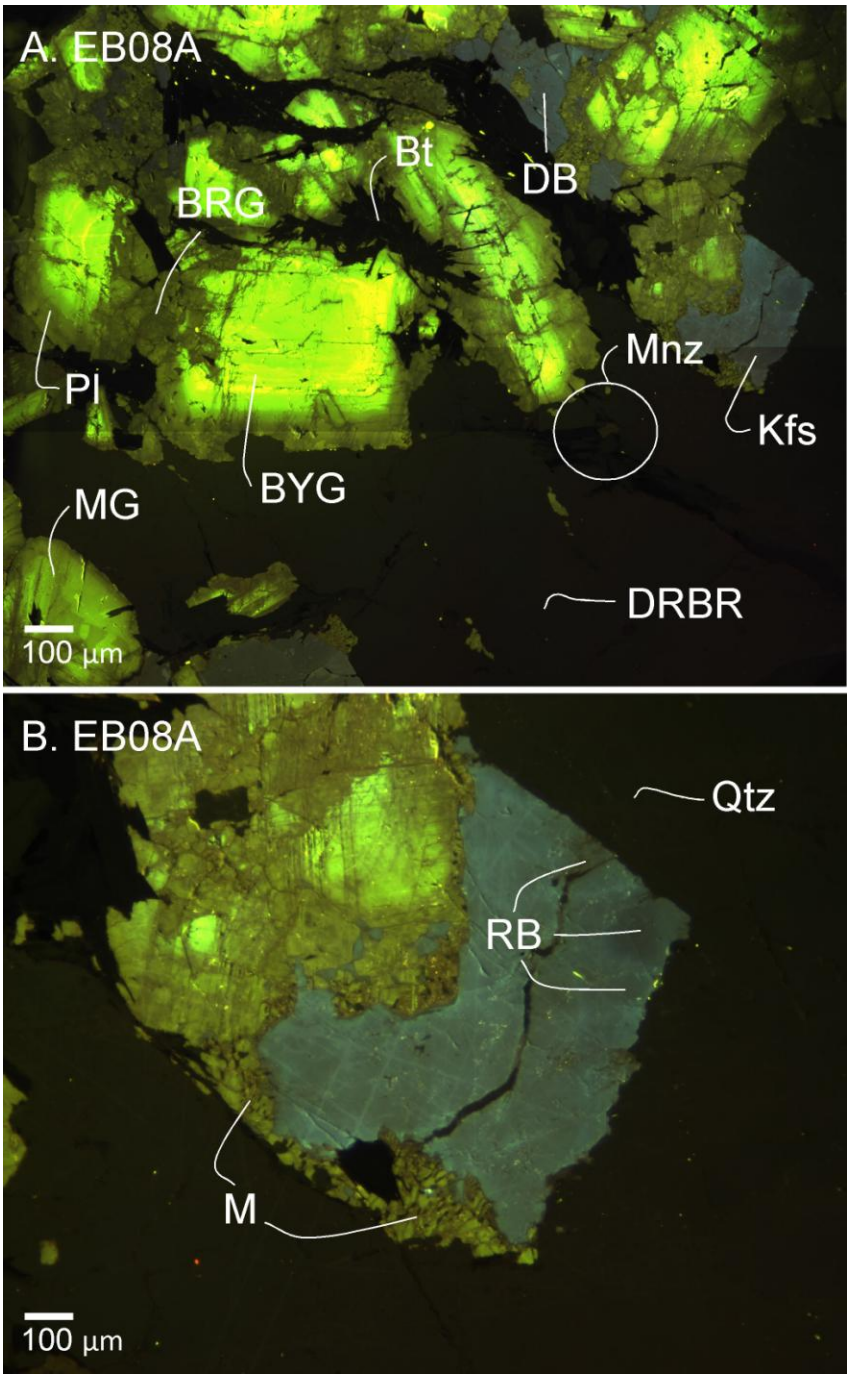

Figure 6.10. CL image of the Turgutlu granite. Abbreviations are the same as Figure 6.1. (A) CL image shows zonation in the plagioclase. (B) CL image of the Turgutlu granite at 10x. Image shows k-feldspar, plagioclase, and myrmekites around the k-feldspar

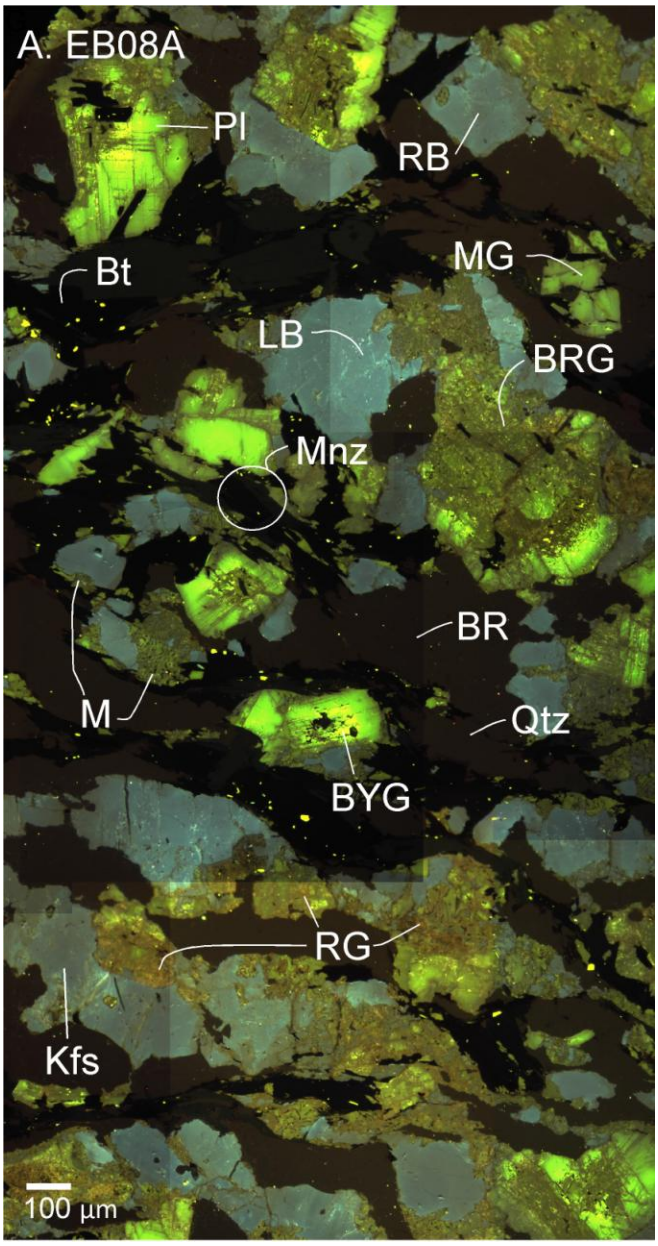

Figure 6.11. CL image of the Turgutlu granite. Abbreviations are the same as 6.1. Image shows large monazite located in plagioclase surrounded by myrmekite.

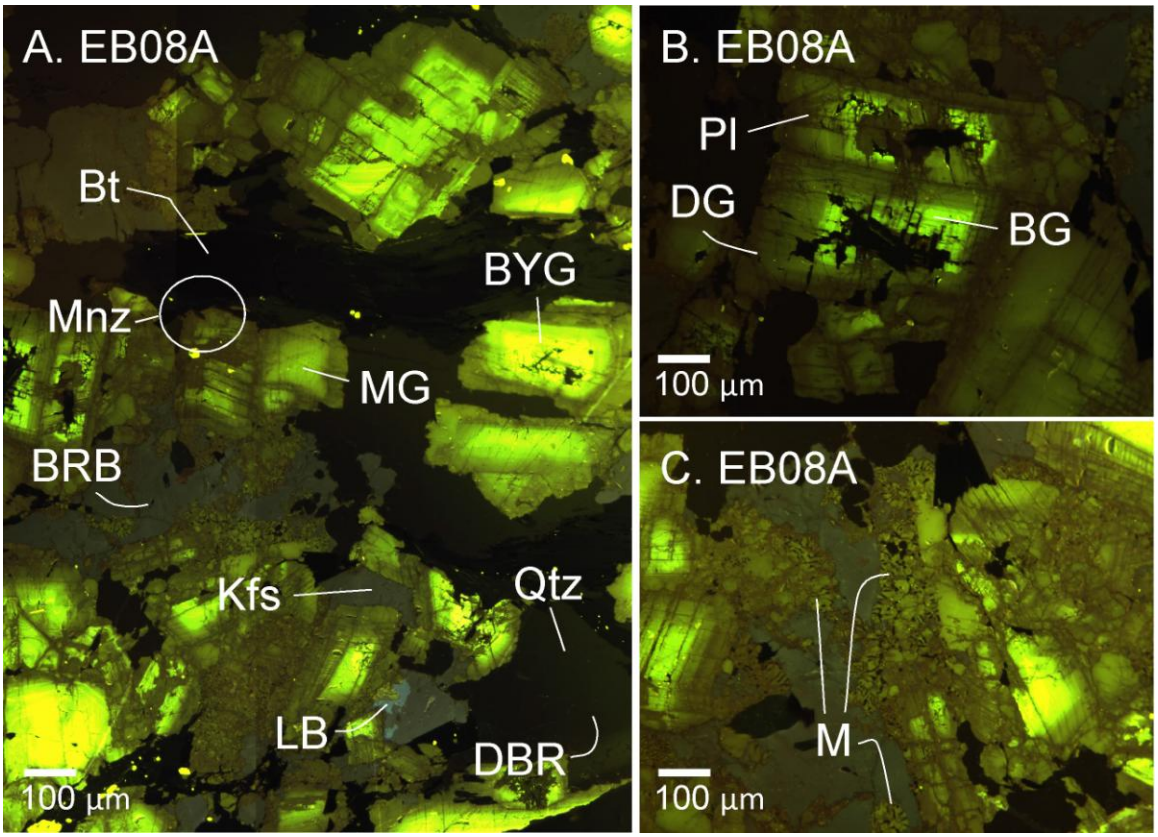

Figure 6.12. CL image of Turgutlu granite. Abbreviations are the same as 6.1. (A) Image of Turgutlu granite. (B) CL image of Turgutlu granite at 10x. Image shows plagioclase with corroded core and dashed line represents zonation in the plagioclase grain. (C) CL image of Turgutlu granite at 10x. Image shows myrmekites.

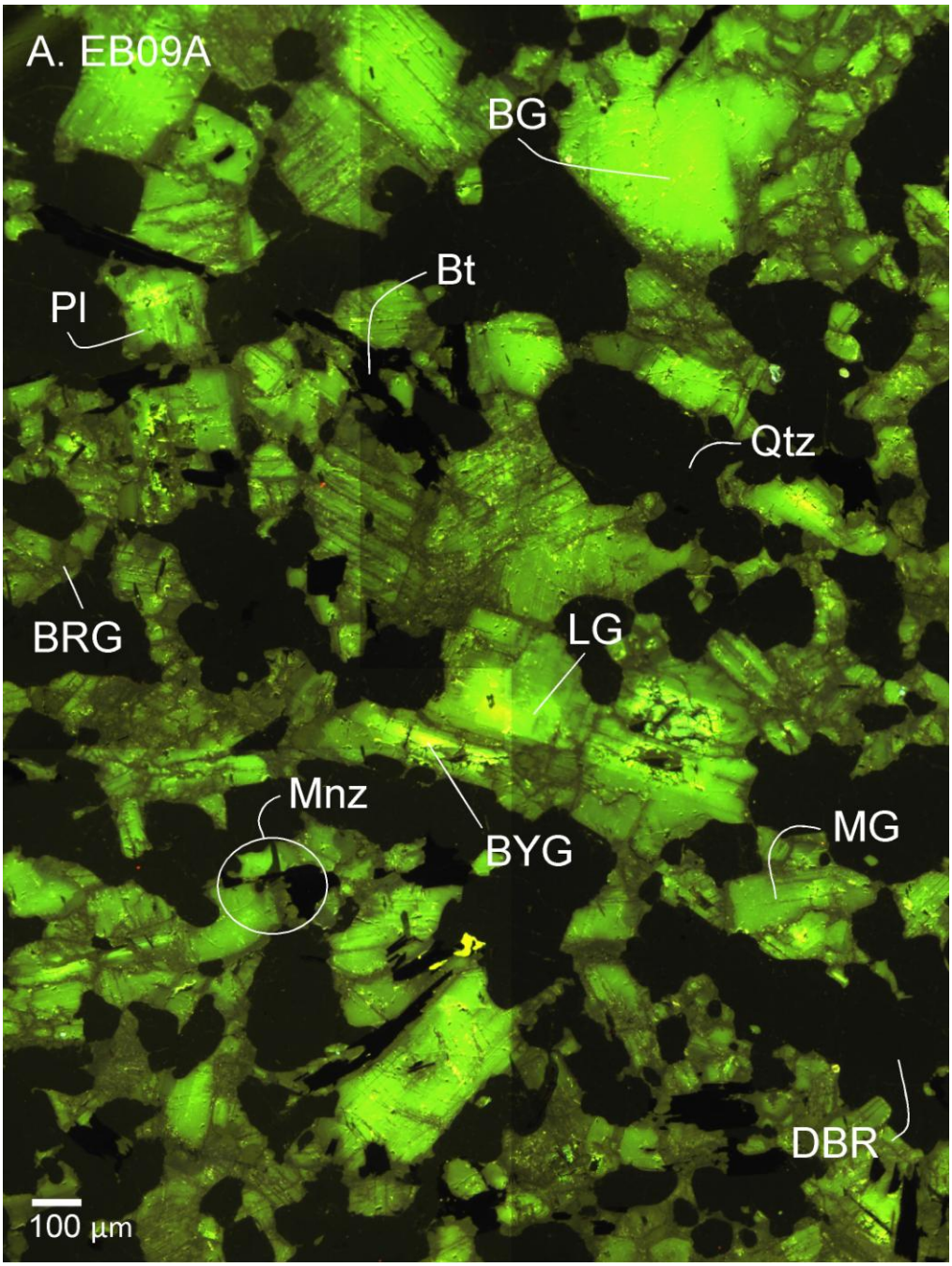

Figure 6.13. CL image of Turgutlu granite. Abbreviations are the same at 6.1. Image of Turgutlu granites shows no k-feldspar present and little or no corroded cores in the plagioclase.

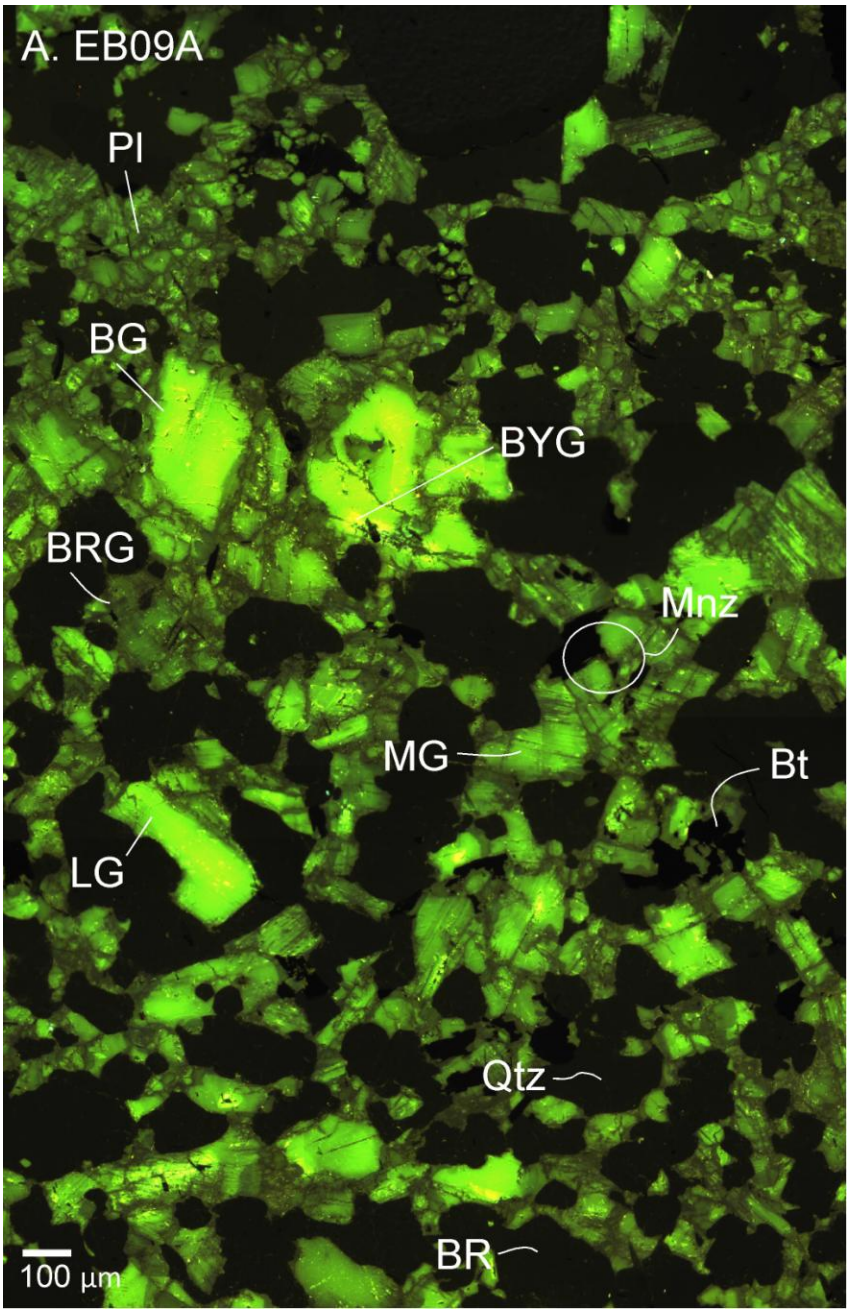

Figure 6.14. CL image of the Turgutlu granite. Abbreviations are the same as Figure 6.1. Image of Turgutlu granite shows no k-feldspar present and little or no corroded cores in the plagioclase.

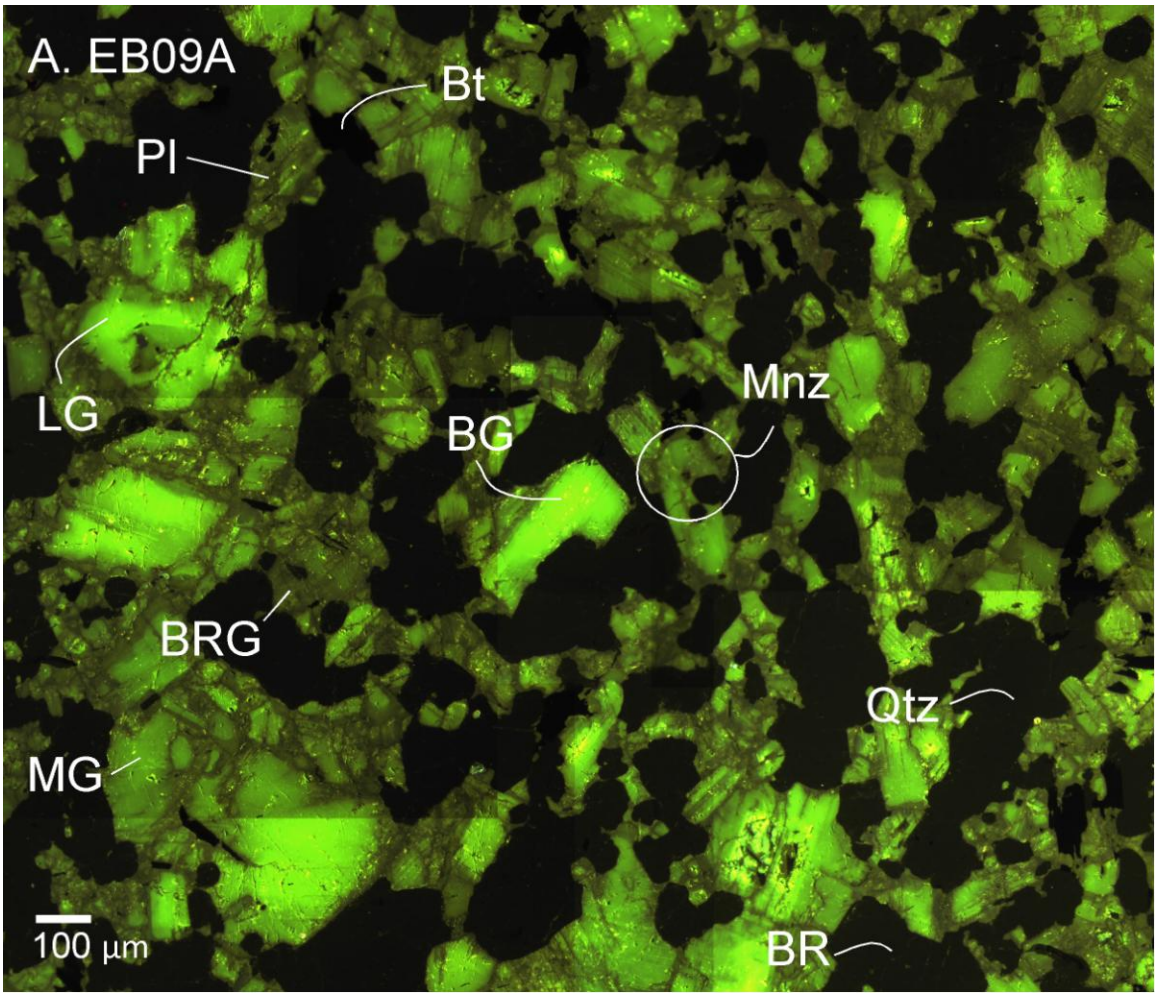

Figure 6.15. CL image of the Turgutlu granite. Abbreviations are the same as Figure 6.1. Image of Turgutlu granite shows no k-feldspar present and no corroded cores in the plagioclase.

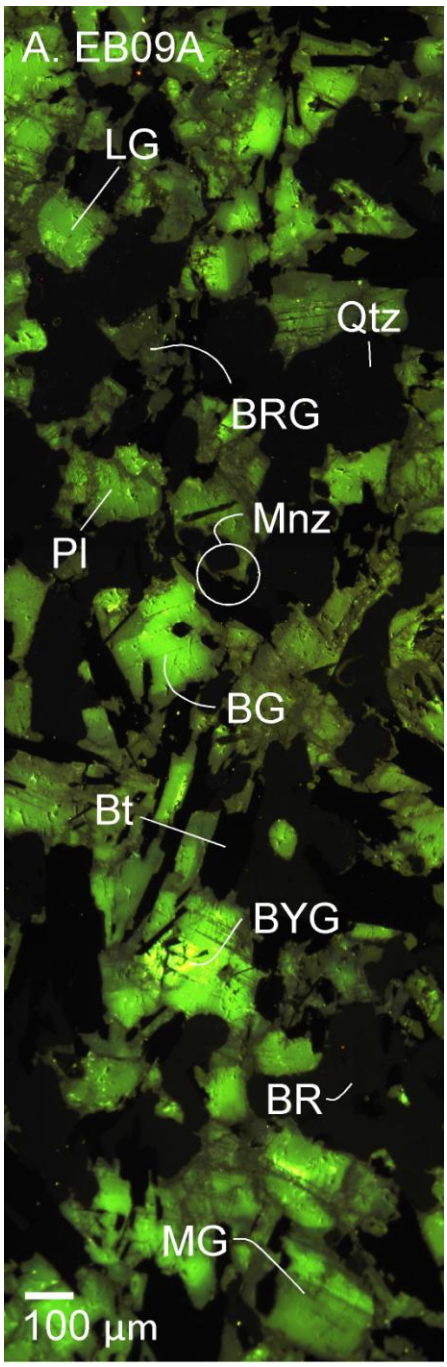

Figure 6.16. CL image of the Turgutlu granite. Abbreviations are the same as Figure 6.1. Image of Turgutlu granite shows no k-feldspar present and little or no corroded cores in the plagioclase.

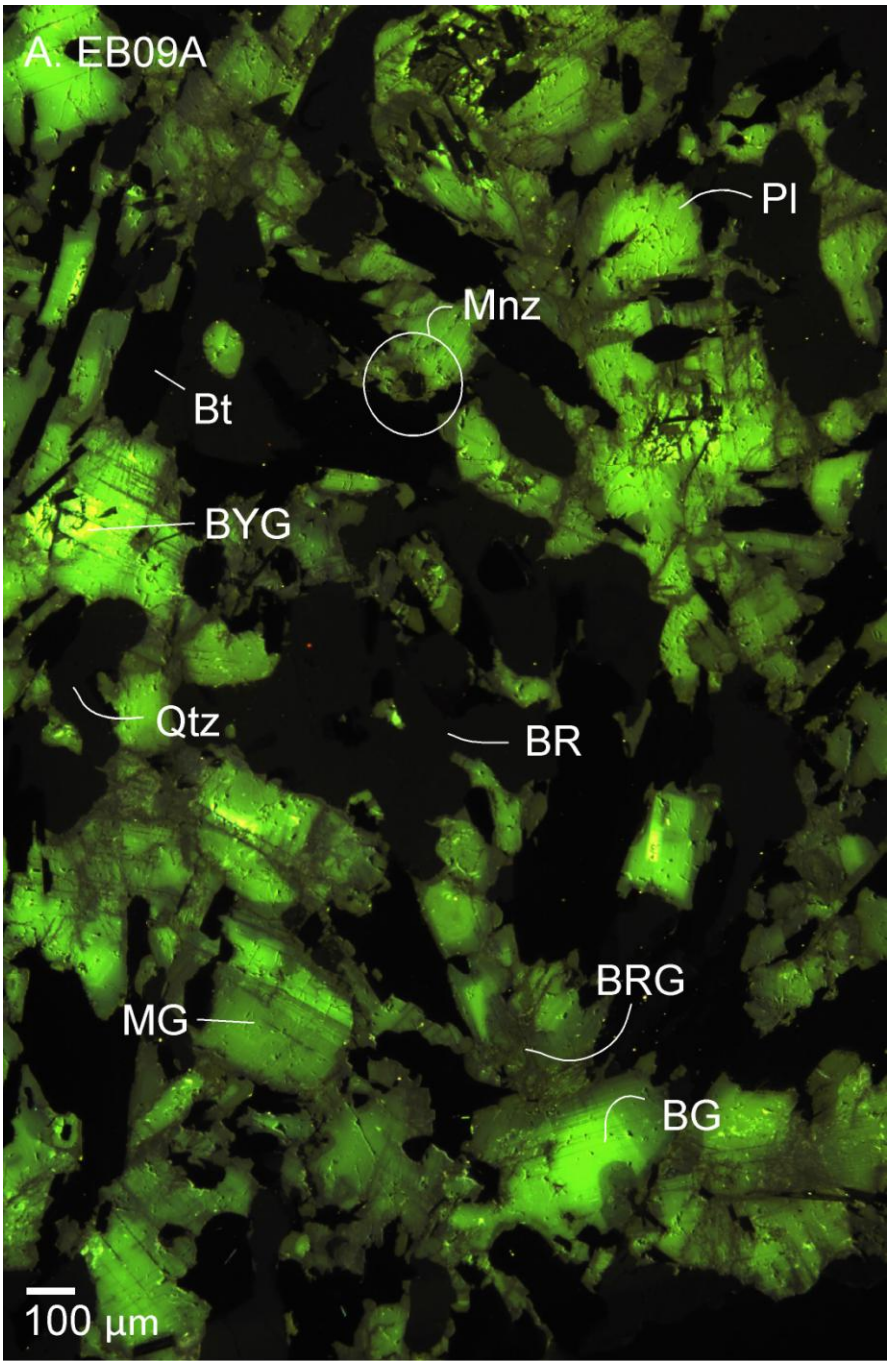

Figure 6.17. CL image of the Turgutlu granite. Abbreviations are the same as Figure 6.1. Image of Turgutlu granite shows no k-feldspar present and no corroded cores in the plagioclase.

CHAPTER VII

TIMING AND MODE OF EXTENSION IN THE MENDERES MASSIF

7.1. Introduction

Geochemical and geochronological data from the Menderes Massif can discriminate between the various proposed models for large-scale extension in the Aegean region. The s-type peraluminous granites (Salihli and Turgutlu) were possibly generated as the Eastern Mediterranean seafloor subducted along the Hellenic trench (Figure 1.1). The three proposed models that are thought to explain the tectonic evolution of the Menderes Massif include 1.) lateral extrusion/tectonic escape, 2.) back arc spreading, and 3.) orogenic collapse. Studies have shown that the initiation of extension in the tectonic escape model occurred around 5 Ma (Dewey and Sengor, 1979; Bozkurt and Sozbilir, 2004) and an intermediate age of 12 Ma is applied to the initiation of back arc spreading as subduction along the Hellenic arc shifted southwest (McKenzie, 1978; Meulenkamp et al., 1998). As stated in Chapter 1 subduction may have occurred around 26 Ma during the late Miocene (McKenzie, 1978; Le Pichon and Angelier, 1979; Le Pichon and Angelier, 1981; Jackson and McKenzie, 1988; Meulenkamp et al., 1988; Spakman et al., 1988; Seyitoglu and Scott, 1996). The final model orogenic collapse has

an older initiation age of 20 Ma after the Eocene thickening subsided (Dewey, 1988; Seyitoglu and Scott, 1992). Although the Salihli and Turgutlu granites share many similar characteristics, they likely evolved from compositionally distinct magma sources. Understanding the timing of movement within the Menderes Massif has important implications for our understanding of the mantle-scale processes that drive extension in the Aegean. Data reported in this study can be used to help identify the tectonic model that best explains the evolution from compressional to extensional processes. Th-Pb isotope dating of in-situ monazites provide critical data to decipher the complex set of processes that have resulted in the exhumation of the Aegean metamorphic complexes.

7.2. Salihli and Turgutlu Magma Sources

A series of discrimination diagrams were created both with geochemical data from the Salihli and Turgutlu granites (this study) and data from previous studies (Delaloye and Bingol, 2000; Glodny and Hetzel, 2007; Catlos et al., 2008) to identify magma sources and gain insight into the tectonic evolution of the granites and their relationship with each other (de la Roche et al., 1980). While discrimination diagrams can be useful, they do rely on the assumption that the trace element geochemistry of the rocks has not been significantly affected by post-crystallization alteration reactions (Pearce et al., 1984; Twist and Harmer, 1987). Geochemical data presented in Chapter 4 showed that both granites formed in a volcanic arc setting, experienced fractional crystallization and, moreover, that these two granites were derived from two compositionally-distinct sources. For example, the Salihli samples generally contain allanite [$A_2M_3Si_3O_{12}(OH)$] as

the main accessory mineral, with the exception of sample CC20, while the Turgutlu samples contain monazite [(CeTh)PO_4].

CL imagery demonstrated that these two granites experienced a similar deformation history. For example, the CL images from the Salihli and Turgutlu granites show secondary alteration textures and multiple episodes of deformation. However, despite these similarities in deformation mechanics, REE systemactics indicate that the Salihli granites were likely exposed to slightly higher temperatures during their evolution as compared to most of the Turgutlu samples. This is seen in the higher degree of flattening of the REE pattern which could be an indication of higher temperatures of metamorphic recrystalization (Bea and Montero, 1999). The only exception is Turgutlu sample EB09 **(**Figures 6.13-6.17). EB09 was collected from the western portion of the study area and has a flatter chondrite normalized REE pattern that is more similar to the Salihli samples.

7.3. Geochronological results and the tectonic evolution of the Menderes Massif

Monazite is a useful tool for geochronology studies because it is stable over a wide range of pressure-temperature conditions. Monazite ages can thus be important pieces of data when constraining tectonic models in a region, since they can record the timing of wide range of processes, with only small errors arising from the resetting of ages by dissolution-reprecipitation reactions along a retrograde path (Seydoux-Gullaume, et al., 2002; Catlos et al., 2009). Salihli sample CC20 contains monazite in the matrix and in the rims of plagioclase grains. Such spatial relationships suggest that the monazite formed relatively late in the crystallization sequence. Monazite is impervious to Pb loss

(Cocherie and Legendre, 2007; Catlos et al., 2009). If it is assumed that this is true for the Salihli granites, then their monazite ages constrain the last episode of plagioclase growth in the rock to 9.6±1.5 Ma, based on a monazite crystal located in the rim of a plagioclase grain in sample CC20. Thus, this ages likely times the latest episode of deformation in the rock rather than crystallization. Another monazite found in Salihli sample CC20 yields three different ages (21.7±4.5 Ma, 16.0±1.6 Ma, and 11.6±2.3 Ma). These ages reflect reprecipitation/dissolution reactions which indicate the presence of chemically reactive fluids.

A monazite from Turgutlu sample EB08A has a very young age of 11.5±0.8 Ma. This monazite is located in the rim of a feldspar grain close to encroaching mrymekite (Figure 6.9). The formation of mrymekite may be from igneous crystallization, solid state exsolution, progressive or retrograde metamorphism, metasomatism or even as a result of complicated deformation mechanisms (Zachar and Toth, 2001). However, the origin of the mrymekite texture has been the focus of much debate (Zachar and Toth, 2001). The young age and the presence of mrymekite is a further indication of fluid infiltration which reset the monazite age. These ages are similar to the youngest determined for the Salihli samples. Taken together, the petrology and dates also indicate fluid flow and the occurrence of late-stage chemical reactions. The source of these fluids (e.g. hydrothermal versus meteoric waters) cannot be determined with the dataset in the current study. However, fluid flow was most likely triggered as these granites were exhumed along the Alaşehir detachment These results cannot, however, distinguish between the proposed models: subduction, collision and orogenic collapse, and lateral extrusion along strike-

slip faults (Pichon and Angelier, 1979; Sengor and Yilmaz, 1981; Sengor et al., 1985; Meulenkamp et al., 1988; Dewey, 1988; Seyitoglu and Scott, 1996; Cemen et al., 1999).

7.4. Conclusions

The geochemical and geochronological data indicate that the Salihli and Turgutlu granites formed in a compressional regime from north-dipping subduction of the Eastern Mediterranean floor along the Hellenic trench. These two granites differ in their source, period and number of tectonic events, degree of alteration and interaction with fluids, and their P-T history. Differences in accessory minerals (allanite versus monazite) indicated that these granites were generated from compositionally distinct magma sources. Cathodoluminescence data indicates that the two granites experienced similar deformation histories after crystallization, which is apparent with the presence of secondary alteration textures, generations of mineral growth and multiple episodes of deformation. Data (ages, CL imagery, and geochemistry) collected from the monazites in the Salihli and Turgutlu granites for this study has been reported here and indicate consistency with extension initiating in the Menderes Massif due to subduction roll back. However, problems do arise in linking the ages from the granites to a specific tectonic event due to presence of complex textures, generations of mineral growth, and multiple episodes of deformation.

CHAPTER VIII

CONCLUSION

Several analytical techniques including electron microprobe, ion microprobe and cathodoluminescence have been used to understand the growth history of the Salihli and Turgutlu granites in the Menderes Massif. These granites have a complicated growth history, which has been constrained by the CL and geochemical data. Understanding the growth history of the Salihli and Tugutlu granites further constrains the complicated tectonic history of the Menderes Massif. The data obtained in this thesis shows:

1. Both Salihli and Turgutlu samples are are peraluminous- S-type rocks.
2. The majority of the Salihli samples are granodiorites and the majority of the Turgutlu samples are granites.
3. The Salihli granodiorites are magnesian and the Turgutlu granites are ferroan.
4. Turgutlu granites are alkali-calcic and calcic-alkalic, whereas the Salihli samples are clacic.
5. All samples can be considered volcanic-arc granites, and are enriched in Rb, Th, U, Ta, Nb, Hf, and Y and depleted in Ba, Sr, P, Zr, and Ti (Brown et al., 1984).

6. Geochemical data suggests that the Salihli and Turgutlu granites generated from different sources, which can be seen by the differences in their accessory minerals (ie., allanite found in Salihli samples and Monazite found in Turgutlu samples).

7. Monazite ages suggest that the Menderes Massif has undergone multiple stages of deformation. CL images indicates that the two granites experienced similar deformation histories after crystallization, which is apparent with the presence of secondary alteration textures, generations of minerals growth and multiple episodes of deformation.

8. The abundant ~15 Ma ages recorded by these granites (Glodny and Hetzel, 2007) likely time the crystallization of the monazite grain in this rock, but the ages, however, may be affected by dissolution-reprecipitation reactions.

9. The average of all the Salihli and Turgutlu monazites date is 15.0±2.8 Ma (MSWD=3.8).

10. Data including the Th-Pb ages, CL imagery and geochemical data collected from the Salihi and Turgutlu granites for this study has been reported here and indicate a consistency with extension initiating in the Menderes Massif due to subduction roll back.

11. However problems do arise in linking the ages from the granites to a specific tectonic event due to the presence of complex textures, generations of mineral growth, and multiple episodes of deformation.

REFERENCES

Akkok, R., 1981, Metamorphic conditions of gneisses and schists from Menderes massif, Alasehir-Manisa: Bull Geol Soc Turkey, v. 24, pp. 11-20.

Aksu, A.E., Piper, D.J.W., Konuk, T., 1987, Quarternary growth patterns of Buyyuk Menderes and Kucuk Menderes deltas, western, Turkey: Sedimentary Geology, v. 52, pp. 227-250.

AlDahan, A.A., 1988, Low temperature alterations in granititc rocks from the Siljian Ring structure, central Sweden: Springer-Verlag, v. 1, pp. 209-216.

Aleinikoff, J.N., Wintsch, R.P., Fanning, C.M., and Dorais, M.J., 2002, U-Pb geochronology of zircon and polygenetic titanite from the Glastonbury Complex, Connecticut, USA: An integrated SEM, EMPA, TIMS, and SHRIMP study: Chemical Geology, v. 188, pp. 125-147.

Altunkaynak, S., 2007, Collision-driven slab breakoff magmatism in Northwestern Anatolia, Turkey: The Journal of Geology, v. 115, pp. 63-82.

Arculus, R.J., 1987, The significance of source versus process in the tectonic controls of magma genesis. In: Tectonic controls on magma chemistry, Weaver, S.D., and Johnson, R.W. (eds.), Journal of Volcanology and Geothermal Research, v. 32, pp. 1-12.

Avigad, D., and Garfunkel, Z., 1991, Uplift and exhumation of high-pressure metamorphic terrains; the example of the Cycladic blueschist belt (Aegean Sea); Tectonophysics, v. 188, pp. 357-372.

Axen, G.J., and Bartley, J., 1997, Field tests of rolling hinges: Existence, mechanical types and implications for extensional tectonics: Journal of Geophysical Research, v. 102, pp. 20,515-20,537.

Ayers, J., Miller, C., Gorisch, B., and Milleman, J., 1999, Textural development of monazite during high-grade metamorphism: Hydrothermal growth kinetics, with implications for U, Th-Pb geochronology: American Mineralogist, v. 84, pp. 1766-1780.

Barka, A., 1997, Neotectonics of the Marmara regions, in Schindler, C., and Pfister, M., eds., Active tectonics of northwestern Anatolia: The Marmara Ploy-Project, a multidisciplinary approach by space-geodesy, geology, hydrogeology, geothermic and seismology: Zurich, Vdf Hochschulverlag AG an der ETH, pp. 55-87.

Bea, F., and Montero, P., 1999, Behavior of accessory phases and redistribution of Zr, REE, Y, Th and U during metamorphism and partial melting of metapelites in the lower crust; an example from the Kinzigite Formation of Ivrea-Verbano, NW Italy: Geochimica et Cosmochimica Acta, v. 63, pp. 1133-1153.

Bingol, E., Akyurek, B., Korkmazer, B., 1975, Geology of the Biga Peninsula and some characteristics of Karakaya Formation: International Geodynamics Project: report of Turkey.

Bonev, N., Stampfli, G., 2008, Petrology, geochemistry and geodynamic implications of Jurassic island arc magmatism as revealed by mafic volcanic rocks in the Mesozoic low-grade sequence, eastern Rhodope, Bulgaria: Lithos, v. 100, pp. 210-233.

Bonev, N., Burg, J., Ivanov, Z., 2006, Mesozic-Tertiary structural evolution of an extensional gneiss dome-the Kesebir-Kardamos dome, eastern Rhodope (Bulgaria-Greece): Int. J. Earth Sci., v. 93, pp. 318-340.

Boyanov, I., and Goranov, A., 2001, Late Alpine (Palaeogene) superimposed depressions in parts of southeast Bulgaria: Geologica Balcanica, v. 31, pp. 3-36.

Bozkurt, E., and Mittwede, S., 2001, Introduction to the geology of Turkey; a synthesis: International Geology Review, v. 43, pp. 578-594.

Bozkurt, E., and Oberhänsli, R., 2001, Menderes Massif (western Turkey): structural, metamorphic and magmatic evolution- a synthesis: Int. J. Earth Sci., v. 89, pp. 679-708.

Bozkurt, E., and Park, R.G., 1997a, Microstructures of deformed grains in the augen gneisses of southern Menderes Massif (western Turkey) and their tectonic significance: Geol Rundsch, v. 86, pp. 103-119.

Bozkurt, E., and Park, R.G., 1997b, The extensional evolution of the central Menderes Massif as a metamorphic core complex in western Anatolia, Turkey: Abstracts with programs, Geological Society of America, v. 29, pp. 318.

Brown, G.C., Thrope, R.S., and Webb, 1984, The geochemical characteristics of granitoids in contrasting arcs and comments on magma sources: Journal Geological Society of London, v. 141, pp. 411-426.

Broska, I., and Siman, P., 1998, The breakdown of monazite in the West-Carpathian Veporic orthogneisses and Tatric granites: Geologica Carpathica, Bratislava, v. 49, pp. 161-167.

Broska, I., Petrik, I., and Williams C.T., 2000, Coexisting monazite and allanite in peraluminous granitoids of the Tribec Mountains, Western Carpathians: American Mineralogist, v. 85, pp. 22-32.

Buick, I.S., 1991, The late Alpine evolution of an extensional shear zone, Naxos, Greece: Journal of the Geological Society, London, v. 148, pp. 93-103.

Burg, J-P., Ricou, L-E., Ivanov, Z., Godfriaux, I., Dimov, D., and Klain, ?L., 1996, Syn-metamorphic nappe complex in the Rhodope Massif, structure and kinematics: Terra Nova, v. 8, pp. 6-15.

Burt, D.M., 1989, Compositional and phase relations among rare earth element minerals: Reviews in Mineralogy, v. 21, pp. 259-307.

Bozkurt, E., and Park, R.G., 1994, Southern Menderes Massif: an incipient metamorphic core complex in western Anatolia, Turkey: Journal of the Geological Society, London, v. 151, pp. 213-216.

Broska, I., and Uher, P., 2001, Whole rock chemistry and genetic typology of the western Carpathian Variscan granites: Geol. Carpath., v. 52, pp. 79-90.

Campbell, H.K., Craddock, J.P., Klein, T.H., 2003, Calcite twinning constraints on Alpine nappe emplacement, Hellenic Arc, Crete, Greece: Abstracts with programs, Geological Society of America, v. 35, pp. 31.

Candan, O., and Kun, N., 1991, Possible Pan-African metavolcanics in the Odemis Submassif of the Menderes Massif, western Turkey: Bulletin of the Mineral Research and Exploration Institute of Turkey, v. 112, pp. 1-16.
Catlos, E.J., Gilley, L.D., and Harrison, M.T., 2002, Interpretation of monazite ages obtained via in situ analysis: Chemical Geology, v. 188, pp. 193-215.
Catlos, E.J., Dubey, C.S., Harrison, T.M., and Edwards, M.A., 2004, Late Miocene movement within the Himalayan Main Central Thrust shear zone, Sikkim, north-east India: Journal of Metamorphic Geology, v. 22, pp. 207-226.
Catlos, E.J., and Çemen, I., 2005, Monazite ages and the evolution of the Menderes Massif, western Turkey: Int. J. Earth Sci., v. 94, pp. 204-217.
Catlos, E.J., Baker, C.B., Cemen, I., and Ozerdem, C., 2008, Whole rock major element influences on monazite growth: examples from igneous and metamorphic rocks in the Menderes Massif, western Turkey: Mineralogia, v. 38, pp. 5-18.
Catlos, E.J., Baker, C.B., Sorensen, S.S., Cemen, I., Hancer, M., 2009, Geochemistry, geochronology, and cathodoluminescence imagery of the Salihli and Turgutlu granites (central Menderes Massif, western Turkey): Implications for Aegean tectnoics, Tectonophysics, doi:10.1016/j.2009.06.001.
Çemen, I., Göncüoglu, C., and Dirik, K., 1999, Structural evolution of the Tuzgölü Basin in Central Anatolia, Turkey: The Journal of Geology, v. 107, pp. 693-706.
Çemen, I., Catlos, E.J., Göğüs, O., Özerdem, C., 2006, Postcollisional extensional tectonics and exhumation of the Menderes massif in the Western Anatolia extended terrane, Turkey: Geological Society of America, Special Paper, pp. 353-379.
Cemen, I., Gonguoglu, M.C., Erler, A., Kozlu, H., and Perincek, D., 1993, Identation tectonics and associated lateral extrusion in east, southeast, and central Anatolia: Abstracts with programs, Geological Society of America, v. 25, pp. 116-117.
Chappell, B.W., and White, A.J.R., 1974, Two contrasting granite types: Pacific Geology, v. 8, pp. 173-174.
Cherniak, D.J., Watson, E.B., Grove, M., and Harrison, T.M., 2004, Pb diffusion in monazite: A combined RBS/SIMS study: Geochimica et Cosmochimica Acta, v. 68, pp. 829-840.
Compston, W., Williams, I.S., and Meyer, C.E., 1984, U-Pb geochronology of zircons from lunar breccia 73217 using a sensitive high mas-resolution ion microprobe: Journal of Geophysical Research, v. 89, pp. 525-534.
Cox, R.A., Dempster, T.J., Bell, B.R., and Rogers, G., 1996, Crystallization of the Shap Granite: evidence from zoned k-feldspar megacryst: . Geol. Soc., London, v. 153, pp. 625-635.
Cuney, M., and Friedrich, M., 1987, Physicochemical and crystal-chemical controls on accessory mineral paragenesis in granitoids: implications for uranium metallogenesis: Bull. of Mineral., v. 110, pp. 235-247.
Delaloye, M., Bingöl, E., 2000, Granitoids from Western and Northwestern Anatolia: Geochemistry and modeling of geodynamics evolution: International Geology Review, v. 42, pp. 241-268.
De St. Jorre, L., and Smith, D.G.W., 1988, Cathodoluminescence Ga-en-riched feldspars from the Thor Lake rare-metal deposits, NW Territories, Canada: Can. Mineral, v. 26, pp. 301-308.

De La Roche, H., Leterrier, J., Grande Claude, P., and Marchal, M., 1980, A classification of volcanic and plutonic rocks using R1 and R2 diagrams and major element analysis: Its relationship to and current nomenclature: Chemical Geology, v. 29, pp. 183-210.

Del Moro, A., Innocenti, F., Kyriakopoulos, C., Manetti, P., and Papadopoulous, P., 1988, Tertiary granitoids from Thrace (northern Greece): Sr isotopic and petrochemical data: N. Jb. Miner. Abh., v. 159, pp. 113-135.

Dilek, Y., and Moores, E.M., 1990, Regional tectonics of the Eastern Mediterranean ophiolites, in Malpas, J., Moores, E.M., Panayiotou, A., and Xenophonotos, C., (eds.), Ophioites, oceanic crustal analogues: Nicosia, Cyprus, The Geological Survey Department, Proceedings of the Symposium, "Troodos 1987", pp. 295-309.

Dilek, Y., Thy, P., Hacker, B., and Grundvig, S., 1999, Structure and petrology of Tauride ophiolites and mafic dike intursions (Turkey): Implications for the Neo-Tethyan ocean: Bulletin of the Geological Society of America, v. 111, pp. 1192-1216.

Dilek, Y., 2006, Collision tectonics of the Mediterranen region: causes and consequences: Geological Society of America, Special Paper, pp. 1-13.

Dilek, Y., Altunkaynak, S., 2007, Cenozoic crustal evolution and mantle dynamics of post-collisional magmatism in western Anatolia: International Geology Review, v. 49, pp. 431-453.

Dinter, D.A., 1998, Late Cenozoic extension of the Alpine collisional orogen, northeastern Greece: origin of the north Aegean basin: Geol. Soc. Amer. Bull., v. 110, pp. 1208-1230.

Dewey, J.F., and Sengor A.M.C., 1979, Aegean and surrounding regions: complex multiplate and continuum tectonics in a convergent zone: Geol.Soc. Am. Bull., v. 90, pp. 84-92.

Dewey, J.F., 1988, Extensional collapse of orogens: Tectonics, v. 7, no. 6, pp. 1123-1139.

Dora, O.O., Candan, O., Durr, S., and Oberhansli, R., 1995, New Evidence of the geotectonic evolution of the Menderes Massif. In: Piskin, O., Ergun, M., Savascin, M.Y., Tarcan, G., (eds.) Proc Int Earth Sci Colloquium on the Aegean Region 1995, Izmir, Turkey, v. 1, pp. 53-72.

Durr, S., Altherr, R., Keller, J., Okresch, M., and Seidel, E., 1978, The median Aegean crystalline belt: Stratigraphy, structure, metamorphism, magmatism: In: Closs, H., Roeder, D., and Schmidt, K. (eds.), Alps Aooeninnes, Hellenides, Schweizerbart. Stuttgart, v. 537, pp. 564.

Erdoğan, B., and Güngör, T., 2004, The problem of the core-cover boundary of the Menderes Massif and emplacement mechanism for regionally extensive gneissic granites, western Anatolia (Turkey): Turkish Journal of Earth Sciences, v. 13, pp. 15-36.

Finger, F., Krenn, E., Riegler, G., Romano, S., and Zulauf, G., 2002, Resolving Cambrian, Carboniferous, Permian , and Alpine monazite generations in the polymetamorphic basement of eastern Crete (Greece) by means of the electron microprobe: Terra Nova, v. 14, pp. 233-240.

Fassoulas, C., Kilias, A., and Mountrakis, D., 1994, Postnappe stacking extension and exhumation of high-pressure/low-temperature rocks in the island of Crete, Greece: Tectonics, v. 13, no. 1, pp. 127-138.

Fedo, C.M., Young, G.M., Nexbitt, H.W., and Hanchar, J.M., 1997, Potassic and sodic metasomatism in Southern Province of the Candian Shield; evidence from the Paleoproterozoic Serpent Formation, Huronian Supergroup, Canada: Precambrian Research, Elsevier: Amsterdam, International, v. 84, pp. 17-36.

Frost, B.R., Barnes, G.C., Collins, W.J., Arculus, R.J., Ellis, D.J., and Frost, C.D., 2001, A geochemical classification for granitic rocks: Journal of Petrology, v. 42, no. 11, pp. 2033-2048.

Finch, A.A., and Klein, J., 1999, The causes and petrological significance of cathodoluminescence emissions from alkali feldspar: Contrib Mineral Petrol, v. 135, pp. 234-243.

Finger, F., Broska, I., Roberts, M.P., and Schermaier, A., 1998, Replacement of primary monazite by apatite-allanite-epidote coronas in an amphibolites facies granite gneiss from the eastern Alps.: Am. Mineral., v. 83, pp. 248-258.

Force, E.R., 1997, Geology and mineral resources of the Santa Catalina Mountains, southeastern Arizona, in Monographs in Mineral Science, Center for Mineral Resources, Tucson, AZ, v. 1, pp. 1-135.

Garcia, D., Pascal, M-L., and Rouz, J., 1996, Hydrothermal replacement of feldspars in igneous enclaves of the Velay granites and the genesis of myrmekites: Eur. J. Mineral., v. 8, pp. 703-717.

Gautier, P., and Brun, J-P., 1994, Ductile crust exhumation and extensional detachments in the central Aegean (Cyclades and Evvia Islands): Geodinamica Acta., v. 7, pp. 57-85.

Götze, J., Habermann, D., Kempe, U., Neuser, R.D., and Richter, D.K., 1999, Cathodoluminescence microscopy and spectroscopy of plagioclase from lunar soil: American Mineralogist, v. 84, pp. 1027-1032.

Goetze, J., Krbetschek, M.R., Habermann, D., and Wolf, D., 2000, High-resolution cathodoluminescence studies on feldspar minerals: In: Cathodoluminescence in Geoscience (M.Pagel et al., eds), pp. 245-250.

Greer, R.T., and Weber, J.N., 1968, Correlation of mineral luminescent phenomena: American Geophysical Union, v. 49, pp. 745.

Gessner, K., Ring, U., and Johnson, C., 2001, An Active bivergent rolling-hinge detachment system: Central Menderes metamorphic core complex in western Turkey: Geology, v. 29, no. 7, pp. 611-614.

Gilotti, J.A., and McClelland, W.C., 2005, Leucogranites and the time of extension in the East Greenland Caledonides: Journal of Geology, v. 113, pp. 399-417.

Gokten, E., Havzoğlu, T., and Şan, Ö., 2001, Tertiary evolution of the central Menderes Massif based on Structural investigations of metamorphic and sedimentary cover rocks between Salihli and Kiraz (western Turkey): Int. J. Earth Sci., v. 89, pp. 745-756.

Gorur, N., Oktay, F.Y., Seymen, I., and Sengor, A.M.C., 1984, Paleotetonic evolution of Tuzgolu basin complex, Central Turkey: In: Dixon, J.E., and Robertson, A.H.F., eds. The geological evolution of the Eastern Mediterranean. Spec. Publ. Geol. Soc., v. 17, London, Blackwell Scientific, pp., 81-96.

Glodny, J., and Hetzel, R., 2007, Precise U-Pb ages of syn-extensional Miocene intrusions in the central Menderes Massif, western Turkey: Geol. Mag., v. 144, pp. 235-246.

Gessner, K., Ring, U., Passchier, C.W., Hetzel, R., 2002, Disscusion on "Stratigraphic and metamorphic inversions in the central Menderes Massif: a new structural model", by Aral I. Okay: Int. J. Earth Sci., v. 91, pp. 168-172.

Greake, J.E., Walker, G., Telfer, D.J., Mills, A.A., and Garlick , G.F.J.,1973, Luminescence of lunar terrestrial and synthetic plagioclase caused by Mn^{2+} and Fe^{3+}: Geochem Cosmochim Acta, v. 3, pp. 181-189.

Harkovska, A., Yanev, Y., and Marchev, P., 1989, General features of the Paleogene orogenic mamgatism in Bulgaria: Geol. Balc., v. 19, pp. 37-72.

Hetzel, R., Romer, R.L., Candan, O., and Passchier, C.W., 1998, Geology of the Bozdag area, central Menderes massif, SW Turkey: Pan-African basement and Alpine deformation: Geol Rundsch, v. 87, pp. 394-406.

Hetzel, R., and Reischmann, T., 1996, Intrusion age of Pan-African augen gneisses in the southern Menderes Massif and the age of cooling after Alpine ductile extensional deformation: Geol. Mag., v. 133, pp. 565-572.

Hetzel, R., Ring, U., Akal, C., and Troesch, M., 1995a, Miocence NNE-directed extensional unroofing in the Menderes Massif, southwestern Turkey: Journal of the Geological Society, London, v. 152, pp. 639-654.

Hetzel, R., Passchier, C.W., Ring, U., and Dora, O.O., 1995b, Bivergent extension in orogenic belts: The Menderes Massif (southwestern Turkey): Geology, v. 23, pp. 455-458.

Harrison, T.M., McKeegan, K.D., LeFort, P., 1995, Detection of inherited monazite in the Manaslu leucogranites by 208Pb/232Th ion microprobe dating: Crystallization age and tectonic implications: Earth and Planetary Science Letters, v. 133, pp. 271-282.

Harrison, T.M., Grove, M., and Lovera, O.M., 1997, New insights into the origin of two contrasting Himalayan granite belts: Geology, v. 25, pp. 899-902.

Harrison, T.M., Grove, M., McKeegan, K.D., Coath, C.D., Lovera, O.M., and LeFort, P., 1999, Origin and emplacement of the Manaslu intrusive complex, Central Himalayan: J. Petrol., v. 40, pp. 3-19.

Harrison, T.M., Aikman, A., Holden, P., Walker, A.M., McFarlane, C., Rubatto, D., and Watson, E.B., 2005, Testing the Ti-in-zircon thermometer: Eos, Transactions, American Geophysical Union, v. 86, iss. 52.

Hopson, R.F., and Ramseyer, K., 1990, Cathodoluminescence microscopy of myrmekite: Geology, v. 18, pp. 336-339.

Hoskin, P.W.O., 2005, Trace-element composition of hydrothermal zircon and the alteration of Hadean zircon from the Jack Hills, Australia: Geochimica et Cosmochimica Acta, v. 69, pp. 637-648.

Işik, V., Seyitoğlu, G., and Çemen, I., 2003, Ductile-brittle transition along the Alasehir detachment fault and its structural relationship with the Simav detachment fault, Menderes massif, western Turkey: Tectonophysics, v. 374, pp. 1-18.

Işik, V., and Tekeli, O., 2001, Late orogenic crustal extension in the northern Menderes massif (western Turkey): evidence for metamorphic core complex formation: Int. J. Earth Sciences, v. 89, pp. 757-765.

Ilbeyli, N., Pearce, J.A., Thirlwall, M.F., and Mitchell, J.G., 2004, Petogenesis of collision-related plutonics in Central Anatolia, Turkey: Lithos, v. 72, pp. 163-182.

Jackson, J., and McKenzie, D., 1988, The realstionship between plate motions and seismic moment tensors and rates of active deformation in the Mediterranean and Middle East: Geophysical Journal, v. 93, pp. 45-73.

Janoušek, V., Bowes, D.R., Braithwaite, C.J.R., and Rogers, G., 2001, Microstructural and mineralogical evidence for limited involvement of a Hercynian high-K calc-alkaline intrusion: the Kozarovice granodiorite, Central Bohemian Pluton, Czech Republic Trans. R. Soc. Edinb: Earth Sci., v. 91, pp. 15-26.

Janoušek, V., Braithwaite, C.J.R., Bowes, D.R., and Gerdes, A., 2004, Magma-mixing in the genesis of Hercynian calc-alkaline granitoids: an integrated petrographic and geochemical study of the Sázava intrusion, Central Bohemian Pluton, Czech Republic: Lithos, v. 78, pp. 67-99.

Jolivet, L., Brun, J-P., Gautier, P., Lallemant, S., and Patriat, M., 1994, 3D-kinematics of extension in the Aegean region from the early Miocene to the Present, insights from the ductile crust: Bull. Soc. Geol. France, v. 165, pp. 195-209.

Kopp, O., 1981, Cathodoluminescence petrography a valuable tool for teaching and research: Journal of Geological Education, v. 29, pp. 108-113.

Koralay, O.E., Satir, M., and Dora, O.O., 1998, Geochronologic evidence of Triassic and Precambrian magmatism in the Menderes Massif, west Turkey: In: Third International Turkish Geology Symposium, Ankara, v. 285.

Katzir, Y., Avigad, D., Matthews, A., Garfunkel, Z., and Evans, B.W., 2000, Origin, HP/LT metamorphism and cooling of ophiolitic mélanges in southern Evia (NW Cyclades), Greece: J. Metamorphic Geol., v. 18, pp. 699-718.

Klein, T.H., Zulauf, G., Craddock, J.P., and Heidelbach, F., 2004, Metamorphic Tripolitza rocks on top of non-metamorphic sediments: consequences for the geological evolution of Crete. 10th International Congress of the Geological Society of Greece, pp. 15-17, Thessaloniki, Greece.

Katzir, Y., Avigad, D., Matthews, A., Garfunkel, Z., and Evans, B.W., 1999, Origin and metamorphism of ultrabasic rocks associated with a subducted continental margin, Naxos (Cyclades, Greece): J. Metamorphic Geol., v. 17, pp. 301-318.

Kilias, A., Fassoulas, C., and Mountrakis, D., 1994, Tertiary extensional of continental crust and uplift of Psiloritis metamorphic core complex in the central part of the Hellenic Arc (Crete, Greece): Geol. Rundsch., v. 83, pp. 417-430.

Peytcheva, I., Kostitsin, Y., Salnikova, E., von Quadt, A., Kamenov, B., and Klain, L., 1999, Alpine evolution of the magmatism is the West-Rhodopes: Rb-Sr and U-Pb isotope data: J. Conf. Abstr., v. 4, pp. 470.

Konak, N., 2002, The Geologic Map of Turkey: General Directorate of Mineral Research and Exploration. Izmir Area Map.

Kingsbury, J.A., Miller, C.F., Wooden, J.L., and Harrison, T.M., 1993, Monazite paragenesis and U-Pb systematic in rocks of the eastern Mojave Desert, California, USA: implications for thermochronometry: Chem. Geol., v. 110, pp. 147-167.

Kretz, R., 1983, Symbols for rock-forming minerals: American Mineralogist, v. 68, pp. 277-279.

Krohe, A., and Mposkos, E., 2002, Multiple generations of extensional detachments in the Rhodope Mountains (northern Greece): Blundell, D.J., Neubauer, F., von Quadt, A., (eds.), The Timing and Location of Major Ore Deposits in an Evolving Orogen: Geol. Soc. London Sp. Publ., v. 204, pp. 151-178.

Lee, D.E., and Dodge, F.C.W., 1964, Accessory minerals in some granitic rocks in California and Nevada as a function of calcium content: American Mineralogist, v. 49, pp. 1660-1669.

Le Pichon, X., and Angelier, J., 1979, The Hellenic arc and trench system: a key to the Neotectonic evolution of the eastern Mediterranean area: Tectonophysics, v. 60, pp. 1-42.

Le Pichon, X., and Angelier, 1981, The Aegean Sea: Phil. Trans. R. Soc. Lond., v. 300, pp. 357-372.

Leven, E.J., and Okay, A.I., 1996, Foraminifera from the exotic Permo-Carboniferous limestone blocks in the Karakaya Complex, northwest Turkey: Rivista Italiana Paleontologia e Stratigrafia, v. 102, pp. 139-174.

Liati, A., Gebauer, D., and Wysoczanski, R., 2002, U-Pb SHRIMP-dating of zircon domains from UHP garnet-rich mafic rocks and late pegmatoids in the Rhodope zone (N Greece); evidence for Early Cretaceous crystallization and Late Cretaceous metamorphism: Chemical Geology, v. 184, pp. 281-299.

Liati, A., 2005, Identification of repeated Alpine (ultra) high-pressure metamorphic events by U-Pb SHRIMP geochronology and REE geochemistry of zircon: the Rhodope zone of Northern Greece: Contrib. Mineral. Petrol., v. 150, pp. 608-630.

Lips, A.L.W., White, S.H., and Wijbrans, J.R., 2000, Middle-Late Alpine thermotectonic evolution of the Southern Rhodope Massif, Greece: Geodin. Acta., v. 13, pp. 281-292.

Lips, A.L.W., Cassard, D., Sözbilir, H., Yilmaz, H., and Wijbrans, J.R., 2001, Multistage exhumation of the Menderes Massif, western Anatolia (Turkey): Int. J. Earth Sciences, v. 89, pp. 781-792.

Liati, A., and Gebauer, D., 1999, Constraining the prograde and retrograde P-T-t path of Eocene HP rocks by SHRIMP dating of different zircon domains: inferred rates of heating, burial, cooling and exhumation for central Rhodope, northern Greece: Contrib. Mineral Petrol., v. 135, pp. 340-354.

Lister, G., Banga, G., and Feenstra, A., 1984, Metamorphic core complexes of cordilleran type in the Cyclades, Aegean sea, Greece: Geology, v. 12, pp. 221-225.

Loos, S., and Reischmann, T., 1999, The evolution of the southern Menderes Massif in SW Turkey as revealed by zircon dating: Journal of the Geological Society, London, v. 156, pp. 1021-1030.

Long, J.V.P., and Agrell, S.O., 1965, The cathodoluminescence of minerals in this section: Mineral Magazine, v. 34, pp. 318-326.

Leichmann, J., Broska, I., and Zachovalova, K., 2003, Low-grade metamorphic alteration of feldspar minerals: a CL study: Terra Nova, v. 15, pp. 104-108.

Long, J.V.P., and Agrell, S.O., 1965, The cathodoluminescence of minerals in this section: Mineralogical Magazine, v. 34, pp. 318-325.

Mariano, A.N., and Ring, P.J., 1975, Eu-activated cathodoluminescence in minerals: Geochim Cosmochim Act, v. 39, pp. 640-660.

Marshall, D.J., 1977, Suggested standards for the reporting of cathodoluminescence results: Journal of Sedimentary Research, v. 48, pp. 651-653.
Matter, A., and Ramseyer, K., 1985, Cathodoluminescence microscopy as a tool for procenance studies in sandstones. In: G.G. Zuffa (Editor), Provenance of Arenites. Reidel, Boston, pp. 191-211.
McKenzie, D., 1978, Active tectonics of the Alpine-Himalayan belt: the Aegean Sea and surrounding regions: Geophysical Journal of Royal Astronomical Society, v. 55, pp. 217-254.
Montel, J-M., 1993, A model for monazite/melt equilibrium and application to the generation of granitic magmas: Chem. Geol., v. 110, pp. 127-146.
Montel, J.M., Kornprobst, J., and Vielzeuf, D., 2000, Preservation of old U-Th-Pb ages in shielded monazite: example from the Beni Bousera Hercynian kinzigites (Morocco): J. Metamorphic Geol., v. 18, pp. 335-342.
Mora, C.I., and Ramseyer, K., 1992, Cathodoluminesscence of coexisting plagioclase, Boehls Butte anorthosite: CL activators and fluid flow path: American Mineralogist, v. 77, pp. 1258-1265.
Meldrum, J.E., Boatner, L.A., Weber, W.J., and Ewing, R.C., 1998, Radiation damage in zircon and monazite: Geochimica et Cosmochimica Acta, v. 62, pp. 2509-2520.
Meulenkamp, J.E., Wortel, M.J.R., Van Wamel, W.A., Spakman, W., and Hoogerduyn, S.E., 1988, On the Hellinic subduction zone and the geodynamic evolution of Crete since the late middle Miocene: Tectonophysics, v. 146, pp. 203-215.
Metcalfe, I., 1999, The ancient Tethys oceans of Asia: How many? How old? How deep? How wide?: UNEAC Asia paper, no. 1, pp. 1-9.
Murphy, M.A., and Harrison, T.M., 1999, Relationship between leucogranites and the Qomolangma Detachment in the Rongbuk Valley, South Tibet: Geology, v. 27, pp. 831-834.
Okay, A.I., Satir, M., Maluski, H., Siyako, M., Monie, P., Metzger, R., and Akyuz, S., 1996, Paleo- and Neo-Tethyan events in northwest Turkey: geological and geochronological constraints: In Tectonics of Asia (eds) Yin, A., and Harrison, M., pp. 420-41.
Okay, A.I., Siyako, M., and Burkan, K.A., 1991, Geology and tectonic evolution of the Biga peninsula, northwest Turkey: Bulletin Technical University of Istanbul, v. 44, pp. 191-256.
Okay, A.I., Tansel, İ., and Tüysüz, O., 2001, Obduction, subduction and collision as reflected in the Upper Cretaceous-Lower Eocene sedimentary record of western Turkey: Geol. Mag., v. 138, pp. 117-142.
Okay, A.I., and Satir, M., 2000, Coeval plutonism and metamorphism in a latest Oligocene metamorphic core complex in northwest Turkey:Geol. Mag., v. 5, pp. 495-516.
Oberhänsli, R., Monié, P., Candan, O., Warkus, F.C., Partzsch, J.H., and Dora, O.Ö., 1998, The age of blueschist metamorphism in the Mesozoic cover series of the Menderes Massif: Schweiz. Mineral Petrogr. Mitt., v. 78, pp. 309-316.
Oberhänsli, R., Candan, O., Dorra, O.Ö., and Dürr, St.H., 1997, Eclogites within the Menderes Massif/ western Turkey: Lithos, v., 41, pp. 135-150.
Okay, A.I., 2001, Stratigraphic and metamorphic inversions in the central Menderes Massif: a new structural model: Int. J. Earth Sciences, v. 89, pp. 709-727.

Overstreet, W.C., 1967, The geologic occurrence of monazite: Geological Survey of America Professional Papers, v. 530, pp. 1-327.
Pan, Y., 1997, Zircon- and monazite- forming metamorphic reactions at Manitouwadge, Ontario Can.: Mineral., v. 35, pp. 105-118.
Papanikolaou, D.J., and Demirtasli, E., 1987, Geological correlation between the Alpine segments of the Hellenides-Balkanies and Taurides-Pontides. In: Pre-Variscan and Variscan events in the Alpine-Mediterranean Mountain Belts, Flugel, H.W., et al., (eds.), Bratislava, Alfa Publishers, pp. 387-396
Pearce, K.A., Harris, N.B.W., and Tindle, A.G., 1984, Trace element discrimination diagrams for tectonic interpretation of granititc rocks: Journal of Petrology, v. 25, pp. 956-983.
Pickett, E.A., and Robertson, A.H.F., 1996, Formation of the Late Paleozoic-Early Mesozoic Karakaya Complex and related ophiolites in NW Turkey by Paleotethyan subduction-accretion: Journal of the Geological Society, London, v. 153, pp. 995-1009
Pidgeon, R.T., Nemchin, A.A., van Bronswik, W., Geisler, T., Meyer, C., Compston, W., and Williams, L.S., 2007, Complex history of a zircon aggregate from lunar breccias 73235: Geochimica et Cosmochimica Act, v. 71, pp. 1370-1381.
Ramseyer, K., Baumann, J., Matter, A., and Mullis, J., 1988, Cathodoluminescence colours of α-quartz: Mineralogical Magazine, v. 52, pp. 669-677.
Ramseyer, K., AlDahan, A.A., Collini, B., and Landström, O., 1992, Petrological modifications in granitic rocks from the Siljan impact structure: evidence from cathodoluminescence: Tectonophysics, v. 216, pp. 195-204.
Raouzaios, A., Lister, G.S., and Foster, D.A., 1996, Oligocene exhumation and metamorphism of eclogite-blueschists from the Island Sifnos, Cyclades, Greece: Abstracts-Geological Society of Australia, v. 41, pp. 358.
Rapp, R.P., Watson, E.B., 1986, Monazite solubility and dissolution kinetics; implications for the thorium and light rare earth chemistry of felsic magmas: Contrib. Mineral. Petrol., v. 94, pp. 304-316.
Reischmann, T., 1998, Pre-Alpine origin of tectonic units from the metamorphic complex of Naxos, Greece, identified by single zircon Pb/Pb dating: Bull. Geol. Soc. Greece, v. 3, pp. 101-111.
Robertson, A.H.F., and Mountrakis, D., (eds.), 2006, Tectonic Development of the Eastern Mediterranean Region: Geological Society, London, Special Publications, v. 260.
Rougvie, J.R., and Sorensen, S.S., 2002, Cathodoluminescence record of K-metasomatism in ash-flow tuffs: Grain-scale mechanisms and large-scale geochemical implications: Geological Society of America, v., 30, pp. 307-310.
Romano, S.S., Dörr, W., and Zulauf, G., 2004, Cambrian granitoids in pre-Alpine basement of Crete (Greece): evidence from U-Pb dating of zircon: Int. J. Earth Sci., v. 93, pp. 844-859.
Ricou, L-E., Burg, J-P., Godfriauz, I., and Ivanov, Z., 1998, The Rhodope and Vardar: the metamorphic and the olistostromic paired belts related to the Cretaceous subduction under Europe: Geodin. Acta., v. 11, pp. 285-309.
Ridley, J., 1984, Listric normal faulting and reconstruction of the synmetamorphic structural pile of the Cyclades. In: The Geological Evolution of the Eastern

Mediterranean, Dixon, J.E., and Robertson, A.H.F. (eds.), Geological Society Special Publication, v. 17, pp. 755-762.
Ring, U., Willner, A.P., Lackmann, W., 2001, Stacking of nappes with different pressure-temperature paths: an example from the Menderes nappes of western Turkey: American Journal of Science, v. 301, pp. 912-944.
Ring, U., Gessner, K., Güngör, T., and Passchier, C.W., 1999, The Menderes Massif of western Turkey and the Cycladic Massif in the Aegean—do they really correlate?: Journal of the Geological Society, London, v. 156, pp. 3-6.
Robertson, A.H.F., and Dixon, J.E., 1984, Introduction: aspects of the geological evolution of the Eastern Mediterranean: In: Robertson, A.H.F., and Dixon, J.E., (eds.), Tectonic Evolution of the Eastern Mediterranean: Geol. Soc. London, Sp Pub., v. 17, pp. 1-74.
Rollinson, H., 1993, Using Geochemical data: Evaluation, Presentation, Interpretation: John Wiley and Sons, Tottenham.
Royden, L., 1993, Evolution of retreating subduction boundaries formed during the continental collision: Tectonics, v. 12, pp. 629-638.
Rubatto, D., Williams, I.S., and Buick, I.S., 2001, Zircon and monazite response to prograde metamorphism in the Reynolds Range, central Australia: Contrib. Mineral. Petrol., v. 140, pp. 458-468.
Slaby, E., Götze, J., 2004, Feldspar crystallization under magma-mixing conditions shown by cathodoluminescence and geochemical modeling—a case study from the Karkonosze pluton (SW Poland): Mineralogical Magazine, v. 68, pp. 561-577.
Smith, J.V., and Stenstrom, R.C., 1965, Electron-excited luminescence as a petrologic tool: Journal of Geology, v. 73, pp. 627-635.
Sorensen, S.S., Harlow, G.E., and Rumble III, D., 2006, The origin of jadeitite-forming subduction-zone fluids: CL-guided SIMS oxygen-isotope and trace-element evidence: American Mineralogist, v. 91, pp. 979-996.
Satir, M., and Friedrichsen, H., 1986, The origin and evolution of the Menderes Massif, W-Turkey: A rubidium/strontium and oxygen isotope study: Geologische Rundschau, v. 75, pp. 703-714.
Seidel, M., and Theye, T., 1993, High pressure/ low temperature metamorphism in the external Hellenides (Crete, Peloponnese): Bull. Geol. Soc. Greece, v. 28, pp. 49-55
Seidel, M., Seidel, E., and Stöckhert, B., 2007, Tectono-sedimentary evolution of lower to middle Miocene half-graben basins related to an extensional detachment fault (western Crete, Greece): Terra Nova, v. 19, pp. 39-47.
Sippel, R.F., and Glover, E.D., 1965, Structures in carbonate rocks made visible by luminescence petrography: Science, v. 150, pp. 1283-1287.
Smith, H.A, aand Giletti, B.J., 1996, Lead diffusion in monazite: Geochimica et Cosmochimica Acta., v. 61, no. 5, pp. 1047-1055.
Smith, H.A., and Barreiro, B., 1990, Monazite U-Pb dating of staurolite grade metamorphism in pelititc schists: Contrib. Mineral Petrol., v. 105, pp. 602-615.
Sozbilir, H., 2001, Extension tectonics and the geometry of related macroscopic structures; field evidence from the Gediz detachment, western Turkey: Turkish Journal of Earth Sciences, v. 10, pp. 51-67.

Seyitoğlu, G.,and Scott, B.C., 1991, Late Cenozoic crustal extension and basin formation in west Turkey: Geol. Mag., v. 128, pp. 155-166.
Seyitoğlu, G., Scott, B.C., and Rundle, C.C., 1992, Timing of Cenozoic extensional tectonics in west Turkey: Journal of Geological Society, London, v. 149, pp. 533-538.
Seyitoğlu, G., Benda, L., and Scott, B.C., 1994, Neogene palynological and isotopic age data from Gordes basin, western Turkey: Newsletter on Stratigraphy, v. 31, pp. 133-142.
Seyitoğlu, G., and Scott, B.C., 1996, The cause of N-S extensional tectonics in western Turkey: tectonic escape vs. back-arc spreading vs. orogenic collapse: J. Geodynamics, v. 22, pp. 145-153.
Seyitoğlu, G., Çemen, I., and Tekeli, O., 2000, Extensional folding in the Alasehir graben, western Turkey: Journal of Geological Society, London, v. 157, pp. 1097-1100.
Seyitoğlu, G., Tekeli, O., Çemen, I., Sen, S., and Isik, V., 2002, The role of the flexural rotation/rolling hinge model in the tectonic evolution of the Alasehir graben, western Turkey: Geological Magazine, v. 139, pp. 15-26.
Şengör, A.M.C., 1987a, Tectonics of the Tethysides: Orogenic collage development in a collisional setting: Ann. Rev. Earth Planet. Sci., v. 15, pp., 213-244.
Şengör, A.M.C., 1987b, Cross-faults and differential stretching of hanging alls in region of low angle normal faulting: Examples from western Turkey: Geological Society, London, Special Publication, v. 28, pp. 575-589.
Şengör, A.M.C., 1987c, The North Anatolian transform fault: its ages, offset and tectonic significance: Journal of the Geological Society of London, v. 136, pp. 269-282.
Şengör, A.M.C., 1979, The North Anatolian Transform Fault: its age, offset and tectonic significance: Journal of he Geological Society, London, v. 136, pp. 269-282.
Seyitoğlu, G., Tekeli, O., Çemen, I., Şen, Ş., and Işik, V., 2002, The role of the flexural rotation/rolling hinge model in the tectonic evolution of the Alaşehir graben, western Turkey: Geol. Mag., v. 139, pp. 15-26.
Şengör, A.M.C., Satir, M., and Akkok, R., 1984, Timing of tectonic events in the Menderes Massif, western Turkey: Imlications for tectonic evolution and evidence for Pan-African basement in Turkey: Tectonics, v. 3, no. 7, pp. 693-707.
Şengör, A.M.C., Gorur, N., and Saroglu, F., 1985, Strike-slip deformation basin formation and sedimentation: Strike-slip faulting and related basin formation in zones of tectonic escape: Society of Economic Paleontologists and Mineralogist Special Publications, v. 37, pp. 227-264.
Scherrer, N.C., Engi, M., Gnos, E., Jakob, E., and Liechti, A., 2000, Monazite analysis; From sample preparation to microprobe age dating and REE quantification: Schweizerische Mineralogische and Pertrographische mitteiungen, v. 80, pp. 93-105.
Schuiling, R.D., 1962, On petrology, age and structure of the Menderes migmatite complex (SW-Turkey): Bull. Res. Expl. Inst. Turkey, v 58, pp. 71-84.
Schuiling, R.D., 1959, Uber eine pra-herzynische Faultings-phase in Kazdag Kristallin: Bulletin of the Mineral and Research Exploration Institute, Turkey, v. 53, pp. 89-93.

Şengör, A.M.C., and Yilmaz, Y., 1981, Tethyan evolution of Turkey: A plate tectonic approach: Tectonophysics, v. 75, pp. 181-241.
Seydoux-Guillaume, A-M, Paquette, J-L, Wiedenbeck, M., Montel, J-M., and Heinrich, W., 2002, Experimental resetting of the U-Th-Pb systems in monazite: Chemical Geology, v. 191, pp. 165-181.
Soldatos, T., and Christofides, G., 1986, Rb-Sr geochronology and origin of the Elatia Pluton, Central Rhodope, North Greece: Geol. Balc., v. 16, pp. 15-23.
Spakman, W., Wortel, M.J.R., and Vlaar, N.J., 1988, The Hellenic subduction zone, a tomographic image and its geodynamic implications: Geophysical Research Letters, v. 15, pp. 60-63.
Stampfli, G.M., Mosar, J., Favre, P., Pillevuit, A., and Vannay, J-C., 2001, Permo-Triassic evolution of the western Tethyan realm: the Neotethys-east Mediterranean basin connection: In: Ziegler, P.A., Cavazza, W., Robertson, A.H.F., Crasquin-Soleau, S., (eds.), Peri-Tethys Memoir 6: Peri-Tethyan Rift/Wrench Basins and Passive Margins. Mem. Mus. Natn. Hist. Nat. Paris, v. 186, pp. 51-108.
Stampfli, G.M., Borel, G.D., Cavazza, W., Mosar, J., and Ziegler, P.A., 2001, Paleotectnic and palaeogeographic evolution of western Tethys and peri-Tethyan domain: Episodes, v. 24, pp. 222-228.
Stern, R.A., and Sanborn, N., 1998, Monazite U-Pb and Th-Pb geochronology by high-resolution secondary ion mass spectrometry. Radiogenic Age and Isotopic Studies, Report 11, Curr. Res. 1998-F. Geological Survery of Candan, Ottawa, ON, Canada, pp. 1-18.
Stirling D., Duncan, A.M., Guest, J.E., and Finch, A.A., 1999, Petrogenesis of plagioclase phenocryst of Mount Etna, Sicily, with particular reference to the 1983 eruption: contribution from cathodoluminescence petrography: Miner. Mag., v. 63, pp. 189-199.
Taymaz, T., Yilmaz, Y., and Dilek, Y., 2007, The geodynamics of the Aegean and Anatolia: introduction: Geological Society, London, Special Publication, v. 291, pp. 1-16.
Townsend, K.J., Miller, C.F., D' Andrea, J.L., Ayers, J.C., Harrison, T.M., and Coath, C.D., 2000, Low temperature replacement of monazite in the Ireteba granite, Southern Nevada: geochronological implications: Chem. Geol., v. 172, pp. 95-112.
Thomson, S.N., Stockher, B., Raushe, H., and Brix, M.R., 1998, Apatite fission-track thermochronology of the uppermost tectonic unit of Crete, Greece: implications for the post-Eocene tectonic evolution of the Hellinic Subduction System. In: Van den Haute, P., De Corte, F., (eds), Advances in fission-track geochronology. Kluwer, Dordrecht, pp. 187-205.
Twist, D., and Harmer, R.E.J., 1987, Geochemistry of contrasting siliceous magmatic suites in the Bushveld Complex; genetic aspects and implications for tectonic discrimination diagrams, In: Tectonic controls on magma chemistry, Weaver, S.D., and Johnson, R.W. (eds.), Journal of Volcanology and Geothermal Research, v. 32, pp. 83-98.
Verge, N.J., 1995, Oligo-Miocene extensional exhumation of the Menderes Massif, Western Anatolia: Terra Abstracts, v. 7, pp. 117.

Walker, T.R., 1984, Diagentic albitization of potassium feldspar in arkosic sandstones: Sediment. Petrol., v. 54, pp. 3-16.
Wilson, M., 1989, Igneous petrogenesis, Unwin Hyman, London.
Wiebe, R.A., Wark, D.A., and Hawking, D.P., 2007, Insights from quartz cathodoluminescence zoning into crystallization of the Vinalhaven granite, coastal Maine: Contrib. Mineral. Petrol., v. 154, pp. 439-453.
Wing, B.A., Ferry, J.M., and Harrison, T.M., 1999, The age of andalusite and kyanite isograds in New England from Th-Pb ion microprobe dating of monazite. 1998 Annual Meeting Toronto, ON, Canada, Abstr. Progr., v. 30, Geological Society of Ameica, Boulder, CO, pp. 27.
Wernicke, B.P., 1985, Uniform-sense normal simple shear of the continental lithosphere: Canadian Journal of Earth Sciences, v. 22, pp. 108-125.
Wernicke, B.P., 1988, On the role of isostasy in the evolution of normal fault systems: Geology, v. 16, pp. 848-851.
Yilmaz, H., Alpaslan, M., and Temel, A., 2007, Two-stage felsic volcanism in the western part of the southeastern Anatolian Orogen; petrologic and geodynamic implications: International Geology Review, v. 49, pp.120-141.
Zhu, L., Mitchell, B.J., Akyol, N., Cemen, I., and Kekovali, K., 2006, Crustal thickness variations in the Aegean region and implications for the extension of continental crust: Journal of Geophysical Research, v. 111, pp. 1-10.
Zulauf, G., Kowalczyk, G., Krahl, J., Petschick, R., and Schwanz, S., 2002, The tectonometamorphic evolution of high-pressure low-temperature metamorphic rocks of eastern Crete, Greece: constraints from microfabrics, strain, illite crystallinity and paleostress: J. Struc. Geol., v. 24, pp. 1805-1828.
Zhu, X.K., and O'Nions, R.K., 1999a, Zonation of monazite in metamorphic rocks and its implications for high temperature thermochronology: a case study form the Lewisian terrain. Earth Planet: Sci. Lett., v. 171, pp. 209-220.
Zhu, X.K., and O'Nions, R.K., 1999b, Monazite chemical composition: some implications for monazite geochronology. Contrib. Mineral. Petrol., v. 137, pp. 351-363.

VITA

Courteney Blaire Baker

Candidate for the Degree of

Master of Science

Thesis: DECHIPHERING THE EVOLUTION HISTORY OF THE SALIHIL AND TURGUTLU GRANITES, MENDERES MASSIF, WESTERN TURKEY USING THE ELECTRON MICROPROBE, ION MICROPROBE AND CATHODOLUMINESCENCE

Major Field: Geology

Biographical:

Personal Data: Born in Houston, Texas, April 28, 1982, the daughter of Rodney and Alice Brisco.

Education: Graduated from Putnam City North High School, Oklahoma City, Oklahoma in May 2000; received Bachelor of Science degree in Geology from Oklahoma State University in Stillwater in May of 2006; completed the requirements for the Master of Science in Geology at Oklahoma State University, Oklahoma, May, 2009.

Experience: Visiting graduate research assistant at the University of Texas at Austin, August 2007-December 2007; Research Fellow at the Smithosonian National Museum of Natural Research, Summer 2007; Graduate Research/Teaching Assistant at Oklahoma State Universtiy, August 2006-May 2008; Summer Intern for Waller Exploration LLC, Summer 2004.

Professional Memberships: Oklahoma State University Geological Society, Association of Women in Geology, Association of American Petroleum Geologist

Name: Courteney Blaire Baker Date of Degree: May, 2010

Institution: Oklahoma State University Location: Stillwater, Oklahoma

Title of Study: DECHIPHERING THE EVOLUTION HISTORY OF THE SALIHIL AND TURGUTLU GRANITES, MENDERES MASSIF, WESTERN TURKEY USING THE ELECTRON MICROPROBE, ION MICROPROBE AND CATHODOLUMINESCENCE

Pages in Study: 107 Candidate for the Degree of Master of Science

Major Field: Geology

Scope and Method of Study: The Menderes Massif, western Turkey is a large scale metamorphic core complex. This study focuses on determining the timing of movement along one of the main exhumation mechanisms of the Menderes Massif: the Alasehir Detachment. To address the timing of extension, granodiorites samples (S-type, peraluminous) were collected from two outcrops along the Alasehir detachment, located near the towns Salihli and Turgutlu. Monazite $(CeLaTh)PO_4$ in the rocks were dated in situ (in thin section) using an ion microprobe. To better understand the monazites ages x-ray element maps, geochemical data and cathodoluminescence (CL) images of the dated samples were obtained.

Findings and Conclusions: Th-Pb ages range from the Late to Early Miocene, which indicate that the massif has undergone multiple stages of extension. The CL images provided evidence of fluid flow that indicate dissolution/reprecipitation reactions and document a multistage tectonic history. Geochemical data suggests that the Salihli and Turgutlu granites may have been generated under a compressional régime due to north dipping subduction of the Eastern Mediterranean floor along the Hellenic trench. The major and trace element geochemistry show differences between the two granites; which could indicate that the Salihli and Turgultu granites do in fact have different sources, degree of alteration and interaction with fluids, duration and number of tectonic events experienced by the granites, even their P-T history.

ADVISER'S APPROVAL: Dr. Anna Cruse